Spring 2016

Carbon and Boron Nitride Nanotube Fabricated Supercapacitors

Derek Christian Demuth
Old Dominion University

CARBON AND BORON NITRIDE NANOTUBE FABRICATED

SUPERCAPACITORS

by

Derek Christian Demuth
B.A. May 2007, Virginia Polytechnic and State Institute
B.S. December 2014, Old Dominion University

A Thesis Submitted to the Faculty of
Old Dominion University in Partial Fulfillment of the
Requirements for the Degree of

MASTER OF SCIENCE

ELECTRICAL AND COMPUTER ENGINEERING

OLD DOMINION UNIVERSITY
May 2016

Approved by:

Gon Namkoong (Director)

Helmut Baumgart (Member)

Abdelmageed Elmustafa (Member)

ABSTRACT

CARBON AND BORON NITRIDE NANOTUBE FABRICATED SUPERCAPACITORS

Derek Christian Demuth
Old Dominion University, 2016
Director: Dr. Gon Namkoong

The fabrication of supercapacitor devices consisting of boron nitride nanotubes (BNNTs) and carbon nanotubes (CNTs) has great theoretical capabilities of high specific capacitance, energy density, and power density. Various methods of dispersion and deposition are utilized to optimize such supercapacitors with BNNTs and CNTs, and also to produce devices with only CNTs to use as a benchmark. In addition to capacitance measurements, BNNTs that were exposed to nitric acid were compared to fabricated devices without acid exposure.

Dispersion has been accomplished through the trial of many solvents and surfactants for both CNTs and BNNTs. Deposition techniques that are utilized rely heavily on vacuum filtration and spray deposition techniques. The resultants of fabrication have been tested with capacitance voltage measurements and transmission electron microscopic images are used to analyze solutions.

The highest specific capacitance was found in a fabricated device without including BNNTs, as a device fabricated from CNTs as the electrode, a polymer electrolyte, a dielectric separator of nafion, and foil contacts, had a specific capacitance of 0.51 mF/g. This device also had 0.13 Wh/kg for energy density, and 3.02 kW/kg for power density. However, despite this measurement of highest specific capacitance achieved without using BNNTs, a device made of only CNTs, BNNTs, foil contacts, and electrolyte, had the highest energy density of 0.15 Wh/kg and power density of 4.29 kW/kg. This device also had one of the highest measured specific

capacitances of 0.27 mF/g.

The CNTs and BNNTs were chosen to be used together because of costs and availability and their ideal structures for use as an electrode and a separator, respectively. Both materials have lattice structures that can be rolled into tubes to create bonds and also strengthen the material between walls. The porous structures also allow an electrolyte to seep into the pores to promote charge separation. Carbon is an ideal electrode and boron nitride has high dielectric properties suited for a capacitor separator.

The devices showed consistent capacitance characteristics with higher power density than energy density. The techniques used for fabrication, measurement, and further optimization are mentioned throughout this paper. Cleaning BNNTs in nitric acid proved to promote better physical and electrical properties for the resultant solutions and devices.

This thesis is dedicated to my mother and my grandfather, who helped me start school but could not be around to see me finish.

ACKNOWLEDGMENTS

There are many people who have contributed to the successful completion of this thesis. I extend many thanks to my committee members for their patience and hours of guidance on my research and preparation of this manuscript.

I would specifically like to thank the other graduate students who assisted me through the entire process of completing my thesis in Raihan, Nizam, Xin, Pengtao, Tanzilla, and Haider. Without their direction and assistance, none of this would be possible. Also the undergraduate students Doug, Louis, and Brandon for assistance in experiments.

I would like to thank my family; through my sister offering advice on how to navigate through graduate school, and my father by giving me motivation to complete my degree as soon as possible.

A special thanks is given to all the faculty at Old Dominion in the Electrical Engineering department with their wisdom and opportunities presented to me. A specific thanks to Dr. Ali for offering me lab experience at Jefferson Lab during my undergraduate career. Dr. Xin and Dr. Backens who helped me financially during my last year as an undergraduate student. Also, Dr. Namkoong for the financial backing, experimental, and scholarly advice, and his untiring efforts to help push me to further enhance my research.

Dr. Cao deserves special recognition for helping me gather data and also for his direction for experimental procedures. Also, the college of William and Mary for their resources at Jefferson Lab during my research. This work is partially supported by the NSF SoLEAP program.

I would also like to thank God. I have said many prayers to help me get through my graduate work.

NOMENCLATURE

A Area, m^2

a_{cc} Molecular C-C Bond Length, m

C Capacitance, F

C_s Specific Capacitance, F/g

d Thickness, m

d' Ideal Diameter of rolled Nanotube Sheets, m

ε Dielectric Constant, F/m

I Current, A

m Mass of Active Material in a Single Electrode, g

M Mass of Active Material in Both Electrodes, g

n Index of Unit of Nanotube Cut, (No Units)

n,m Index of Unit of Nanotube Cut, x-y axis, (No Units)

P Voltage, V

R Resistance, Ω

Q Stored Charge, C

V Voltage, V

V_a Voltage at Anode, V

V_c Voltage at Cathode, V

v_s Scan rate, V/s

V_w Voltage Window, V

TABLE OF CONTENTS

LIST OF TABLES

Table   Page

LIST OF FIGURES

CHAPTER I

INTRODUCTION

Supercapacitors, also called ultracapacitors, are a necessity moving forward in powerful energy storage systems where rechargeable batteries are used. This is true whether energy is collected by wind, water, or the sun. As large grids, or energy farms, are becoming more prevalent and taxing on current batteries, rechargeable batteries are limited in such systems due to their acceptance, delivery of energy, as well as their charge and discharge cycles [1], [2]. Also, in hybrid electric cars, supercapacitors are used for battery systems load leveling, providing peak power under acceleration or traveling up gradients, cold-start assistance, and catalytic converter preheating [3]. The idea of capacitors has been around for hundreds of years and the first documented capacitor dates back to 1746 in the Netherlands [4]. Supercapacitors are used to help carry the load for many new powerful systems due to their achievable higher power than batteries, rapid charging and discharging, pulse power supply, long cycle life, high dynamic of charge propagation, ability to work in extended temperature ranges, low level of heating, long term operation stability, and no disposable parts [1], [5], [6].

The next section defines a brief background given of common terms, or topics, that appear throughout this paper. This background will give all readers the same level of understanding of what key concepts are when they appear in various sections.

SOLUTES, SOLVENTS, SURFACANTS

As a variety of solid materials are used in the fabrication of devices, and some of these solids need to be changed into a liquid form. When solids need to be changed into liquid form, they acquire

the definition of solutes, which mix with liquids, known as the solvent, and will mix into a liquid the same way powder drinks do. Quite often solids and liquids do not mix so easily, such as sand and water. Although salt and water mix well, such as with ocean water, sand will sink to the ocean floor, despite constant mixing through waves and ocean currents. It has been found however, by adding various acids to a sand and water mixture, that the sand will become a liquid solution [7]. For this reason, specific solvents may be needed to help dissolve a solid into a liquid solution. Solvents can also be in a solid or gas form [8], [9]. Not all solutes have a solvent that will allow for a quality mixture to completely change a solute into a solution, and an extra material known as surfactants may be necessary [10].

Surfactants lower surface tension allowing for a more dispersed resultant liquid between two materials through an amphipathic molecular structure in which a hydrophile is connected to a hydrophobe, or a lipophile [11]. Because of this structure, the surfactant can adsorb onto a surface and alter, typically lower, the interfacial free energies of the surface [12]. The interfacial free energy is the minimum amount of work required to create the interface of the surfaces [12]. The surfactant exists as an amphipathic structure because the hydrophile is attracted to water and the hydrophobe is attracted to the non aqueous part of the solution [11]. The hydrophile distorts the structure of the solvent through expelling some of the surfactants molecules into the interfaces of the system [12]. The surface of the solvent then becomes covered with a layer of the surfactant, with the hydrophilic groups pointed towards the air, resulting in a decrease of surface tension at the surface [12]. This is due to molecules at the surface tend to have a higher potential energy than the interior molecules because of the strong interaction between the molecules, so work is required to move a molecule from the interior to the surface [12]. The hydrophobe group prevents the

surfactant from being expelled from the solvent as a separate phase [5]. The surfactant used is heavily dependent on the type of solvent used and can be anionic, cationic, zwitterionic, or nonionic, based on charge [12]. The hydrophobic group is usually a long chain hydrocarbon group, and an increase in length results in increases of solubility in organic solvents, of tighter packed surfactant molecules at the interface, of the surfactant to adsorb at an interface, and a decrease in solubility in water [12]. So, surfactants are based on the solvent used in the solution and help the solubility of materials, also known as dispersion.

DISPERSION AND DEPOSITION

Dispersion, in regards to chemistry, refers to a system in which particles of one kind are intermixed in a continuous phase of another composition or state [10]. Variations exist for dispersion in such that a dispersed solution can be considered a true solution or a colloidal solution [10]. A true solution exists in that the particles are dissolved in the continuous phase in a homogenous mixture with particle size around tens of nanometers [10]. These dispersed true solutions mix well with only a solvent being necessary [10]. In the case of colloidal solutions, the particles being dissolved are usually larger, in the range of nanometers to micrometers, and do not mix as well as true solutions, so surfactants are added to help thermodynamically and kinetically stabilize the solution [10]. The colloidal solutions tend to change degree of dispersion over time, typically having the solutes settle at the bottom of the container as time passes [10]. For certain materials, further distinctions can be made to differentiate the dispersed solutions, as in the case of carbon nanotubes (CNTs) being designated as macrodispersions, with dispersion of the bundles, and nanodispersions, being dispersions of the non bundles of carbon nanotubes [10]. A well dispersed

solution will allow the solute to reach the desired mixture phase, and for the solution to be deposited easier.

Deposition is the process of placing particles on a desired surface typically achieved through chemical vapor deposition [13], atomic layer deposition [14], vacuum filtration [15] – [22], spray deposition [23], physically pressing materials such as 'domino pushing' of CNTs [24], ion-assisted physical vapor deposition (PVD) methods such as magnetron sputtering, biased plasma deposition, or ion-beam deposition [25]. All of these methods have their own benefits and disadvantages, so selection of the desired deposition method must be considered based on the substrate and desired result. Chemical vapor deposition and physical vapor deposition are ideal for fabricating nanotubes in their pure form, but have more fabrication costs in regards to time and equipment needed than other methods when attempting to make nanotube mats [13], [15] – [19]. Vacuum filtration and spray deposition require a basic setup and are easy methods to replicate in a basic laboratory setting [15], [23]. Deposition allows particles to move from one substrate to another [13]. Various methods are applicable for specific purposes of fabrication. The main uses of deposition used in this experiment are of vacuum filtration and spray deposition techniques, because of the ease of setup to produce nanotube films.

MOLECULAR BONDING

Described in further detail later in the literature review section is molecular bonding. To introduce molecular bonding, a simple equation to determine a nanotube diameter (d') of a single wall carbon nanotube (SWCNT) uses C-C bond length between atoms and is shown on the next page in equation 1 [26].

$$d'=0.955na_{cc} \tag{1}$$

The term *d'* is used because the carbon graphene sheets are rolled and do not always produce an exact cylindrical shape so the prime nomenclature represents an ideal cylindrical shape, which equals the lattice indices representing the type of cut (n), discussed in greater detail in further in this section, multiplied by 0.955 and the bond length (a_{cc}) [26]. Equation 1 shows that the type of bond is important to basic calculations to characterize the carbon nanotube structure [26]. Also, mentioned throughout the paper is the bonding of molecular orbitals, specifically the sp^2 and sp^3 bonds experienced by CNTs and boron nitride nanotubes (BNNTs), so a brief explanation is given to build a fundamental understanding of the importance of such bonds.

Carbon is the sixth element in the periodic table, with corresponding atomic number 6 [27]. This means that there are 6 electrons which occupy its orbital structure [27]. The first orbital houses 2 electrons and the second orbital can hold up to 8, but only needs 4 for the remaining electrons in regards to carbon [27]. The carbon simple electron configuration can be written as $1s^2\,2s^2\,2p^2$ [27]. So pure carbon uses sp^2 bonding in its basic form, but CNTs are rolled graphene sheets so additional bonds are made during methods of fabrication [28], [29]. This is due to an increase in density from an ion having enough energy to penetrate the surface layer, causing it to take on a metastable interlayer sp^3 configuration typically achieved through neutron irradiation [28], [29]. Irradiation is done to improve mechanical strength of the nanotubes and exists as the transformation path between graphite and diamond under electronic excitation as diamond has sp^3 bonds which results in the material being much stronger than graphene [29], [30]. If the ion energy

is too high, the sp^3 bond can relax back to the sp^2 bond, and only a fraction of sp^3 bonds exists [29], [31]. Boron nitride shares similar bonds dependent on structure as the atomic number of boron is 5 and nitrogen is 7 and is discussed in further detail further in this paper [27], [32]. Now that certain details have been discussed, a background will be given on the main topic, supercapacitors.

BATTERIES

There are many similarities in comparison of batteries and supercapacitors, but a brief examination of current rechargeable batteries will show the need for supercapacitors in conjunction with batteries. Currently, lithium ion batteries are preferred for use in powerful systems due to their smaller physical size while having more desirable electrical characteristics of batteries when compared to batteries made of nickel or cadmium [2]. In lithium ion batteries, the fabrication materials have low costs and the batteries have a low operational voltage, around 4 volts, because they are made by using inexpensive carbon as the anode in conjunction with a cathode capable of stability at high voltages [2]. An electrolyte, explained in greater detail further in this chapter, in these batteries allows lithium ions to move through the device because of its structure housing conductive ions during charging and discharging cycles [2], [33]. A separator layer is placed between these electrodes to isolate the anode and cathode, creating a sandwich geometry similar to that of supercapacitors, which is discussed in further detail below [2], [33], [34]. A common issue with early lithium ion batteries was when the metal electrodes had contact with a liquid electrolyte, as sometimes this reaction would cause fires and explosions [33]. Typically, in electric vehicles, battery life is expected to be near 10 years, as this is the typical life of a car [35]. New materials and advancements are making lithium ion batteries lifetimes longer and able to handle harsher conditions during charge and discharge cycles [2], [33], [35], [36]. However,

the main issues that these batteries suffer from are low power density and poor cycle life, usually around 1000 cycles, despite being able to store large amounts of energy [2], [33], [35], [36]. Supercapacitors, on the contrary, suffer from low energy density, but have excellent power density and can undergo many more charge and discharge cycles while maintaining adequate performance [36]. Combining supercapacitors with lithium-ion batteries, commonly referred to as hybrid supercapacitors, allow for a system that has both high energy and high power densities [36]. The hybrid supercapacitors follow the same structure as lithium ion batteries and supercapacitors, but combine both types of battery and capacitor in the electrodes to fabricate the device utilizing both faradic and non faradic reactions allowing for both high power and high energy densities [36], [37]. As improvements are continuously being made to these structures, supercapacitors are not being phased out as supercapacitors are still needed for operations where fast cycle life is needed, such as emergency doors on airplanes [1]. For these reasons, supercapacitors with low manufacturing costs are a necessity for constantly changing technology, and are described in further detail below.

SUPERCAPACITORS

A supercapacitors structure involves two nonreactive porous plates known as electrodes, containing an electrolyte, contained within two current collectors in which voltage is applied divided by a separator [38]. The supercapacitor has a much higher capacitance than a regular capacitor because of a larger surface area of the active material in the electrode region, commonly accomplished by using activated carbon [39]. A typical supercapacitor structure consists of current collectors of opposite charges, due to the difference in applied voltage potential, on the edges of the supercapacitor pressed against an electrode with the corresponding charge type,

positive or negative, as each current collector [34]. An electrolyte is applied on, or in, the electrodes, and the opposite charges of the supercapacitor are segregated by a separator layer [34]. Each layer is described in further detail below and a basic diagram of a typical supercapacitor can also be seen below in Figure 1 [34]. Figure 1 is reprinted with permission from (V. Musolino, L. Piegari, and E. Tironi. "New Full-Frequency-Range Supercapacitor Model with Easy Identification Procedure." *IEEE Transactions on Industrial Electronics* 60.1 (2013): 112-20.). Copyright (2013). (IEEE).
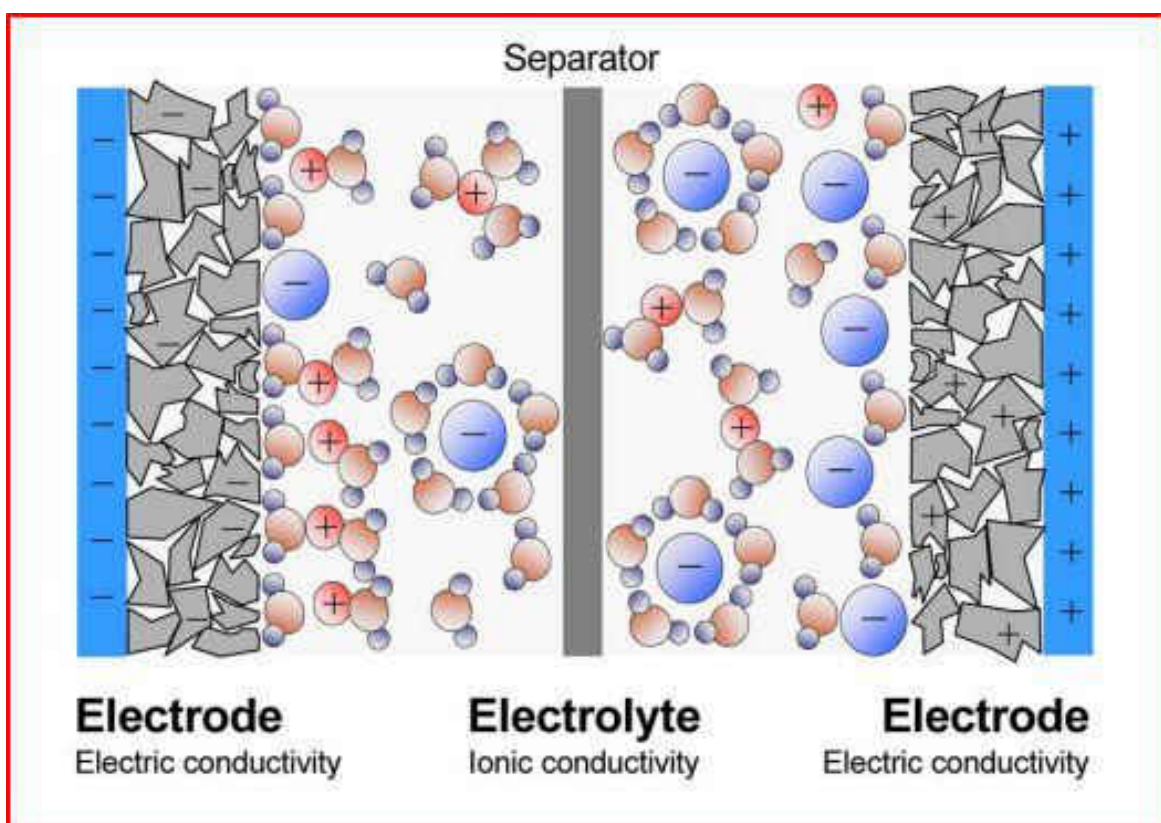

Figure 1: Basic supercapacitor structure layers [34] © 2013 IEEE

The current collectors are located on the edge of the supercapacitor to transport charges produced by the active materials in the electrode and electrolyte along the length of the supercapacitor with high efficiency to minimize energy loss [34], [40]. These edges of the supercapacitor device carry the same charge, positive or negative, as the electrode that they are pressed against [34]. Typically, aluminum is used as the current collector, but other materials such as carbon coated aluminum through chemical vapor deposition, carbon film, gold, nickel, platinum, silver, copper, along with various combinations of such materials, have been tested for improved supercapacitor performance [3], [40] – [42]. Although aluminum and nickel are commonly used as current collectors, copper has been proven to extend the potential window from 1 volt to 1.4 volts, allowing for a larger range of operation [3], [37], [40], [41], [43]. The potential window increase is attributed mainly to an increase in the electrochemical performance of the device through an oxidation of the coppers surface by the electrolyte used, which could vary by type of electrolyte, which results in an increase in energy density and power density [40]. Although the current collectors are made from conductive material, one of the factors that limit a supercapacitors potential is the contact resistivity between the current collector and the electrode, so materials that interact well at the bonding site of the current collector and electrode are imperative to keep internal resistance down, which increases power density [43].

The electrode layer, often considered the most important layer in the supercapacitor in regards to performance because it contains the active material and it has an interface with both the current collector and the electrolyte [34]. The electrode layer is typically fabricated from nanoscale materials that have high surface areas and high porosity to allow the electrolyte to seep through [34], [44]. To overcome the supercapacitors naturally low energy density, new materials are being

examined and developed as improvements are constantly being made to the electrode layer to increase a supercapacitors performance [44], [45].

Many different materials such as metal oxides, conducting polymers, and various carbon materials, such as activated carbon or carbon nanotubes (CNTs), have been tried as the electrode layer in supercapacitors [46]. For the following reasons described below, CNTs were chosen as the electrode material. Research on various types of carbon have become prominent in recent years due to carbon's high specific capacitance and high power density [46]. However, the low conductivity of porous carbon materials limits the supercapacitors power density, so CNTs, detailed in further sections, have gained interest in the supercapacitors electrode layer due to their improved conductivity and surface area over conventional carbons [46]. Carbon nanotubes have not yet reached their full expectations of capacitance, mainly believed to be due to the contact resistance between the electrode and the current collector [46]. Some research has proven there is improvements when growing CNT film on graphene to reduce the contact resistivity between the electrode and current collector [42], [46]. The interface between the current collector and electrode is just as important as the interface between the electrode and the electrolyte, as the electrolyte will seep into the electrodes pores, causing charge separation [34]. The electrodes pores allow for not only the storage of charged ions through the electrolyte, but also the separation of charges between the electrolyte and the electrode material, which causes an electric field and helps promote higher efficiency of the device [44].

The electrolyte layer is just as important as the electrode layer to create the charge separation as the electrolyte will exist through the electrodes pores [34]. The electrolyte layer contributes to the

stability and conductivity of the supercapacitor through constant time, nominal voltage, and cycle life [47]. Typical characteristic requirements for use of an electrolyte in a supercapacitor include a wide voltage window, high electrochemical stability, low resistivity, low viscosity, low volatility, high ionic concentration with low solvated ionic radius, and maintaining a high purity at low cost [44]. Electrolytes can be classified into three categories: aqueous, organic, and ionic liquids [44]. Aqueous electrolytes, such as H_2SO_4, are liquid based and demonstrate a high ionic concentration with a low resistance [44]. These electrolytes are easy to create, but have a small voltage window, which leads to limitations in both energy and power densities [44]. Organic electrolytes provide a voltage window almost three times that of aqueous electrolytes, but issues arise from organic electrolytes are that of low flash points of materials, such as acetonitrile, causing major safety concerns, or such issues as the electrolyte having poor conductivity at low temperatures due to poor viscosity, such as polypropylene carbonate [47]. Other materials used for organic electrolytes include ethyl acetate, organic salts such as triethylmethylammonium tetrafluoroborate, and ester solvents with methoxy or fluorine groups being added to ethylene carbonate [44], [47]. The third classification type, ionic liquids, are created by melting salts [44]. Most of the work being done on organic electrolytes is focused on making the materials safer by raising their flashpoint to allow for safe operation and fabrication under higher temperatures, while maintaining ideal characteristics of the materials, such as acetonitrile, or the focus concentrates on increasing the conductivity of materials like polypropylene carbonate by adding ionic liquids to allow better physical characteristics at lower temperatures [47]. An issue from aqueous electrolytes and electrolytes in liquid form is that liquid electrolytes can leak out of the device and lead to corrosion or harmful acid around the device [48]. Gel electrolytes, based off aqueous electrolytes, are widely used in supercapacitors because they minimize low conductivity,

poor contact, high internal resistance, and low mechanical strength [48]. Gel electrolytes have shown comparable performance to ionic liquids and are easy to make and apply [48]. However, gel electrolytes are difficult to regulate in terms of deposition and can lead to shorts as the paste is often pressed between materials causing the gel to leak out and vacate certain areas that were under high pressure [23]. The most commonly used electrolyte in commercial supercapacitors is tetraethylammonium tetrafluoroborate (ET_4NBF_4) in non-aqueous solvents, while in aqueous systems, sulfuric acid or potassium hydroxide is used [39].

The supercapacitor uses not only a sandwich geometry as seen previously in Figure 1, but typically layers will be the same on opposite sides of the device mirroring each other [34]. The middle section of the supercapacitor is known as the separator layer [34]. This layer is a porous dielectric separator, so that it will act as both an electric insulator and also as a proton conducting separator so that the two sides of the device can interact [23], [38]. This phenomenon occurs from the electrolyte material seeping into the separator membrane, as the membrane is typically hydrophilic in that it absorbs solution [6], [49]. This layer keeps the positive and negative electrodes apart to prevent short circuits and also allows ionic charge carriers to rapidly pass through, to complete the capacitance circuit [50]. Thus, the separator material should not only be a good insulator, but also have the ability to conduct ions well [50]. The separator is mesoporous in nature and influences the relaxation frequencies during charge and discharge cycles, and influences the energy density and power density. In addition, the separator layer has an effect on the ionic charge transfer rate between the positively and negatively charged electrodes [51]. To increase the performance of the separator layer, optimization must be taken in consideration of the thickness, the wettability, and limitation of the molar conductivity of ions in the separator. Also, to increase performance,

optimization must keep the molar conductivity in the electrode and electrolyte layer, as the separator needs to have minimal conductivity in the capacitor [52]. As with all the layers, lower fabrication costs with optimal performance are considered when selecting the material for each layer in such performed experiments [50].

The physical characteristics of the layers in the device can be used to calculate the capacitance using the equation below, equation 2, when a small separator layer is used, such as that found in supercapacitors [44].

$$C = \frac{A\varepsilon}{4\pi d} \qquad (2)$$

In this equation above, the capacitance of the electrode and electrolyte interface (C) is found by multiplying the area engulfed by the current collectors (A) by the dielectric constant of the material between the electrodes (ε) and dividing this by 4π times the thickness between the electrodes (d) [44]. However, the capacitance for this research will be calculated by measuring a capacitive device to minimize error. Equation 1 is mentioned to show the possibility of defining capacitance by such physical characteristics.

Although there are many different materials and methods used for the fabrication of each layer of a supercapacitor, the device can be classified based on how it creates the capacitance [1]. Supercapacitors are classified into two categories, electrical double layer capacitors (EDLCs), and pseudocapacitors, which are defined based strictly on their energy storage mechanism [1], [38].

EDLC SUPERCAPACITOR

With EDLCs, the capacitance is non faradic, as no electron transfer takes place, but rather the capacitance comes from the pure electrostatic charge accumulation at the electrode and electrolyte interface [1], [38]. A separation of ionic charges occurs at the interfaces of layers between the ionic solutions and solids [4]. In EDLCs the supercapacitors are based on a double electric charge layer effect, existing only in electrolytic capacitors [6]. The mechanism behind the EDLC relies purely on the electrostatic accumulation of surface charge through surface dissociation and ion adsorption [44]. An excess or deficit of charges accumulate on the electrode side of the electrolyte interface, so counterbalancing charges are then formed on the electrolyte side to counter the imbalance of charges [44]. This phenomenon is called electroneutrality, and is seen during charging when energy is stored in the double-layer surface as cations move toward the negative electrode, and anions move towards the positive electrode [44]. This process is reversed during the discharge cycle [44]. Through these processes, no charge transfers or net ion exchanges occur between the electrode and the electrolyte, implying that the electrolyte ion concentration remains constant during charging and discharging [44]. These supercapacitors store much more energy than conventional capacitors because of a large interface area and the atomic distance of charge separations [1]. The EDLC supercapacitors always use a porous material as the separator so that a liquid electrolyte can penetrate into its pores [6].

The concept of EDLCs dates back to the 1800's when Hermann von Helmholtz investigated the distribution of opposite charges at the interface of colloidal particles [1]. In his work, he found that two layers of opposite charges form at the electrode interface and are separated by an atomic distance [1]. He also found that charged electrodes immersed in an electrolyte solution will repel

the coions, while attracting counterions to their surfaces [53]. The two compact layers of charges formed at the electrode and electrolyte interfaces is called the "electric double layer" (EDL) [53]. His created structure resembles typical dielectric capacitors that utilize the separation of multiple charged plates [1], [53]. Von Helmholtz created equations to solve the specific capacitance for a planar electrode, a cylindrical electrode, and a spherical electrode [53]. Years later, this work was later scientifically added to by Gouy and Chapman first, and again later by Stern [1], [53]. Stern combined research from his predecessors to create a capacitance model with two regions of ion distribution [1]. One region is called the compact layer, also known as the Stern layer, which is the inner layer closest to the positively charged surface and resembles the work from von Helmholtz, as seen on the following page in Figure 2 [1]. In this region, ions are strongly absorbed by the electrode and there are no free charges [1], [53]. The other region is known as the diffuse layer, which is derived from the works of Gouy and Chapman, and in the outer region a continuous distribution of electrolyte ions in the electrolyte solution are being driven by thermal motion [1]. Figure 2 is a representation of the three models from von Helmhotlz, Gouy, Chapman, and Stern [53]. Figure 2 is reprinted with permission from (H. Wang, and L. Pilon. "Accurate Simulations of Electric Double Layer Capacitance of Ultramicroelectrodes." *Journal of Physical Chemistry C* 115.33 (2011): 16711-6719.). Copyright (2011). (American Chemical Society).
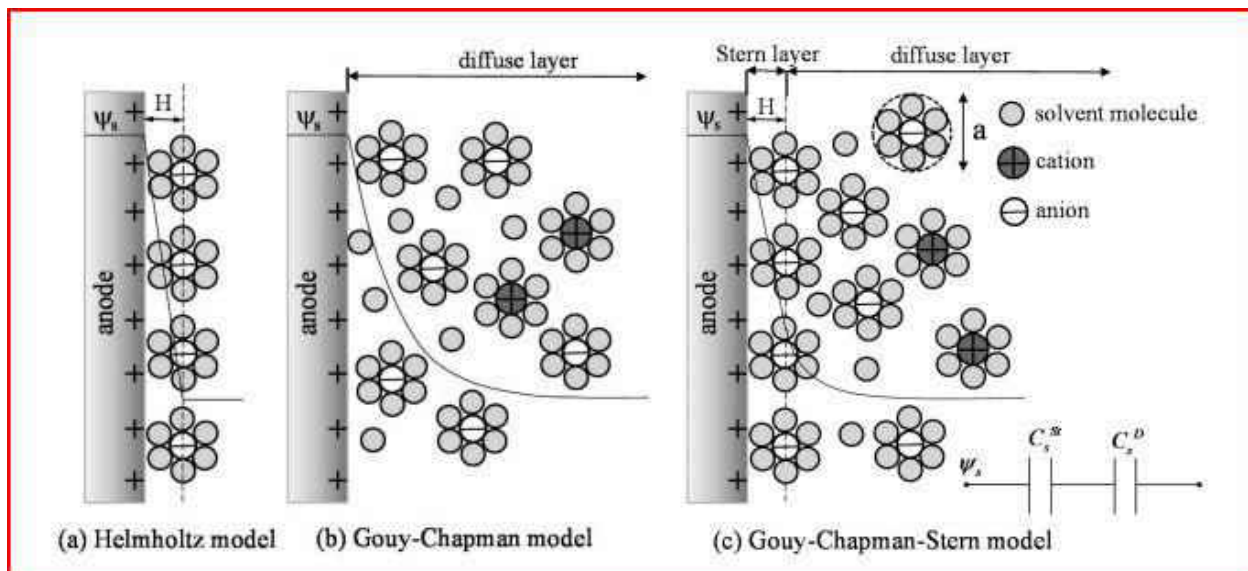
Figure 2: *The advancement in EDLC models [53] © 2011 ACS*

The total calculated capacitance of the Stern model uses the two regions in series to calculate the total capacitance [1], [53]. This is shown below in equation 3 [1].

$$\frac{1}{CEDL} = \frac{1}{CSTERN} + \frac{1}{CDIFF}$$

(3)

The factors that determine the EDL behavior at the electrode surface, mathematically a planar flat surface for the electrode, include the electric field across the electrode, the types of electrolyte ions, the solvent in which the electrolyte ions are dissolved, and the chemical relation between the adsorbed ions and the electrode surface [1]. However, the typical electrode is a porous material with a high specific surface area so the EDL behavior at the surface of the electrode is more complex than a planar model [1]. The ion size and ion concentration also play a major role in capacitance, as the Poisson-Boltzmann equations used to create these EDL models only account

for low ion concentration and low electric potential [53]. Modified Poisson-Boltzmann equations have been created based on local density and mean-field approximations to create a more convenient mathematical approach [53].

PSUEDOCAPACITOR SUPERCAPACITOR

The other type of supercapacitor, pseudocapacitors, create capacitance due to a fast and reversible faradic charge transfer process, in which electron transfer produces changes in the chemical or oxidation state [1], [38]. This is due to the thermodynamics of charge acceptance, or charge stored, and a change in potential voltage to formulate the capacitance charge [1], [54]. Taking the derivative of the charge acceptance (q) over that of the potential voltage, or voltage window (V_w) allows for the capacitance (C) to be found as seen below in equation 4 [1]. The voltage window is the difference in voltage between the anode and the cathode [23].

$$C = \frac{d\Delta q}{d\Delta Vw} \tag{4}$$

Pseudocapacitance is accomplished by using electrode materials that have the electrochemical signature of a capacitive electrode, such as ruthenium oxide or manganese oxide [54]. Other common active species used are vanadium nitride, electrically conducting polymers, and surface functional groups containing oxygen or nitrogen [1]. Such materials excel as pseudocapacitors due to their nanotubular arrayed porous structures that have properties consistent with a hydrous nature and metallic conductivity [1]. Although pseudocapacitance can be higher than EDL capacitance, pseudocapacitors suffer from a low power density and lack of stability during cycling [1].

Some supercapacitors are not limited to one category as both capacitance mechanisms can operate simultaneously depending on the nature of the electrode material [1]. For example, an EDLC with various high-area carbon electrodes can also exhibit a small, but significant pseudocapacitance due to electrochemically active redox functionalities [38].

SUPERCAPACITOR CHARACTERISTIC EQUATIONS

The performance of supercapacitors is mainly evaluated on their energy density, power density, specific capacitance, cyclability in regards to lifetime, charge and discharge times, minimal self-discharging energy loss, safe operation, and low cost [1]. The capacitance of a supercapacitor can be used to calculate the electrical energy (E), also referred to as stored energy, as it is directly related to capacitance (C), stored charge (Q), and voltage (V) and is seen below in equation 5 [38]. The stored energy is found by multiplying one half of the voltage squared by capacitance [38].

$$E = \frac{CV^2}{2} = \frac{QV}{2} \tag{5}$$

In this equation, the capacitance and stored charge depend on the electrode material used, and the operating voltage is determined by the stability window of the electrolyte [38]. The large amount of charges that can be stored allow the supercapacitor to provide higher amounts of power than batteries [38]. However, when storing energy in layers, an equivalent series resistance is created [1]. This is shown in the power density (P) equation below, equation 6, where voltage (V) is squared and divided by four times the device's series resistance, or equivalent series resistance

(ESR) [1], [38]. Examining equations 5 and 6, it is clear that energy and power are improved when using materials of high capacitance and low resistance [38].

$$P = \frac{V^2}{4ESR} \qquad (6)$$

Other calculations important for capacitors which draw from equations 5 and 6 are that of energy and power density, as seen on the following page in equations 7 and 8. Equation 7, energy density, is taken from equation 5 of stored energy, in which capacitance (C) is multiplied by voltage (V) squared and divided by 2 times the mass (M) of both electrodes, with typical units of Wh/kg [55]. Equation 8 is power density, which is taken from the max power, equation 6, and is calculated by squaring the voltage (V), and dividing by 4 times the resistance (ESR) and the mass (M) of the two electrodes [55]. The units are typically kW/kg [6], [56].

$$E = \frac{CV^2}{2M} = \frac{QV}{2M} \qquad (7)$$

$$P = \frac{V^2}{4ESRM} \qquad (8)$$

Supercapacitors, operate in the farad range, where regular capacitors are in the picofarad to microfarad range. The development of capacitors with both a high power density and a high energy density are needed for practical applications as stronger batteries are being developed [3]. Optimizing the energy density without deteriorating the high power capability is key for the development of supercapacitors [1]. Of current technologies, lithium-ion batteries have the highest energy density at around 150 Wh/kg, but have a very limited life cycle [6],

[37]. Supercapacitors highest known power density and energy density capabilities exist in the hundreds of kW/kg and hundreds of Wh/kg [57].

The key factors in determining the power of supercapacitors through resistance are the resistivity of the electrode, the resistivity of the electrolyte in the electrodes pores, and the contact resistance between the electrode and the current collector [3], [43]. So, the internal characteristics will determine the capabilities of the capacitor. Carbon material has been widely used in supercapacitors because of its ideal properties as an electrode [6]. Also, recent advancements in energy storage techniques have shifted from conventional structured electrodes to nanostructured electrodes to relieve surface tension between the interfaces, as well as supply smaller pores for the electrolyte to exist [37]. Early studies of carbon in capacitors used activated carbon fiber cloth separated by glass fiber filter paper [6]. As time passed, carbon nanotubes have since become widely studied for such applications [1], [3], [5], [6], [37], [38], [58].

CARBON NANOTUBES

The research of CNTs began in the 1970's through a synthesis of vapor grown carbon fibers achieved from the decomposition of hydrocarbons at high temperatures in the presence of transition metal catalyst particles less than 10 nm in diameter [58]. Although a few labs in varying countries were experimenting with this approach, there was a general consensus that carbon was thought to only exist in the allotropes of diamonds and graphite. Not until 1985, by means of using an intense pulsed laser, a stream of helium gas carried vaporized carbon into a mass spectrometer in which C_{60} had been defined [59]. C_{60} had formed very easily as a new allotrope in the shape of a sphere, known as a fullerene, and was called 'buckminsterfullerene', or 'buckyball' for short,

which later led to the terms 'buckytube' and 'buckypaper' [59]. In 1991, through the use of a High Resolution Transmission Electron Microscope, multiwall carbon nanotubes (MWCNTs) were first reported [60]. MWCNTs, as opposed to single wall carbon nanotubes (SWCNTs), have slightly different characteristics detailed in the next sections [61]. In addition to these discoveries, other carbon atoms were being found soon after [62] – [65]. By the turn of the century, a Nobel prize was awarded to the group in 1985 for discovering fullerenes, which led to the advancement in finding more carbon types including C_{36} [62], C_{70} [63], C_{74} [64], and C_{86} [65]. Examining these structures common geometry shows a fullerene structure comprised of 12 pentagonal faces and varying hexagonal faces that are two-dimensionally isotropic, allowing for easy manipulation of the physical structure [66]. This led to the discovery that the carbon atoms can form long cylindrical tubes [59]. Utilizing the carbon structure, a variety of cuts and rolls of layers of the graphite tubes allow for further manipulation of the CNTs [38]. The CNTs unique tubular porous structures allowed for finding the CNTs superior electrical properties that favor fast ion and electron transportation [1]. Because of the CNTs hexagonal structure, there are a variety of cuts that can be made to produce various qualities in the nanotubes, such as electronic properties and growth dynamics [67].

CARBON NANOTUBES - BONDING

MWCNTs are preferred typically in commercial applications due to their lower cost and availability, as they are to easier to manufacture than SWCNTs [61]. However, SWCNTs have a theoretical tensile strength near 100 GPa, but because of their brittle nature, they suffer from fabrication defects that lower their actual, measured strength [61]. Other limitations of the brittle SWCNTs include resistance to compressive loading due to buckling, limited by the pore space in

the nanotube, and the process of functionalizing in acid to enhance coupling to a matrix can introduce strength-limiting flaws [28]. MWCNTs suffer from these same characteristics when van der Waals coupling is used [28]. Van der Waals force is the electrodynamic coupling between the polarized states, and there is an increase in the relative density of photonic states during excitation by drawing atoms close to the CNT sheet creating a bond [68]. Experiments have been performed on C_{60} tubes to verify the molecular accommodation when van der Waal potential energy forces are present [69]. Certain arrangements of the nanotubes can be made to utilize the van der Wall forces, such as nestling of CNT layers similar to a Russian doll [28]. However, van der Waal forces are not always enough for MWCNTs to overcome buckling from loads, leaving energy dissipation between layers and a broken telescopic effect [28]. Utilizing sp^3 molecular orbitals of CNTs has proven to strengthen the bond between MWCNT layers [28], [61]. The sp^3 bonds allow bridges to form between CNT walls by applying chemistry and allowing bonds to occur through manipulation of the molecules natural state [28], [61]. Sp^2 bonds exist in carbon, but more so in perfect lattice structure such as graphene sheets, but defects on CNTs, quite often intentional through irradiation or acid treatment, leave the structure with comparatively stronger sp^3 bonds [28], [70]. Often times a hybridization of sp^2 and sp^3 bonds are used to classify the molecular bond CNTs experience [71]. Sp^3 molecular bonds in MWCNTs increases intrawall bonding, buckling resistance, and load transfer, thus decreasing the chance of a sword and sheath fracture, but instead leads to planar fracture, which can handle more load, up to 45 GPa [28], [61]. From simple modifications, MWCNTs will have the same actual strength as SWCNTs, which was one of the main points to use SWCNTs, due to its theoretically preferred mechanical properties [61]. MWCNTs are favored in supercapacitor research as the cost to manufacture these are much lower than SWCNTs [61].

CARBON NANOTUBES – LATTICE CUTS

The three main lattice cuts that can be made on CNTs are zigzag, armchair and chiral [67]. These different cuts of the CNTs honeycomb tubular structure can be seen below in Figure 3 [1]. These cuts can be further detailed as zigzag has a cut of (n,0) meaning that x-axis can go 'n' steps along the graphene sheet [1], [72]. This means that each step in the lattice, or hexagonal honeycomb structure, is one, and many steps can be made for different outcomes [1]. Figure 3 is reprinted with permission from (L. L. Zhang, and X. S. Zhao. "Carbon-based Materials as Supercapacitor Electrodes." *Chemical Society Reviews*. 38.9 (2009): 2520-2531.). Copyright (2009). (Chemical Society Reviews).
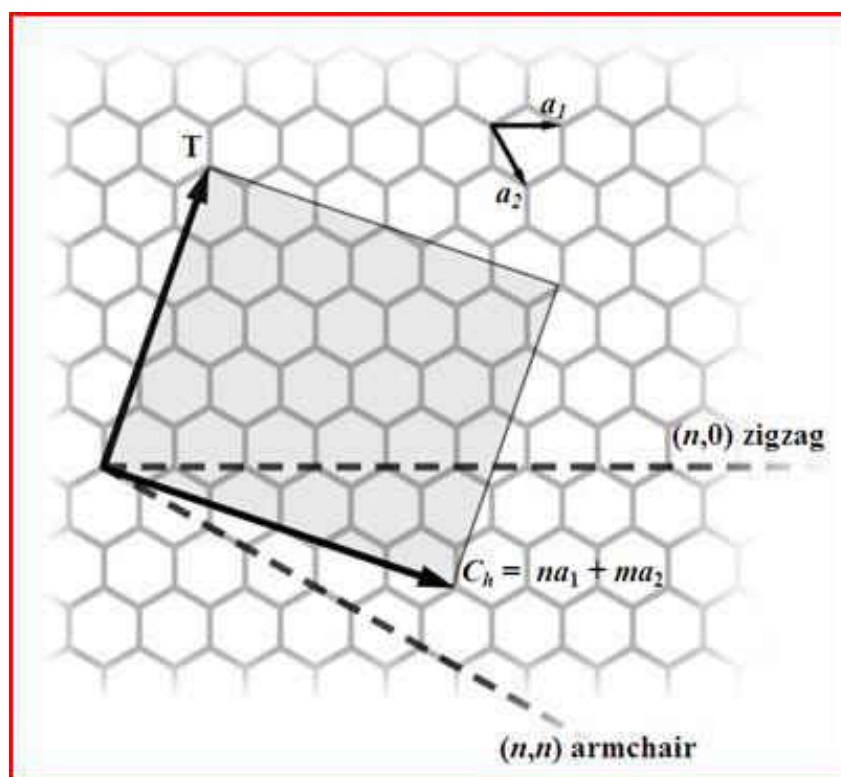
Figure 3: *Zigzag (n,0), armchair (n,n), and chiral, C_h (na_1+ma_2) cuts of CNTs [1] © 2009 Chemical Society Reviews*

The specific cut used can determine if the CNTs will be metallic or semiconducting [72]. The chiral cut can be simplified to (n,m) as a_1 and a_2 FROM Figure 3 are unit vectors [72]. The chiral cut leaves a semiconducting CNT, except when n - m is a multiple of 3, then a crossing of bands at the Fermi energy will make the CNTs have metallic properties [72]. In the same sense, the armchair cut (n,n) is always expected of being metallic, and zigzag being metallic only when n is a multiple of 3 [72]. However, studies have shown that zigzag cuts of (6,0) and (24,0) results in CNTs being metallic and other cuts of (9,0) (12,0), and (15,0) results in a semiconducting CNT [72]. The diameter of the CNT plays an important role in the energy bandgap in all cuts, with the highest reported bandgap being 0.66 eV for chiral cut (15,5) and 0.8 eV for a zigzag cut of (11,0) [72], [73]. The zigzag cut is favored over the chiral cut as the chiral cut has a large repeat period and the zigzag cut has been theoretically calculated to have a quasiparticle energy band gap of 1.89 eV with a (10,0) cut [73], [74]. The (10,0) zigzag cut has been also experimentally determined to exhibit a .8 eV band gap [75]. This is true because the diameters are very similar of the (11,0) and (10,0) cuts and neither is a multiple of 3, which would make the CNT metallic and have a much lower energy band gap [72]. The band gap relies not only on the diameter of the cut and the length of (n,m) points, but also the bonding of the molecular orbitals created from the cut [76], [77]. The band gap of CNTs is addressed further in the paper but it should be known that these properties make CNTs viable in many implementations, not just capacitors.

CARBON NANOTUBES – APPLICATIONS

Since their fundamental discovery, CNTs have been used in many applications including, but not limited to, biomedics, electronic circuits, batteries, solar cells, thermal detectors for lasers, and

supercapacitors [15] – [19], [42], [78] – [80]. CNTs are used in such applications due to their unique pore structure, narrow distribution size, highly accessible surface area, low electrical resistivity, electrocatalytic active sites for a variety of redox reactions, and high chemical stability [5], [37], [38]. Other reasons that CNTs garner supercapacitor research, and were used in this experiment, are their low cost, variety of medium forms, controllable porosity, and ease of processability [1]. In 1997 it was first suggested to use the CNTs in supercapacitors because of their properties of such adequate bandgaps with high conductivity, large charge sensitivity, and their flexibility [81].

CARBON NANOTUBES – CHARACTERISTCS

In the original study in 1997, certain characteristics demonstrated by the supercapacitor were a specific surface area of 430 m^2/g, a gravimetric specific capacitance of 102 F/g, and an energy density of 0.5 Wh/kg obtained at 1 Hz [81]. These values are discussed below.

Specific surface area is calculated by either determining gas absorption, or by using the Brunauer – Emmett– Teller (BET) isotherm [82]. Surface area is an important characteristic because the larger the surface area of the active material, the greater charge it can hold as such is the case with an ideal theoretical capacitor with 1000 m^2/g could result in a capacitance of 500 F/g [83]. This can allow for a larger capacitance without increasing the size of the electrode, as the energy and power densities will decrease due to the increase in the mass of the electrodes [55]. Although high surface area in carbon materials is typically a characteristic of a highly developed mesoporous structure, it can also be unfavorable for ion transfer through poor electrolyte wetting, typically demonstrated at high current loads [38]. In addition, capacitance also depends on pore size, size distribution,

and conductivity of the electrode [38]. However, combining a high surface area material with a polymer or oxide results in a high power density with stability by utilizing both double layer capacitance and faradic capacitance [38]. So, when combining carbon with a suitable material, an increase in power density is found.

Once specific area is known, the gravimetric specific capacitance can be found through the differential capacitance [84]. The differential capacitance is the incremental capacitance of the BET measured surface area by 1 cm^2 [84]. Following the assumption that the entire surface area measured from BET is accessible to ionic charge, then multiplying the BET surface area by the differential capacitance results in the gravimetric specific capacitance [84]. However, specific capacitance is typically measured by using cyclic voltammogram and through integration [23]. In this case, the specific capacitance is estimated by integrating the area under the current and voltage potential curve, and then dividing by the sweep rate, the mass of film electrode, and the voltage potential window as seen below in equation 9 [23], [85].

$$C_s = \frac{I}{mv_s(Va-Vc)} \int_{Va}^{Vc} I(V)d(V) \tag{9}$$

In this equation, the specific capacitance (C_s) is equal to the charge or discharge current (I) divided by the potential window (V_a-V_c) multiplied by the mass of one electrode (m) and the scan rate (v_s) [23]. This amount is then multiplied by the integral of the charge/discharge current with respect to voltage (I(V)d(V)) through the voltage potential window, or voltage at anode (V_a) to voltage at the cathode (V_c) [23]. Both charge and discharge calculations net the same results as no major distinct reactions occur on the anode or cathode [23]. Specific capacitance is a typical

measurement of a supercapacitors capabilities as farads are calculated while accounting for the size of the electrode, in grams [23], [86]. Once capacitance through cyclic voltammogram measurements is calculated, both energy density and power density, equations 6 and 7, can be calculated [6]. The ESR from equation 7 is found by combining all the resistance of the materials used in the supercapacitor and can also be easily measured with electrochemical impedance spectroscopy, (EIS) [87]. Although this method is typically used in capacitor measurements and calculated through machines, there is always a larger chance of error when more complex calculations are performed. The cyclic voltammogram tests usually output hysteresis graphs, which may lead to miscalculations as the graphs have an odd shape. If capacitance is known, as well as the mass of the active material, a much simpler approach can be taken to calculate the specific capacitance of a capacitor, and this method is shown below in equation 10 [86], [88], [89].

$$C_s = \frac{2C}{m} \tag{10}$$

In this equation, the specific capacitance (C_s) equals twice the measured capacitance (C) divided by the mass of the active material in one electrode (m) [86], [88], [89]. Although a multi-meter could be used for this equation, the results are much more reliable when capacitance is found through capacitance voltage, CV, measurements. Certain criteria are needed for this method to be applicable for calculations however. The supercapacitor must be symmetrical in structure and the weight of the active material must be known [86], [88], [89]. Also, the electrolyte used in the device is not part of the material when calculating the mass of the active material in the electrode, and the mass of the active layer is used for only the weight of one electrode [56], [86], [88], [89]. Energy and power density can both be calculated using this method also as capacitance

voltage measurements typically output such relevant data, in the same manner as from taking the integral of cyclic voltammogram measurement and resistance measurements from EIS [56], [86] – [90].

<div align="center">CARBON NANOTUBES – FABRICATION</div>

Since the first attempt at building a supercapacitor with CNTs, many procedures have remained the same, but with the materials being adjusting to manipulate certain properties [1], [6]. One such example is the pretreatment of CNTs in nitric acid, and using sulfuric acid as the electrolyte to functionalize the nanotubes through catalyst removal while maintaining reversible electron properties during high scan rates [6], [38]. This nitric acid pretreatment process was performed in 1997 and is still used in today's research [6], [38], [81]. Nitric acid treatment produces carboxylic groups, which contribute to the solubility of CNTs [91]. More than 24 hours of exposure to nitric acid was recommended to increase solubility and have the nanotubes align, although many of the smaller particles are lost during this extended acid bath [91]. The greatest benefit achieved with nitric acid treatment before fabricating the supercapacitor device comes from the nanotubes maintaining some catalyst residue while interacting with the functional groups, thus allowing faradic and non faradic processes to be involved in the supercapacitor [38]. It has also been found that nitric acid treatment allows for a greater quantity of quality current paths through mild doping of the CNTs, as well as reducing junction binds and resistance [92]. The use of sulfuric acid as an electrolyte is still used in research of CNT supercapacitors due to the H^+ ions being retained and mobile within the ionomer coating while allowing only electrons to move through the CNTs to the current collectors [23].

Since 1997, higher capacitance values have been reached by adjusting the methods of fabricating CNT supercapacitors beyond pretreatment [1], [6]. Some recent advancements have come from using an oxide composite in conjunction with CNTs, as this creates a stronger pseudocapacitance without losing any double layer capacitance [38]. One of the most commonly used oxides to produce a strong capacitance is ruthenium dioxide, RuO_2 [93] – [96]. Using RuO_2 with CNTs in a supercapacitor has yielded such specific capacitances as 174 F/g [93], 503 F/g [94], and 1652 F/g [96], with variations mainly attributed to the variety of materials and structures composing the supercapacitors. RuO_2 is popular for supercapacitors because of the ease of synthesizing, high capacitance, fast charge and discharge times, low ESR, and long cycle life [94], [96]. An increase in hydrophilicity occurs with combining RuO_2 and the ions have easier access to the electrode and electrolyte interface, which increases the faradic capacitance [38]. However, commercial applications are currently limited due to the low abundance and subsequent high cost of RuO_2 [96]. Other oxides typically used in conjunction with CNTs are manganese dioxide (MnO_2), nickel oxide (NiO_2), cobalt (III) oxide (Co_3O_4), and titanium dioxide (TiO_2) [95] – [97]. All of these materials will typically produce a higher capacitance as opposed to MWCNTs, but the fabrication process does require extra steps and extra fabrication costs [38]. Another type of material that can be mixed with CNTs to raise pseudocapacitance is that of conducting polymers [4], [38].

Conducting polymers combined with CNTs are popular not only because of the increase in capacitance as opposed to MWCNTs, but also because of their improved electrical conductivity and relative low costs [4]. The polymers have an open mesoporous network of nanotubes, which allow ions easy access into the electrode and electrolyte interface [38]. The most commonly used conducting polymers with CNTs are polyaniline (PANI), polypyrrole (PPy), and poly(3,4-

ethylenedioxythiophene) (PEDOT) [4], [38]. These materials have reached high capacitances similar to RuO$_2$, with experimental measurements netting specific capacitances of 775 F/g for PANI, 480 F/g for PPy, and 210 F/g for PEDOT [4]. When combined with MWCNTs, PANI has showed capacitance of 670 F/g when using 1 M sulfuric acid as an electrolyte [4]. However, these polymers typically have issues with depleting ions during charge and discharge cycles, as well as poor stability due to repeated intercalation [4]. There are many variations of CNT supercapacitor fabrication processes, however, some have high manufacturing costs. For this reason, basic and inexpensive CNT supercapacitor structures are studied experimentally for ease of commercial fabrication.

CARBON NANOTUBES – DISPERSION AND DEPOSITION

Dispersion of CNTs vary with experiments in regards to both the solvent used and the concentration of solid to liquid. Such solvents used are deionized water [18], [98], dimethylformamide (DMF) [17], N-methyl-2-pyrrolidone (NMP) [16], sulfuric acid and nitric acid mixture [15], acetone [99], ethanol [99], methanol [10], acetonitrile [10], dimethyl sulfoxide (DMSO) [10], tetrahydrofuran [10], toluene [10], dimethylacetamide (DMAc) [10], and chloroform [10]. Concentrations vary from .0001 to 50 mg of CNTs per milliliter of solvent [10]. The large difference in concentration values is attributed to the final fabrication of the dispersed solution in regards to the deposition method, along with the type of surfactant or polymer used [10]. Surfactants and polymers are both used for CNT dispersions by getting absorbed onto the CNTs surface, making the nanotubes soluble, but using polymers is not ideal as the polymer can participate in hindering electrical events [99]. When polymers cause electrical events, it can be harmful to not only maintaining standards of production, but can cause issues with the device

during fabrication steps, whereas surfactants can easily be washed away leaving a purer CNT surface [99]. Some surfactants used in CNT dispersion are sodium dodecyl benzenesulfonate (SDBS), dodecyltrimethylammonium bromide (DTAB), hexadecyltrimethylammonium bromide (CTAB), octyl phenol ethoxylate (Triton X-100), and sodium dodecyl sulfate (SDS) [99]. Surface modifiers are also used to functionalize mechanical, physicochemical, and irradiation properties of CNTs [10].

For deposition of CNTs, many methods are experimentally used including vacuum filtration [15] – [22], spray deposition [23], and domino pushing [24]. Domino pushing is a dry deposition method in which CNTs are aligned standing vertical on a silicon substrate before being pressed with a membrane [24]. The membrane is then peeled from the silicon and ethanol is passed through the membrane to remove the CNT buckypaper. Spray deposition involves using high pressure around 3 atm, or 44 psi, to deposit a well dispersed CNT solution [23]. The high pressure helps atomize the particles and compact them to form a CNT film, so this type of deposition is done on a specific surface that will collect the CNT deposits [23]. The typical vacuum filtration technique requires using pressure of about 1 atm, or 15 psi, to pull a well dispersed CNT solution through a Buchner funnel with a polyvinylidene fluoride (PVDF) membrane on top of the funnel, passing the solution into an Erlenmeyer flask and collecting a solid CNT film on top of the filter paper [21], [100], [101]. The solid CNT film can be dried and removed, resulting in a CNT buckypaper [18] – [98]. Further details of the spray deposition and vacuum filtration of CNTs procedure can be found in the experimental chapter of this paper.

BORON NITRIDE NANOTUBES

The final goal of the project is to make a supercapacitor, and if CNTs are the electrode layer, a suitable separator layer must be decided. Although some techniques use a nafion membrane, or another material for the separator layer, ideally boron nitride nanotubes (BNNTs) would be selected as the separator layer due to their availability and dielectric properties [23], [102]. Some of the results in the experimental section include nafion membranes as a control for research, as they are known to provide capacitance when paired with CNTs. Thus, for the separator layer, BNNTs will be introduced into the CNTs supercapacitor structure. BNNTs were only first put into theory in 1994 when researchers noted the similarities between the CNT tubular structure and those of boron nitride nanotubes [103]. One year later in 1995, BNNTs were experimentally discovered and could be physically characterized [104]. The molecular bonding and hexagonal geometry of BNNTs are very similar to that of CNTs [105], [106].

BORON NITRIDE NANOTUBES – LATTICE CUTS

In terms of structure, BNNTs and CNTs share similar bond lengths in a hexagonal lattice, such that they can be represented as a one dimensional allotrope through a two dimensional sheet, and are also both isoelectronic [105], [106]. Typically, when combining two separate layers of nanoparticles, these can be done in rod or disk like shapes [106]. When depositing one layer of nanoparticles in a mat form on top of another type of nanoparticle, the term Janus paper is used, named after the two faced Roman god Janus [102], [106]. Some methods for fabrication include electrochemical and photochemical reduction, templating of porous membranes and nanotubes, and surfactant-aided growth [106]. All BNNT sheets are semiconducting independent of the atomic tubular cut, whereas CNTs can be metallic or semiconducting depending of cut [72],

[106]. Because of the variety of properties that CNTs demonstrate based on the specific lattice cut, the functionality of these heterojunction structures can be adjusted by changing the tube length and the tube radius [106]. The highest occupied molecular orbital, and the lowest unoccupied molecular orbital, and thus the energy band gap, of these structures can be manipulated by adjusting the CNTs properties in such that the band gap is decreased when the CNT is of a zigzag structure but increased when an armchair structure is used [106]. Also, if zigzag is used, one end of the lattice will become more conductive due to anisotropy of orbital distribution [106]. BNNTs use the sp^2 bond from its molecular orbit, where MWCNTs use sp^3 to overcome weak van der Waal forces [28], [61], [105]. BNNTs share the same tubular structure and molecular hexagonal geometries as CNTs, so using both together in a structure such as boron carbonitride nanotubes, BCNNTs, is beneficial to the bond of the two materials as both utilize the sp^2 and sp^3 bonds [107], [108].

Similar to how CNTs demonstrate very close lattice characteristics to that of diamond and graphite, BNNTs share the relation to cubic phase-BN and hexagonal phase-BN respectively [109]. The cubic phase-BN is a sp^3 bonded phase where the hexagonal phase-BN is a sp^2 bonded phase [32]. Comparing CNTs and BNNTs specifically, the valence charges of CNTs are equally distributed around C atoms, indicating a strong covalent C-C bond network, but in BNNTs the bonding electrons are more concentrated around N atoms, with an asymmetric charge distribution [110]. Consequently, the electron delocalization on BNNTs is weaker than that on CNTs, but still sufficient to maintain planar sp^2 hybridization [110]. When combining BNNTs and CNTs atomically, the lattice arrangement shifts from C-C and B-N bonds, to C-B and C-N bonds [106], [111]. When combined together, the material is characterized as boron carbonitride nanotubes

(BCNNTs), and these share similar lattice parameters as CNTs and hexagonal BNNTs, so the electronic properties can be easily controlled by manipulating the B-C-N atomic bonds [112]. This lattice change leads to the rehybridization from sp^2 to sp^3 bonds at the newly formed B-C bond sites [110]. Despite this method producing a higher specific capacitance than most CNT supercapacitor measurements, contributed to the well aligned lattice structure and doping of boron and nitride in CNTs, this process typically requires chemical vapor deposition to create the BCNNTs so it will be difficult to replicate in most labs [112]. For this reason, CNTs and BNNTs will be studied as independent layers in the fabricated devices, and not through combining lattice structures. Although, many similarities exist between BNNTs and CNTs, it is the differences that make BNNTs ideal as the separator layer for supercapacitor structures.

BORON NITRIDE NANOTUBES - CHARACTERISTICS

Certain characteristics that differ in BNNTs as opposed to CNTs is that BNNTs exhibit a much wider bandgap of around 5.5 eV, partially ionic structure, greater thermal stability, high thermal conductivity, high mechanical strength, polarizability, high hydrophobicity, resistance to oxidation and heat, high hydrogen storage capacity, high radiation absorption, and high electrical insulation [102], [107], [108], [113]. These characteristics of BNNTs make them useable in many applications where CNTs would not perform as well [108]. The wide band gap is due to the electron density of boron, as the electrons are drawn to the nitrogen atoms because of the higher electronegativity in these areas, causing a partially ionic structure and a large gap between the conduction and valence bands [108]. As the CNTs cut and tube diameter played an impact on the band gap, BNNTs bandgap is practically independent of these characteristics and remains around 5.5 eV no matter how the nanotubes were cut and fabricated [114]. Thermal stability is seen in

BNNTs up to temperatures of 1000º C, where CNTs burn near 500º C, allowing for BNNTs to be used in more applications involving harsh conditions [108], [114].

BORON NITRIDE NANOTUBES - FABRICATION

Fabrication optimization of BNNTs is still being developed and is a major reason that BNNTs do not garner as much attention as CNTs, however, both can be made through arc-discharge, laser ablation, ball milling annealing, pyrolysis, arc-jet plasma, or chemical vapor deposition [107], [114]. These methods produce about 1 gram per hour of BNNTs and tend to produce nanotubes with large diameters, segmented or broken structures, and can introduce catalysts to the BNNTs [107], [115]. Some research has produced greater quality BNNTs using these methods, but by changing fabrication variables and consequently limiting production quantities [107].

However, recent advancements in fabrication techniques have produced BNNTs at a rate of 30 grams per hour using a hydrogen assisted BNNT synthesis (HABS) process, which fabricates BNNTs similar to the high temperature pressure (HTP) method [102], [107], [115]. The HTP method uses a laser to heat a Boron target and introduces nitrogen gas to cool the vapors and forms BNNTs at a rate of 20 milligrams per hour [115]. HABS is performed by using an induction thermal plasma reactor and introduces hydrogen and nitrogen gas into the reactor to allow for a unique thermal flow forming small boron droplets, which are the precursor to BNNTs [107]. After the droplets are formed, a nitrogen reaction stream allows for the droplets to form BNNTs using the root growth mechanism [107]. Both methods do not need a metal catalyst to produce the BNNTs, keeping the nanotubes as pure as possible [102]. The use of hydrogen gas is a necessity to produce the BNNTs, otherwise only a few nanotubes will form with the majority of the resultant

remaining as a boron powder [107]. Using such methods produce BNNTs ranging from a grey to white color in appearance, but also with impurities such as boron nanoparticles encapsulated in a BN shell, amorphous and crystalline BN bundled together, as well as BN nanoparticles which can degrade the characteristics of the BNNTs [102], [115]. So, after this process of fabrication, a raw BNNT material is left and requires purification to further enhance the BNNTs performance in applications [102], [115].

Purification, or cleaning, of raw BNNTs clumps is performed as the boron nitride currently produced for buying may not be an exact 1:1 ratio of Boron to Nitride and could contain many impurities [102], [115], [116]. Currently, three major types of purification are known to help remove unwanted impurities from raw BNNTs [115]. These methods are nitric acid treatment, thermal purification, and surfactant separation [115]. Cleaning with nitric acid will help remove unwanted excess boron nanoparticles and create a more stable 1:1 ratio of dispersed BNNTs, as boron is well known to oxidize in the presence of nitric acid to boric acid, which is water-soluble [115]. Nitric acid has been used previously with nanotubes, such as in CNTs to remove unwanted catalyst and to help functionalize the nanotubes for a higher pseudocapacitance [6], [38], [81]. Heat treatment is designed to remove B_2O_3, which forms during the heating process of fabricating the raw BNNTs [115]. Surfactant separation is implemented to influence interfacial tension allowing for the removal of impurities [115]. Out of these methods, nitric acid treatment is the preferred method for purifying BNNTs as this can be easily performed in a fume hood and is known to increase the surface area of the BNNTs [115].

The nitric acid purification treatment hollows out unstable cubic BNNT crystal structures [117]. The BNNT crystal structures have sharp edges as naturally produced, and pretreatment in nitric acid will allow for a hollow tubular shape of BNNT crystals [117]. Although acid treatment can penetrate and hollow BN shells, the BNNTs can be significantly damaged and alter the BNNTS sp^2 nature of the surface, which is true for performing ultrasonication as well [115]. Sonication of BNNTs has been shown to drastically shorten tube length, while chemical washing methods directly modify the surface structure [115]. Thus, other methods of purifying and dispersing of BNNTs are being sought through introducing solvents that require no ultrasonication time, however, currently all BNNTs dispersion techniques require some sonication [102], [115], [116], [118]. Fabricating and dispersing BNNTs without needed purification and sonication methods will further optimize the BNNTs properties as research suggests that BNNT mats produced after extended ultrasonication times or chemical purification have little or no structural integrity [115]. These ideas will be examined in the experimental section as BNNTs cleaned with nitric acid will be compared to BNNTs that have not undergone any acid treatment.

BORON NITRIDE NANOTUBES – DISPERSION AND DEPOSITION

Due to the raw BNNTs produced being a cotton like solid, dispersion methods are needed for deposition of the BNNTs [116], [118]. Early methods of dispersion recommended using deionized water with methoxy-poly (ethylene glycol) - 1,2-distearoyl-sn-glycero - 3-phosphoethanolamine-N conjugates (mPEG -DSPE) [118]. However, this solution requires an additional surfactant in mPEG that must be rinsed out after deposition to keep the BNNT resultant pure [118]. More recent studies of solutions have recommended dimethylacetamide (DMAc) as a solvent due to the uniform stable solution produced [116]. Other solvents recommended are N,N-

dimethylformamide (DMF) and acetone, and the use of cosolvents to be used are toluene and ethanol [116]. The recommended solvents generally result in a milky stable solution [116], [118]. However, as mentioned later in the experimental section, a milky dispersion free of solid particles is not necessary for deposition.

Deposition techniques for BNNTs are typically that of vacuum filtration to create BNNT mats [102], [107]. Vacuum filtration involves passing a dispersed solution through a polycarbonate track etch (PCTE) membrane placed on top of a Buchner funnel so that only a solid material is left, and thus creating a BNNT buckypaper [102], [107]. Previous research conducted has also suggested that successive filtering of CNTs and BNNTs has resulted in Janus buckypaper [102]. Specific procedures of BNNT deposition are discussed in further detail in the experimental chapter of this paper.

BNNTs with CNTs as supercapacitors have been very seldom mentioned in previous research. One paper draws its idea from a NASA project that was proposed in 2012, however the group seemingly has no updates since June of 2012, and the paper builds a capacitor, but does not mention any capacitance measured [102]. The researchers used vacuum filtration to build a CNT, BNNT, CNT heterojunction device with aluminum contacts using sandwich geometry, took pictures of the device with contacts, but recorded no measurements of any capacitance [102]. The group noted that there is dielectric constant of 3 with no leakage [102]. In the supplementary information the group did demonstrate that if the device is made through successive vacuum filtrations of CNTs, BNNTs, and then CNTs that the device would be conducting and could light an LED with a 9-volt battery [102]. When the structure was made by passing BNNTs through

CNTs layers and assembling the structure by pressing the two resultant filtrations together, that the structure would be insulating [102]. However, no mention, besides the dielectric constant, in regards to capacitance, was recorded during their study [102]. The dielectric constant can help find the capacitance, but only adds an additional constant to the numerator in equation 1 [119].

CHAPTER II

EXPERIMENTAL

The experimental portion of this paper addresses the process developed to create capacitors using carbon and boron nitride nanotubes. The solid nanotubes were dispersed into a liquid solution before being deposited into a device. After deposition, the layers of the final device are combined to fabricate the final capacitor product.

BNNT DISPERSION

The initial focus began on making boron nitride nanotube (BNNT) sheets, also known as mats, or buckypaper. First, dispersion of BNNT was developed to create a solution that is viable to create a BNNT film. Two solutions were prepared of BNNT in methanol, and deionized (DI) water using 5 milliliters of liquid for every 1 milligram of BNNT [118]. It was found that using 200 uM methoxy-poly (ethylene glycol)-1,2-distearoyl-sn- glycero-3-phosphoethanolamine-N, (mPEG-DSPE) as a surfactant is necessary in breaking up the BNNT material in a DI water solution because otherwise the BNNTs will not disperse [118]. MPEG was not used in the solution containing methanol to maintain the purity of the resultant mats. Mixing BNNTs with methanol leaves a cloudy, wispy material in the solution. When mixing BNNTs with DI water and mPEG, the solution became milky with very few solids remaining. After combining the mixture, 2 hours of ultrasonication time is recommended to disperse the BNNTs into the solution [102], [107], [118], [120]. However, the solutions took over 8 hours ultrasonication time to break down the chunks in the solution. This extended ultrasonication time is address later for optimizing the materials.

When not using mPEG in DI water, the solution will have BNNT clumps, flakes, and large particles that cannot be used for film as they cause defects through a non-uniform deposition, leaving holes and gaps through the film. To lower the production costs, mPEG-DSPE costs $160 per gram, and to maintain the BNNT mats purity, tests were performed with just DI water as the solvent, but found that methanol is preferred as the BNNTs are not completely dissolved in DI water. After dispersion techniques were realized, optimizing the dispersion process could ensue.

To begin optimizing dispersion, the methanol and BNNT solution was used to take transmission electron microscopic (TEM) images. To do this, a small liquid sample of the solution was dropped onto a copper grid and dried in an oven for a couple days. The images taken from the TEM can be seen on the following page in Figure 4. The scale bar in the lower left of each image is used to identify the zoom of the image of 0.5 um for the above image and 50 nm for the lower image.
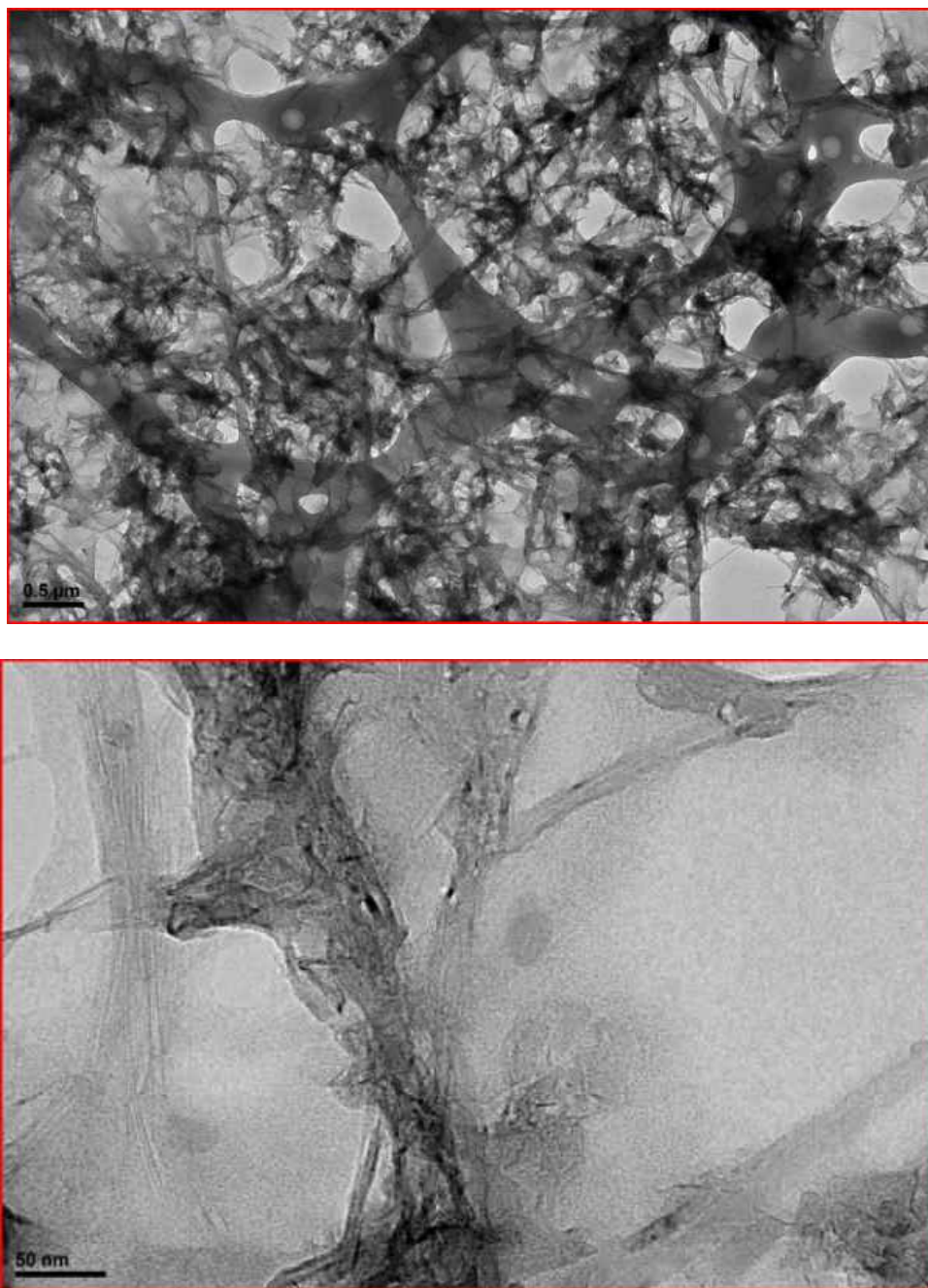
Figure 4: *TEM of BNNTs with methanol after 8 hour ultrasonication at 0.5 um scale bar (above) and 50 nm scale*

bar (below)

The image on the left shows a congregation of the nanotubes, but there is also a film present from where the BNNTs did not disassociate entirely. The image on the right, with 100 times more zoom than the left image, shows a cluster of BNNTs that did not break up well, are densely packed, and very damaged. Further image enhancement of the methanol and BNNT sample can be seen below in Figure 5 as the scale is zoomed in 100 times again to see the damaged wall structure of the BNNTs.
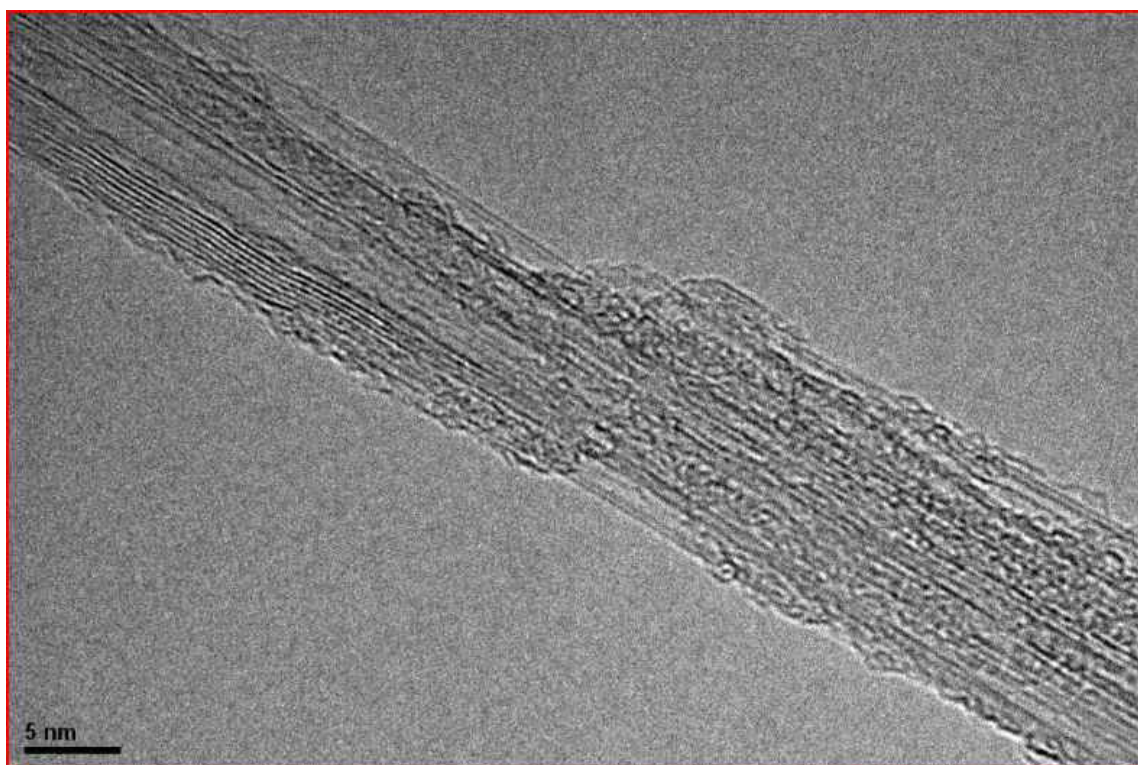
Figure 5: TEM image of BNNTs dispersed in methanol at a 5 nm scale bar

The BNNTs in Figure 5 are very damaged on the sides as parallel lines are expected for the walls. For comparison, TEM images from another research group shows boron nitride multi-walled nanotubes (MWNTs) with minimal defects, and can be seen on the next page in Figure 6 [107]. Comparing the images with previous research, it is clear that bundles are expected, but the bundles that were produced in this stage of the experiment showed many defects formed on the BNNT walls [107]. Figure 6 is reprinted with permission from (K. S. Kim, C. T. Kingston, A. Hrdina, M. B. Jakubinek, J. Guan, M. Plunkett, and B. Simard. "Hydrogen-Catalyzed, Pilot-Scale Production of Small-Diameter Boron Nitride Nanotubes and Their Macroscopic Assemblies." *ACS Nano* 8.6 (2014): 6211-220.) Copyright (2014). (ACS Nano).
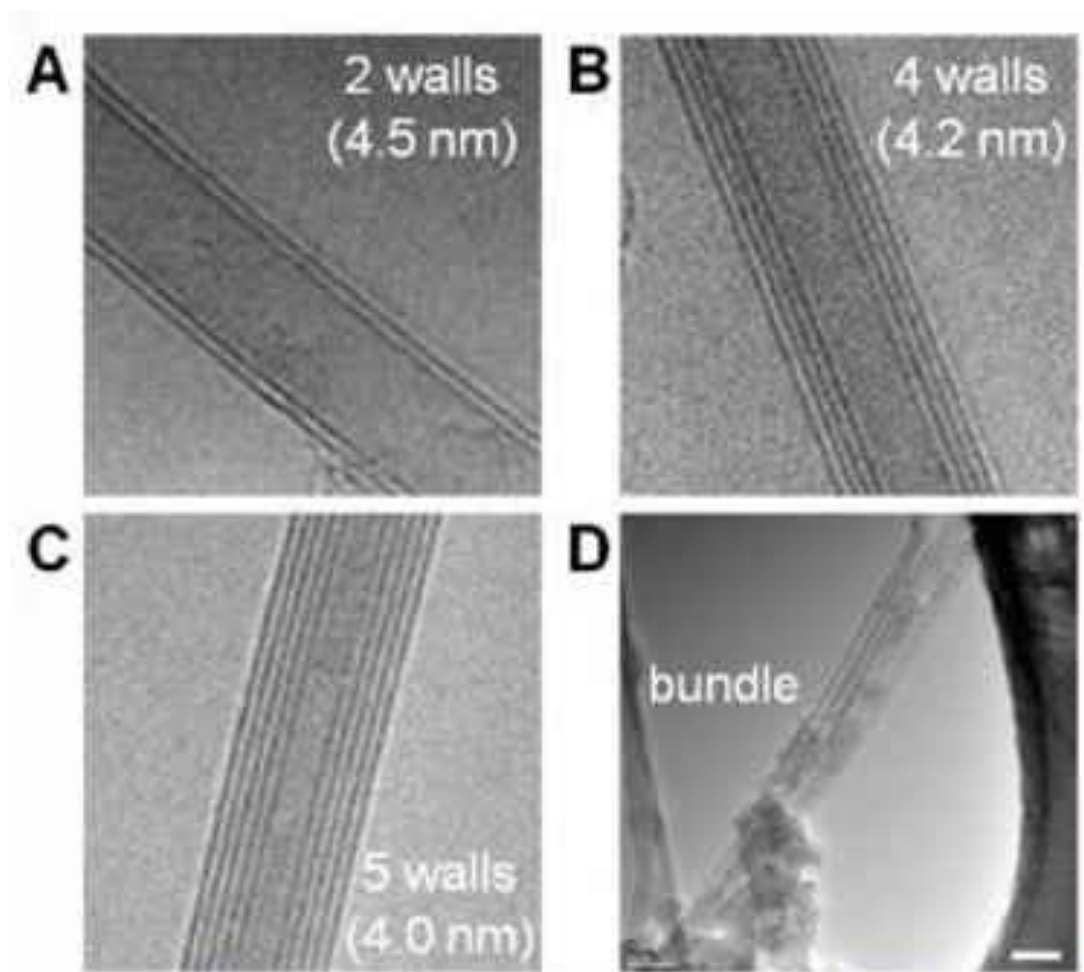
Figure 6: TEM images of various wall structures, diameters, and a bundle of BNNTs [107] © 2014. ACS Nano

The amount of wall numbers varies with how the BNNTs are processed. Similar to CNTs, BNNTs can form long cylindrical tubes when cut due to their pentagonal hexagonal atomic structure [8], [106]. Utilizing the ability to manipulate the structure, a variety of cuts and rolls of layers of the hollow tubes allow for further manipulation of the nanotubes [38], [106]. Each time the tubes are rolled, another wall is formed, hence the manipulation of single wall nanotubes (SWNTs) and MWNTs. The TEM image in Figure 5 shows 8 walls with an expected diameter of less than 10 nm [107]. However, it is clear that the produced walls had major defects. This is attributed to the

ultrasonication time of 8 hours, as opposed to the 2 hours done by other researchers [102], [107], [120]. It is believed that decreasing the sonication time will limit the amount of destruction imposed on the walls because the nanotubes exposure to heat and vibrations will be greatly reduced. After basic dispersion techniques were developed and optimized in further sections, a deposition process was created.

BNNT DEPOSITION

A vacuum filtration technique was implemented for BNNT deposition as vacuum filtration has been used in similar approaches for creating Carbon Nanotube (CNT) buckypaper [15] – [19], [22], as well as BNNT buckypaper [102] – [107]. Most conventional CNT vacuum filtrations are performed at 1 atm, or about 15 psi, but can produce depositions with 30-40 psi [21]. A vacuum filtration device was setup consisting of two Erlenmeyer flasks and a Buchner funnel in the lab, as shown on the following page in Figure 7.

Figure 7: *Vacuum filtration apparatus made for experiments*

The original setup created the vacuum by means of a high density polyethylene vacuum aspirator pump that was connected to a sink faucet and the flask on the left of Figure 7. There is a port on the aspirator that is perpendicular to the water flow that creates a pressure of around 11 psi through the Venturi effect. This flask connected to the pump is taped externally to help eliminate the chance of the glass imploding while under pressure. The taped flask connected to the pump also connects to a second Erlenmeyer flask, which holds the funnel for the solution to pass. The second flask uses a rubber stopper and a porcelain Buchner funnel in which a filter membrane is placed inside the funnel. The dispersed solution is then passed through the funnel under pressure to collect solid material from the solution onto the filter to produce a mat.

The filter paper used for the deposition of CNTs is a polyvinylidene fluoride, (PVDF) membrane, but for BNNT deposition, polycarbonate track etch (PCTE) membranes with 20 micron pores is used [100] – [102], [107], [120]. The PCTE filter is plastic like and allows more liquid to pass through than PVDF allowing for suitable BNNT deposits. An issue that immediately arose was that the PCTE filter has to be manually trimmed to match the funnel diameter as PCTE membranes with diameter of 42 mm, the size of the funnel, could not be found for purchase. Great care is taken in handling and trimming the edges to lower the membrane to the diameter of the filter. Trimming the filter is necessary, especially with PCTE, because solution will pass underneath any raised edge, causing BNNTs to pass through the funnel into the flask, undeposited.

Maintaining the 5:1 liquid solvent to BNNT ratio, 200 ml of methanol solution was ultrasonicated with 40 mg of BNNTs for 2 hours and then centrifuged for 1 hour at 3000 rpm [118]. Centrifuging is recommended to help dissipate the nanotubes and also to remove unwanted material. However, after only 2 hours of ultrasonication, many BNNT clumps still remained in the solution. Using a 5 ml : 1 mg, solutions typically took 4-6 hours of ultrasonication to become dispersed, mostly depending on the sizes of BNNT clumps initially started with, as the raw BNNT clumps varied greatly in sizes.

After depositing on the filter, previous researchers placed the BNNT mat, still adhering to the PCTE membrane, under 1.5 atm pressure sandwiched in between folded parchment paper before placing on a hotplate for 2 hours at 100° C to fully dry [102], [107], [120]. However, if not enough

pressure or BNNT material is used, the BNNT mat will stick to the parchment paper or flake off of the PCTE membrane, as seen below in Figure 8 [102], [107], [120].

Figure 8: Initial BNNT deposition on parchment paper (left) and PCTE membrane (right)

To remedy the poor depositions due to limited pressure, the vacuum pressure line from the faucet aspirator pump was disconnected and reconnected to a small vacuum pump with a pressure control knob and pressure gauge. This was done to not only speed up the vacuum filtration process time, but to help compact the nanotubes better. Having a more compact nanotube structure will allow for a more durable mat.

Attempting vacuum filtration with the vacuum pump attached yielded greater results and a buckypaper of BNNTs was formed. The time needed for drying the BNNT mat on the funnel was also reduced as the dry time dropped from 30 minutes to only a couple minutes. While under

pressure, the methanol passed through the membrane much faster. This allows for much less time for drying in the parchment paper, less excess methanol being evacuated in the parchment paper, and also a much easier final peel of the BNNT mat from the PCTE membrane. Figure 9 is shown below and includes images of the BNNT mat before and after drying in the parchment paper and on the hotplate.

Figure 9: BNNT mat before drying on parchment paper (left) and after drying on hotplate (right)

In a typical vacuum filtration process, wetting the membrane before applying pressure is essential in keeping the membrane in place on the funnel and minimizing the amount of solution that passes underneath. However, with PCTE membranes, because they are plastic like, adding any solution before starting the vacuum only displaces the membrane against the bottom of the funnel because the membrane will float on top of the solution. A remedy for this is to place the membrane on the funnel, then turn on the vacuum. Adding solution slowly at first will minimize the amount of solution passing through the funnel without depositing a solid material on the filter.

Applying pressure first will only minimize this problem because the vacuum will create small cones on the membrane over the funnels pores, thus raising the outer edges of the membrane. By using typical process pressure, around 30 psi, before adding solution, it was found that minimal solution will pass through, and also minimal time is wasted trying to adjust the pressure as solution is continuously added. An example of the edges slightly curling up is seen below in Figure 10 in which there is a visible small gap between the membrane edge and the deposited BNNTs. However, it was found that BNNTs will fill these gaps, stopping future solution to pass underneath, minimizing loss, and also gives room to remove the BNNT mat and membrane from the funnel with tweezers without damaging the deposited mat.

Figure 10: BNNT deposition in which edges of PCTE membrane curl under pressure

BNNT Optimization

A crude, but functional method found in previous research recommended shear mixing to the BNNT clumps prior to ultrasonication [102]. As seen in Figure 11 below, the raw BNNT material is large cotton like clumps.

Figure 11: *BNNTs initial raw state*

Prior attempts at dispersion required having to manually pull apart these chunks with tweezers to get the desired amount of material necessary to maintain a 5 ml to 1 mg ratio. However, it was soon found out that the areas that were pressed with tweezers took the longest time to disperse, usually greater than 10 hours, so much care is taken in not compacting the BNNTs when transporting the clumps. It is recommended to take a large clump and match the amount of liquid

used to maintain a concentration of 5:1. However, these large clumps continued to take much time in the ultrasonic to disperse, about 4 hours, where the desired goal was 2 hours. By using shear mixing, it was possible limit the amount of handling of the BNNTs while having to break up a large clump into much smaller parts, which also allowed for a shorter time in the ultrasonicator, and kept ultrasonication time to around 2 hours.

The first step with BNNTs was to disperse the nanotubes in various solvents. From a recommendation of a research company where the BNNT clumps are produced and purchased, toluene was recommended. Toluene does disperse BNNTs much faster than methanol, and does so with no need for any surfactant or stabilizer. The sample was left to sit for a couple hours after ultrasonication, and only needed a gentle mixing to move the nanotubes throughout the solution as the BNNTs will float near the bottom of a container after an extended time. This could be solved using mPEG to stabilize, but ideally production of pure BNNT mats is sought. Although rinsing the BNNT mat after filtration of the mPEG is possible, mPEG may not be completely removed, so for simplicity and accuracy, no stabilizer is used.

However, the purpose for the dispersion of the BNNTs is to create a BNNT mat. This is done by passing the dispersed solution through a filter membrane and peeling the membrane from the mat. The toluene solution suffers in this filtration method. The toluene reacts with the PCTE filter paper in a negative manner. When the solution is passed through under vacuum, the membrane curls around the edges. This was not experienced with a methanol solution. When the filter curls, the solution passes through the funnels newly exposed pores and the solid in the

solution will pass through to the Erlenmeyer Flask. With the edges curling, the filter membrane could not be reset as the membrane wants to collapse around the pores.

With this issue in mind, an alternative deposition method of spraying the BNNTs was tried. As toluene is commonly used as a paint thinner, the toluene BNNT solution may be ideal for spray deposition of BNNTs using a small paint spray gun. Some samples were made with spraying toluene in addition to CNTs and showed results, but very few samples were prepared because it was soon decided that toluene is not a viable option for deposition as it is a hazardous chemical. Some toluene was saved for TEM images to see how well the nanotube structures fared during the dispersion process, and the images can be found in the data and results chapter, but no toluene was used as a solvent for final device fabrication.

Another approach to optimize the dispersion was done by cleaning the BNNTs through a nitric acid treatment as the boron nitride currently being purchased is not a 1:1 ratio of boron to nitride and contains many impurities. As mentioned in the literature review section, nitric acid has been used previously with nanotubes, as with CNTs to remove unwanted catalyst and to help achieve a higher pseudocapacitance [6], [38], [81].

Similar reactions occur when cleaning the BNNT, as the nitric acid hollows out unstable cubic BNNT crystal structures [117]. The BNNT crystal structures have sharp edges from raw production, and pretreatment in nitric acid will clean the nanotubes to create hollow tubular shapes of BNNT crystals [117]. This will allow for the easier movement of molecules through the dielectric and can allow for an easier bond to CNTs on an atomic level as the BNNTs will have

less rigid defects repelling the CNT crystal lattice. Thus, the shared hexagonal lattices can combine much easier after the nitric acid treatment of BNNTs [105].

To complete the cleaning process, a BNNT clump is mixed with nitric acid in a 1 mg to 1 ml ratio. Typically, more than 50 mg of BNNTs is used so that the clump can be fully submerged in the nitric acid. The solution is heated to 120° C and is occasionally manually stirred with a glass rod to help the clump break up over time. As the solution is heated, the nitric acid goes from a clear liquid, to having a yellowish tint similar to vegetable oil, and then back to clear. This reaction can be seen below in Figure 12.
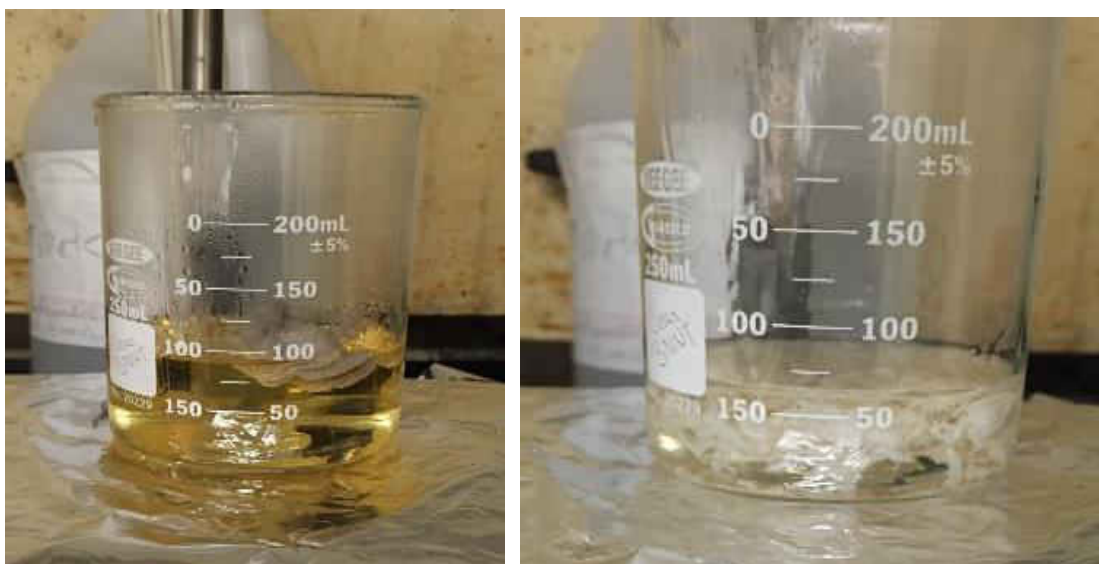
Figure 12: BNNTs and nitric acid solution changes from clear to yellow(left) and then back to clear(right)

This change in color occurs because the impurities are being removed from the BNNTs due to the heating of the nitric acid. These impurities then cook off from the acid. During this time, the BNNT clumps also begin changing from a beige color to a white color as seen in Figure 12. Once the solution reaches the desired temperature, the solution remains heated for 30 minutes to further clean the BNNTs and remove more nitric acid from the solution [117]. The resultant solution containing the broken down BNNTs along with a small amount of remaining nitric acid is rinsed with DI water [118]. This is done by adding DI water to the beaker to not only dilute to nitric acid, but also to allow the BNNT clumps to transfer containers easier for centrifuging. The liquid inside the beaker must be eventually changed from diluted nitric acid to ethanol before deposition.

To accomplish this, the newly cleaned BNNT clumps, nitric acid, and DI water solution is centrifuged. This is done by transferring the solution to smaller vials, capped with rubber stoppers, and centrifuging. Previous BNNT dispersion techniques recommend centrifuging at 3000 rpm for an hour to allow for the BNNT clumps to become untangled [118]. An hour centrifuge is not needed as a syphon of the liquid in the solution will be performed to replace nitric acid with ethanol. 3000 rpms is an ideal spin speed because it pushes the BNNT clumps to the bottom of the vials allowing for most of the liquid to be removed through a pipet. Not all of the liquid can removed as the BNNTs will begin to suction into the pipet, so six centrifuge cycles are needed to dilute the solution further, while limiting the amount of BNNTs that are wasted. Three centrifuge spins for 5 minutes are done exchanging DI water followed by three centrifuge spins for 5 minutes to change from DI water to ethanol. After this is performed, the BNNT and ethanol solution is close to a 1 ml to 1 mg ratio and can be further diluted with ethanol if the 5 ml to 1 mg ratio is needed.

After the final centrifuge, the solution then needs to be ultrasonicated. Following the typical 2 hour recommended sonication time to not damage the BNNT walls, the solution is ready for deposition [118]. Below in Figure 13 is an image of BNNTs that had nitric acid treatment next to BNNTs that did not have acid treatment.
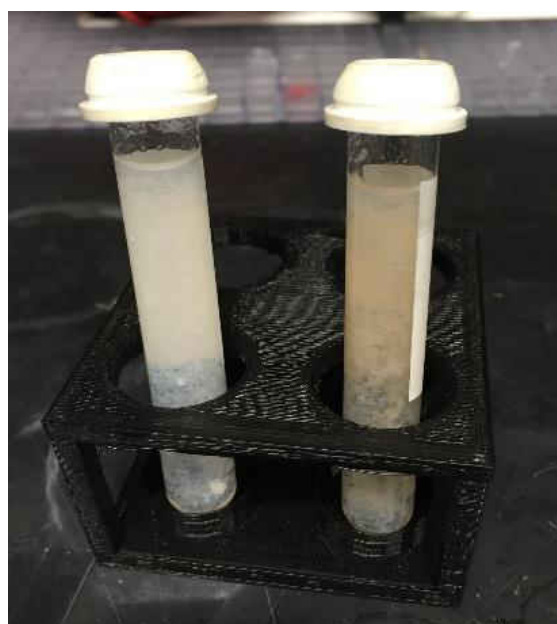
Figure 13: BNNTs that had nitric acid treatment, white, (left) and untreated BNNTs, beige. (right)

A new spray gun was used for depositing the BNNT and resulted in a clean BNNT film as seen on the next page in Figure 14. The smooth surface that was produced showed that the BNNTs that underwent the nitric acid wash could be deposited by spray uniformly with ease.

Figure 14: *Nitric acid treated BNNT spray deposition*

The BNNT solution was sprayed at 30 psi and used about 30 mg of cleaned and ultrasonicated BNNTs. The spray was performed in 3 to 5 second increments to allow time for the BNNTs to dry and adhere to the surface. The defect seen on the bottom of Figure 14 is where the tweezers were holding the sample, so the spray did leave a complete BNNT coated surface. This spray deposition method was used for creating a dielectric on certain fabricated devices, where further details can be found later in this chapter.

Attempts were made to produce a nitric acid cleaned BNNT mat, but had very little productive results. The same process was used to pass 40 mg of BNNTs through a Buchner funnel housing a PCTE membrane with 20 um pores at 30 psi vacuum pressure. The issue with vacuum filtration involving the acid treated BNNTs was that typically many clumps existed after a 2 hour ultrasonication time that were too small to physically remove from the solution, but too big to

allow for a smooth surface after deposition. As experienced previously, any chunks that deposit on the mat during vacuum filtration will cause holes and cracks in the mat upon drying.

When the acid treated BNNTs were ultrasonicated for close to 8 hours, many of the chunks disappeared, but the solution was so well dispersed, in regards to small BNNT particles, that the majority of the solution would pass under the PCTE membrane when exposed to pressure because the membrane lifts up around the outer pores of the Buchner funnel. Larger amounts of cleaned BNNTs, around 55 mg, suffered from the same results of a thin untreated mat, with cracks and holes. So a solution containing a larger amount of BNNTs that are dispersed with minimal chunks is necessary to produce acid treated BNNT mats. Much more attention and refinement is needed to produce acid treated BNNT mats when compared to untreated BNNT mats.

At this point, methanol, toluene, and ethanol have been used to disperse BNNTs. Cleaned and uncleaned BNNTs have been used in ethanol. All of these solutions required at least 2 hours of ultrasonication and shear mixing was used in all BNNT solutions. As mentioned in the literature review section, ultrasonication and acid treatment have been documented to shorten the tube length and modify the surface structure of the nanotubes, so minimizing ultrasonication and acid treatment is needed for optimization [115]. To counter this, a solution was prepared by mixing BNNTs in DMF, in which dispersion should require less than 15 minutes of ultrasonication time but needed to be stirred for four days through a magnetic stirrer [116]. This mixing process was done at room temperature at 950 rpms for 96 hours. However, after the stir time, large clumps of BNNTs still existed in the solution with not much of the solute dispersed, so shear mixing was implemented. A glass rod was used to further break up the BNNT clump by stirring the solution

for 30 seconds, and the solution was soon well dispersed. From all the BNNT solutions made, some were implemented in capacitor fabrication and but more were examined with TEM images.

CNT DISPERSION

For the solvent of CNTs, DI water was chosen over acidic solutions, as not only were the DI water dispersion methods mentioned from previous research more specific with greater detail, but also for the ease and safety of manufacturing the device without using harmful chemicals [18], [98]. An additional material, 1% wt. Triton-X 100, is needed as a surfactant [98]. Also, washing the CNT buckypaper with DI water and methanol after vacuum filtration is needed to rinse of the surfactant, so the BNNT solution containing methanol should not have any adverse effects to the CNT buckypaper when attempting to deposit BNNTs on top of CNTs using vacuum filtration. In regards to the concentration of CNTs in the solution, there is a variety of ratios used, typically ranging from 1:10 to 5:1 mg of CNTs to ml of solvent [15] – [18], [98]. The concentrations varied with the solvents used to disperse the CNTs, so a 1 mg of CNTs to 2 ml ratio of DI water was used. After an ultrasonication of the solution for 2 hours, the solution was ready for deposition [18], [98]. Other concentrations were tried of DMF and sulfuric acid as part of optimizing the dispersion and are discussed in greater detail further in this section.

CNT DEPOSITION

Initially, vacuum filtration was tried with CNTs and the filter paper used was PVDF with 0.4 um pores [98]. The recommended pore size of the membrane is typically from 0.2 um to 0.4 um for CNT deposition [15] – [18], [98]. Similar to the PCTE membranes, some trimming was required of the PVDF membrane so that it would fit in the funnel. Using a lower pressure than BNNT,

around 15 psi, the deposition seemed to settle the CNTs mostly around the pores [21]. After completing a deposition of a 100 ml DI water and 50 mg CNT solution, a CNT mat was left with obvious bubbling and cracking around the locations of the pores in the funnel, as seen below in Figure 15. In this image, the CNTs are still stuck to the PVDF filter.

Figure 15: CNT mat after vacuum filtration

Upon overnight drying under vacuum pressure at room temperature [18], [98], the pores were completely removed when transferring the membrane from a glass petri dish to a plastic sample holder. It was believed a thicker deposition and lower pressure was needed, but using more solution and maintaining a low pressure during vacuum filtration, between 5 and 10 psi, only produced similar results of the CNTs to pop off in small circles where it was once covering the pores, as seen on the next page in Figure 16. If the funnel did not have large pores, then more success from this method is expected.

Figure 16: *CNT mat after drying*

Because of the lack of results from vacuum filtration of CNTs due to the specific funnel used, the methodology of deposition was changed to that of a spray coating. For spray deposition, a ratio of 10 mg of CNTs to 1 ml DMF was used. This solution was then sprayed using an airbrush at around 30 psi through a syphon fed brush. However, the DMF deteriorated the plastic and rubber compound house that drew the solution from a bottle to pass through the gun. Later, a gravity fed airbrush with all metal parts was tried, but suffered similar from lack of a crack free deposition, as this type of spray gun could use no more than 15 psi.

When depositing CNTs, more reliable results came from the higher pressure spray as more solution is being continuously passed through the airbrush gun and a greater force is introduced to compact the CNTs onto the spray surface. Another type of spray gun was used that had all metal parts and was syphon fed, allowing a higher constant pressure that can be maintained when depositing CNTs. This allowed CNTs to be directly deposited on the produced BNNT mats as seen on the following page in Figure 17.
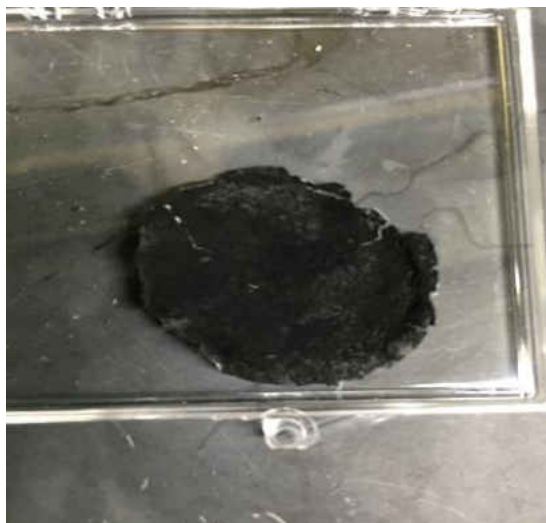
Figure 17: *BNNT mat sprayed with CNTs and DMF*

This CNT deposition seen in Figure 17 was done on a hotplate covered in foil at 70º C, spraying in 5 second intervals, letting the mat dry over the course of three coats. Once one side was dry, the BNNT and CNT mat would be flipped over so that CNTs could be deposited on both sides. The measured capacitance was much lower than expected and it is believed that a thicker CNT deposition, applying an electrolyte, along with better structured BNNTs achieved through cleaning with nitric acid and centrifuge, will increase the capacitance.

It was also tried to spray the CNTs directly on foil. This would allow for BNNT to be spray deposited on top of the CNT deposition which could then be folded in half to double the BNNT thickness and to allow for two separate CNT layers. However, the CNT deposition left many holes and gaps when depositing on foil. If the first CNT layer was not completely covering the foil, BNNT would contact the foil and lead to the device shortage. This leads to instability during measurements because the CNTs do not adhere well to the aluminum foil, and the only research

involving CNT deposition on aluminum foil involved rolling the foil after deposition [121]. Although rolling the foil is simple in the approach, concerns over possible cracks of CNTs as well as introducing BNNTs into this method was questionable. A final deposition method of CNTs was then implemented.

This method involved using a nafion membrane 70 um thick and depositing CNTs mixed with H_2SO_4 on the membrane [23]. The sulfuric acid in the solution acts as the electrolyte to alleviate the need for a gel electrolyte to keep the device from leaking, as well as maintain a standard for fabrication as an electrolyte gel is difficult to control the exact amount being deposited [23]. The nafion sheets available were either 50 um thick, or more than 100 um, so the 50 um film was used, which opened the opportunity to deposit a small amount of BNNTs on the nafion, around 20 um, to achieve similar physical characteristics of the ideal separator layer thickness [23].

The nafion sheet was cut using a razor blade to produce small squares around 5 mm^2. The membranes were then put in a 1 M sulfuric acid bath for 30 minutes at 60º C [23]. The membranes were soaked in acid to promote ion transportation in the separator layer [23]. The CNT solution is mixed with a 2 mg of CNT per 1 ml of .5 M H_2SO_4 with 1% wt. sodium dodecylbenzenesulfonate (SDBS) added as a surfactant [23]. This solution was then ultrasonicated for 15 minutes before the solution was sprayed at 40 psi onto the cut nafion membranes resting on a hotplate at 100º C [23]. The solution was passed through an all metal syphon fed container. Quality metal is needed for the spray gun as corrosion will become apparent after only a couple uses. Foil contacts are then pressed against the electrodes to complete the device [23]. The CNTs did not adhere well to the membrane as seen on the next page in Figure 18.
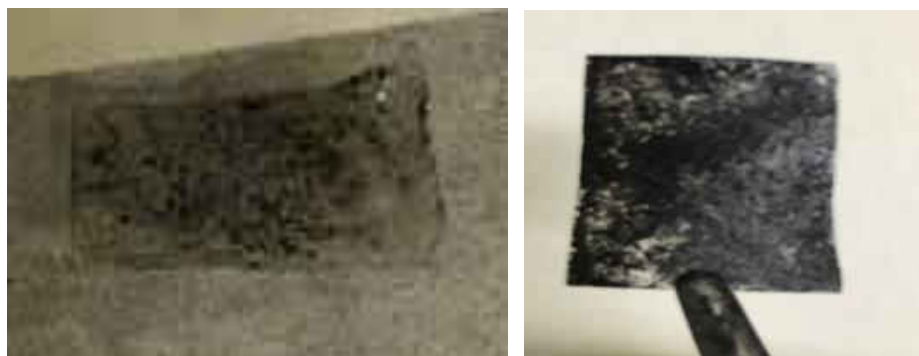
Figure 18: *CNT H₂SO₄ solution on nafion membrane after one spray coat (left) and 3 spray coats (right)*

Even after a longer ultrasonication time and more surfactant added, the nafion membrane took many coats to get a decent CNT deposition accomplished. It is clear the even after three coats, with each coat being 5-10 ml of solution and 10-20 mg of CNT, sprayed on each side of the nafion membrane per coat, the membrane still has gaps of CNT deposition, in which shorts will exist due to the resistive nature of nafion.

The acid solution is required for depositing of CNTs on nafion because using CNTs in a DMF solution caused the nafion membrane to deform when depositing. The DMF caused the nafion to constantly curl up and wrinkle, similar to the PCTE membrane when exposed to toluene. Although the applied heat of 100° C through a hotplate allowed the nafion to slightly reform to its original position, the DMF solution made deposits very difficult due to the sides of the nafion collapsing and leaving a non-smooth surface.

Another issue from the nafion capacitor was pressing the foil contacts onto the electrodes. Even through heating the device with contacts in place for 30 minutes at 100° C under pressure, the foil current collectors would not stick. An electrolyte made of phosphoric acid was made to hold the device together.

ELECTROLYTE FABRICATION

An electrolyte consisting of 50 ml DI water mixed with 5 grams of PVDA and 4.5 ml of phosphoric acid was applied to both sides of the membrane to utilize ion movement and to hold the foil contacts to the membrane [122]. The electrolyte was prepared by following a common technique to prepare the polymer electrolyte by mixing the water and PVDA under 90° C for 2 hours while stirring at 300 rpms [122]. The phosphoric acid was then added to the solution and mixed overnight to create a gel electrolyte [122]. The electrolyte was used in the fabrication of many devices.

DEVICE FABRICATION

The procedures for the individual devices used for final capacitance measurements follow previously mentioned experimental methods and each device's fabrication procedure is further explained below.

The most recent device fabricated, which demonstrated the greatest ideal characteristics for a CNT and BNNT capacitor, was made from aluminum foil, BNNTs, and CNTs. The CNTs were initially cleaned with acid themselves and were acquired after the nanotubes were pretreated with acid. The cleaning of the CNTs allowed for the nanotubes to adhere much better to foil. The CNT and

foil device was weighed before and after the CNT deposition. After this, the electrolyte from PVDA and phosphoric acid was applied to the device before spraying with acid treated BNNTs. This was performed on two separate small pieces which were then manually pressed together to result in a sandwich geometry of aluminum foil, CNTs, electrolyte, and BNNTs on each side. This device is referred to as acid cleaned CNTs with BNNTs.

A PVDF membrane with a 47 mm diameter and 0.45 um pore size was sprayed with a solution of CNTs mixed with .5 M H_2SO_4 using a 2:1 mg per ml concentration and 1% wt. SDBS. H_2SO_4 was used because DMF is not a good solute spray for PVDF as the membrane will begin to deteriorate during sprays. Both sides were sprayed and the membrane was left to air dry as heat also negatively affected the membrane. The fully dried membrane was then weighed on a scale to find the mass of the electrode by comparing it to the membrane before spray. An electrolyte was applied to both sides of the PVDF membrane to allow aluminum contacts to stick.

Similar to the PVDF approach, Whatman student grade filter paper was sprayed with CNTs in DMF with a ratio of 10 mg of CNTs per 1 ml of DMF. The filter paper was cut into a small square for measurements and was then sprayed with CNTs on both sides, allowing the paper dry to over a hotplate set to 60^0 C. The filter paper in this case acts as the dielectric. It is possible, although difficult, to deposit BNNTs also, as both the filter paper and nanotubes are of a white color. Only CNTs were applied in this instance. The electrolyte and foil contacts were then applied.

A nafion capacitor was made following a research paper strictly, but the nafion took about 3 coats to produce a viable product to measure. The H_2SO_4 solution mentioned earlier was used and

sprayed on a nafion membrane at 100° C at 44 psi after soaking the membrane in 1 M H_2SO_4 for 30 minutes at 60° C to rinse the membrane [23]. After the third coat of spray, typically, some parts would be well coated with CNT, but not as uniform as the research paper produced [23]. This caused instability. After drying, the membrane was weighed in comparison to the membrane before the spray to get the weight of the electrodes. The aluminum contacts would not adhere after gentle pressing, or after heating at 100° C for 30 minutes under pressure, so a polymer electrolyte was applied to both sides to allow for the aluminum contacts to stay in place on the final structure.

Due to the lack of success dripping CNTs on office paper, it was decided to try to spray CNTs on office paper. This resulted in a good CNT deposition in regards to uniformity as seen below in Figure 19. The paper was sprayed with the DMF solution using the same previously mentioned concentration on a hotplate at 60^{0} C. The paper was trimmed and weighed after spraying to determine the weight of the electrode before applying the electrolyte and aluminum contacts.
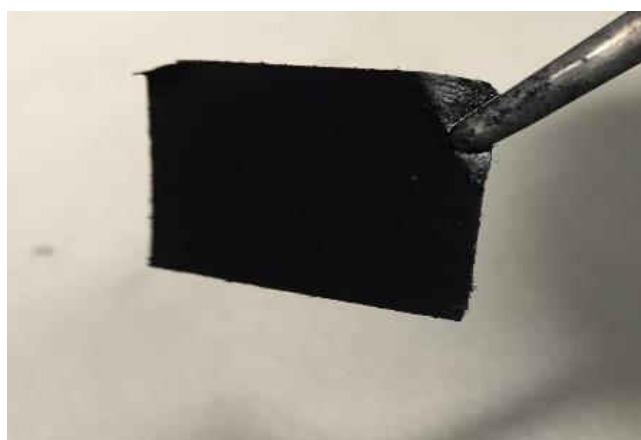
Figure 19: CNT sprayed on office paper with one side coated with BNNTs

A comparison was desired to compare the characteristics of BNNTs in nitric acid and BNNTs without acid treatment, both samples were fabricated under similar conditions. Both devices used a concentration of 5 ml of ethanol to 1 mg of BNNTs and were ultrasonicated for 4 hours. 10 ml of solution was sprayed at 25 psi onto each side of the office paper at 60^0 C on a hotplate. Although a variance in over spray could attribute to small differences, the final weight of both papers was nearly identical when cut to 5 x 5 mm samples. The papers, which were printed black to show the BNNT deposition, can be seen below in Figure 20. CNTs with DMF were then sprayed over a hotplate at 60^0 C with a similar technique of maintaining constant spray amounts. The untreated BNNTs did adhere better to the paper visibly, perhaps due to its beige color. The treated BNNTs did have a layer present, but it appears much lighter on the dried result. Both papers were weighed and then coated with the polymer electrolyte and aluminum contacts were used.
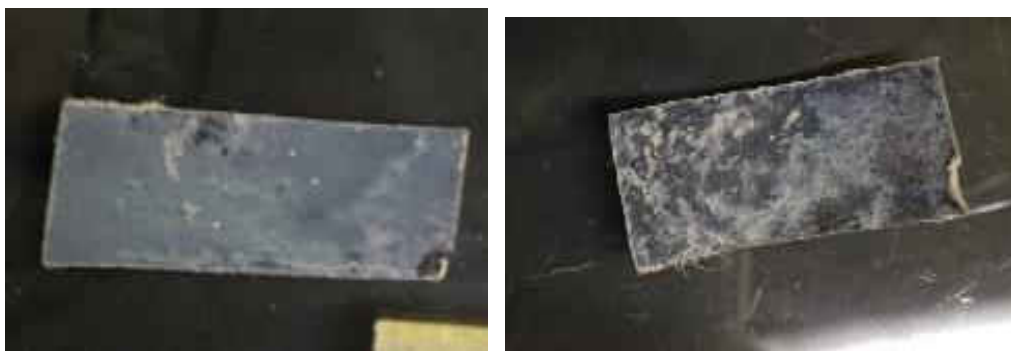
Figure 20: Untreated BNNT paper (left) and nitric acid treated BNNT paper (right)

Similar to the BNNT spray on office paper, BNNTs that underwent nitric acid treatment and BNNTs that did not, were sprayed on nafion in the same ethanol solution mentioned earlier with 5 ml being sprayed on both sides but at 100° C and 35 psi. Similarly, the untreated BNNTs adhered more so to the separator layer on the nafion membrane. Although neither left a complete covering of the nafion, a layer of BNNTs was produced and because nafion and BNNTs would act as the separator, this was left at 5 ml sprayed per each side. Both membranes were weighed after the BNNT spray and showed similar deposited mass and can be seen below in Figure 21. These measurement steps were also done for the CNT and H_2SO_4 solution spray to see how much CNTs were deposited. Both devices followed the same fabrication procedures of the nafion device previously mentioned, and were coated with electrolyte and pressed against aluminum contacts to complete the device.

Figure 21: Untreated BNNTs on nafion (left) and acid treated BNNTs on nafion (right)

Lastly, produced BNNT mats were coated with the polymer electrolyte on both sides and allowed to dry for 1 week, weighed, sprayed with the CNT and DMF solution, and weighed again. Both

the clean and the untreated mats were used for this, although the cleaned BNNT mats have a tendency to produce very thin mats. Because mats are not smooth, but have bumps and waves from vacuum filtration, the aluminum contacts were gently placed and later pressed by pins while taking CV measurements. These two devices are the only devices in which CNTs were sprayed on the electrolyte, although the electrolyte was solid after drying at room temperature for a week. The CNTs could not be sprayed onto a wet electrolyte as the CNTs would run off and not adhere. Below in Figure 22 is an image of a BNNT mat coated with the electrolyte gel as it was hanging to dry during a week's time.
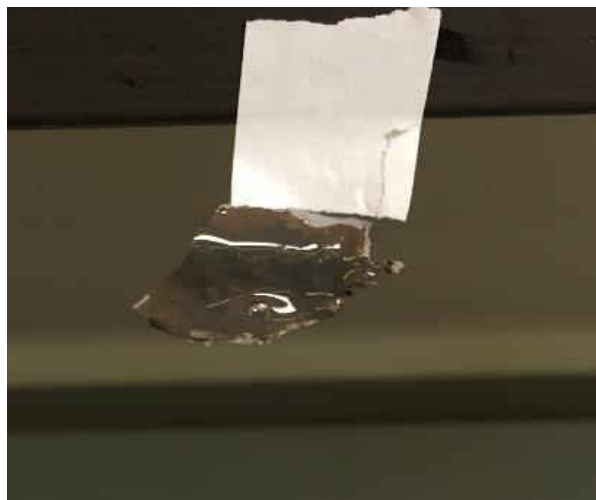
Figure 22: BNNT mat coated with electrolyte gel

Each device, besides the BNNT mats, were trimmed to roughly 5 mm^2 size capacitors. This was done to not only minimize the size of each sample but to give more consistency in the measurements to be taken.

CAPACITANCE CHARACTERISTIC MEASUREMENTS

All the devices were made with a top and bottom of foil pressed against an electrolyte except for the BNNT mats. The design of the machine to be used for capacitance measurements, the Agilent B1500A, uses push pins on a horizontal surface for contacts. Due to this, a small strip of foil was used for a bottom contact for the samples during measurements. A pin was pressed against this strip of foil, and the other pin of the Agilent B1500A was pressed against the top foil contact to hold the device in place and to be sure proper pressure was being applied for the measurement. When BNNT mats were used, two foil strips were used under the same measurement process.

The devices used to measure the fabricated capacitors are an Agilent B1500A to measure capacitance characteristics, and a TEM for enhanced images of solutions. The results section will begin with the measurements found by the Agilent B1500A in which capacitance voltage measurements were taken. This is followed by the TEM microscopic images of BNNT dispersed solutions.

CHAPTER III

DATA AND RESULTS – CALCULATIONS

To begin this section, the procedure and accuracy of measurements is addressed first, and the second part of this chapter will define the measured data and its relation to capacitor efficiency. The data acquired is from an Agilent B1500A, which measures parallel capacitance, conductance, dissipation factor, parallel resistance, series capacitance, reactance, series resistance, impedance, and phase during CV measurements. From this measured data, ESR, stored energy, energy density, max power, power density, and specific capacitance can all be found. Using a machine that can do capacitance voltage measurements differ from taking cyclic voltammogram measurements in that the data is directly found and no math or estimation is required [23], [86], [88], [89].

The first point of measurement discussed is typically taken from cyclic voltammogram measurements, which produce hysteresis plots, is that of specific capacitance. Specific capacitance is the measured capacitance with respect to the mass of one electrode [86], [88], [89]. To refresh the reader on specific equations being implemented in this section, equation 9 is reintroduced.

$$C_s = \frac{I}{mv_s(Va-Vc)}\int_{Va}^{Vc} I(V)d(V) \tag{9}$$

In this equation the specific capacitance (C_s) is equal to the charge or discharge current (I) divided by the potential window (V_a-V_c) multiplied by the mass of one electrode (m) and the scan rate (v_s) [23]. This amount is then multiplied by the integral of the charge/discharge current with respect

to voltage (I(V)d(V)) through the voltage potential window, or voltage at anode (V_a) to voltage at the cathode (V_c) [23]. Both charge and discharge calculations net the same results as no major distinct reactions occur on the anode or cathode [23]. The method for calculating equation 9 is used for cyclic voltammogram measurements in which a hysteresis graph is produced as a relation of current to voltage. The area is calculated inside this graph through integration and used to calculate specific capacitance. Although data is typically measured by machines, which gives an output in spreadsheets, minimizing the chance for mathematical error, simplified calculations limit the risk of error. Such a method is found in equation 10, if the capacitance is known, such as the output from capacitance voltage tests, although specific criteria must be met for this equation to become applicable [86], [88], [89].

$$C_s = \frac{2C}{m} \qquad (10)$$

In this equation, the specific capacitance (C_s) equals twice the measured capacitance (C) divided by the mass of the active material in one electrode (m) [86], [88], [89]. The certain criteria needed for this method to be used for calculations are that the supercapacitor must be symmetrical in structure and the weight of the active material must be known [86], [88], [89]. Also, the electrolyte is not part of the calculation of the mass of the active material in the electrode, so mass calculations must be performed without the electrolyte [56]. The mass of the active layer is used for only the weight of one electrode [86], [88], [89].

Other calculations found in this data section are that of energy and power density from equations 7 and 8 found in the literature review section, and are pictured below for convenience. Equation

7 is energy density, in which capacitance (C) is multiplied by voltage (V) squared and divided by 2 times the mass (M) of both electrodes, with typical units of Wh/kg [55]. Equation 8 is power density, which is calculated by squaring the voltage (V), and dividing by 4 times the ESR times the mass (M) of the two electrodes as seen below [55]. The units are typically kW/kg [6], [56]. Both energy and power density equations are taken from the stored energy and max power equations, but have the additional term of M to account for the mass of both electrodes.

$$E = \frac{CV^2}{2M} = \frac{QV}{2M} \tag{7}$$

$$P = \frac{V^2}{4ESRM} \tag{8}$$

ACCURACY

The accuracy of the experimental data measured by comparing it to capacitance voltage measurements from previous research will be discussed. All found data match the same shape of the results of the capacitance voltage measurements [123] – [129]. Although most measurements produced smooth graphs, some graphs had sharp peaks found from instability of the device, which fabrication techniques were then improved upon.

Noise was measured with no device present, but only using contacts and was found to be less than 2 nanofarads in capacitance. If adding a device, the noise may be slightly higher, but is expected to be minimal, as the measured capacitances are in the micro or millifarad range. Otherwise, any output peaks are from instability of the device. The instability arises from CNT depositions leaving a non uniform homogeneous surface. Once CNT deposited methods were improved for all techniques, the measured output graphs will begin to smooth out.

On the next page, in Figure 23, is the most concise image available comparing carbon material and measured capacitors through capacitance voltage measurements. The top image is from other research taken with permission, while the bottom image is taken from the Agilent B1500A measuring device. Both sets of data start at a lower point of capacitance measured on the y-axis and slowly increase before a plateau only to later lose capacitance just after 0 applied volts [128]. The data continues to lose capacitance, it is only more visible with the graph below, as the image above was taken from a range of -2 V to 2 V, whereas the B1500A has a max range of -5 V to 5 V [128]. The variance of lines in the top image is due to the measurements being taken at different frequencies. The top image in Figure 23 is reprinted with permission from (M. Atif, W. Farooq, A. Fatehmulla, M. Aslam, and S. Ali. "Photovoltaic and Impedance Spectroscopy Study of Screen-Printed TiO2 Based CdS Quantum Dot Sensitized Solar Cells." *Materials* 8.1 (2015): 355-67.). Copyright (2015). (Materials).
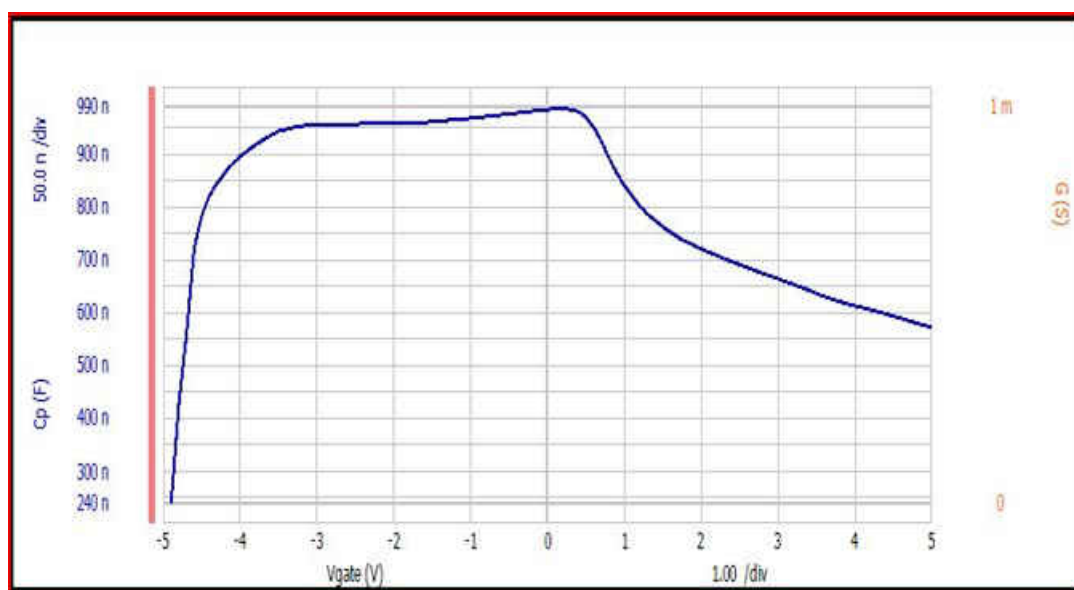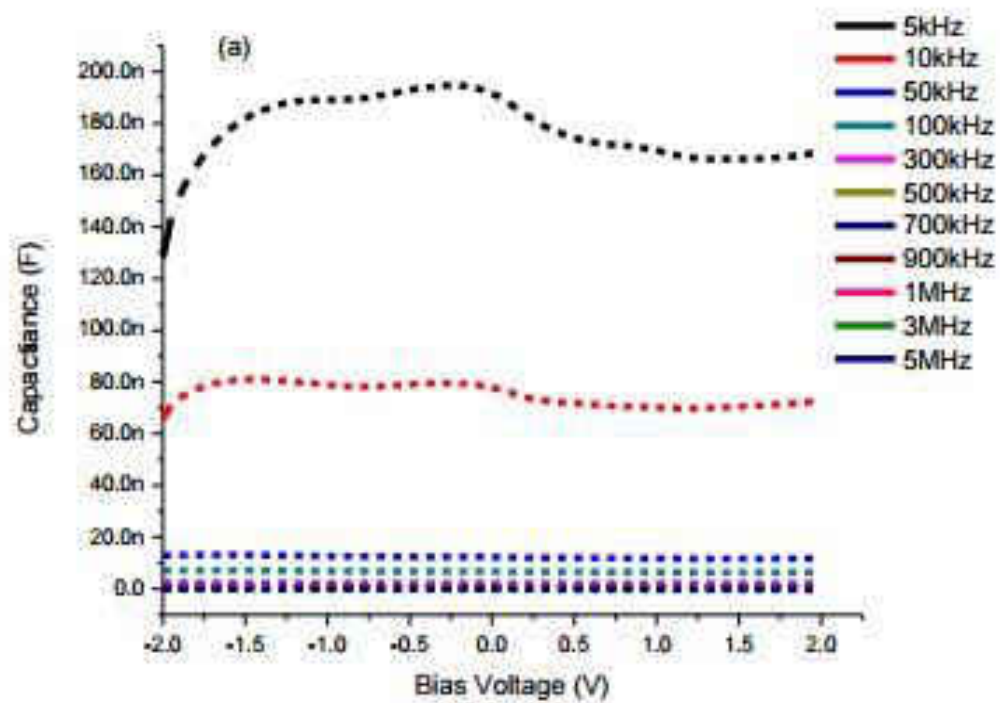
Figure 23: *CV measurements from a research journal [128]© 2015. Materials (above), CV measurements from*

Agilent B1500A (below)

The only major difference in the two images is the measured data appears to drop more after 2 volts, so more images that had a further range in voltage were used in comparison, and it was found that all capacitance voltage data has a sharp drop on the positive voltage side, usually between 3 and 5 volts [123] – [129]. The sharper drop seen on the bottom image is due to a smaller sampling range, and also due to a faster scan rate, explained further below. All of the data found from capacitance voltage measurements in research articles correlates to the measured capacitance voltage data on the Agilent B1500A [123] – [129]. However, operating frequency plays a major role in measured capacitance, as seen in the top image of Figure 23, in which the lesser frequency had the greatest measured capacitance, is explained further in this section. An explanation of the output graph is given below.

The initial increase in capacitance, as seen previously in Figure 23, is due to the charge of the carriers. Capacitance equals charge divided by voltage, so as operating voltage is cycled, the charge plays a major role in capacitance. As the applied voltage decreases from -5 V to 0 V, a constant charge would see an increase in capacitance. This is why the capacitance voltage graphs have a constant increase in the left half of the graph. The initial increase is due to the capacitor becoming charged through the applied voltage. When there is no voltage passing through the capacitor, it is in the discharged state with little ion movement and interaction. Once the capacitance voltage measurement begins, voltage is applied and the charges move to their corresponding electrodes, such as the negative electrode attracting positive ions. This is a fast process of charging the capacitor, but not instantaneous. In addition, because of the ions moving to the oppositely charged conductor, an electric field will form internally due to charge separation. The dielectric separator allows ions to pass through so that they can move to the

cathode and anode of the device. Once the charges are collected to their respective sides, the system will stay relatively neutral in regards to charge as the majority of the ions have been pushed to specific sides.

The decrease seen in the capacitance voltage graphs after 0 V is due to the saturation of the electrode surface. An explanation of the decay is that the electrode active surface is completely covered by ions at a voltage lower than the electrolyte decomposition point. If this is the case, further increasing voltage beyond the voltage value associated with full surface coverage should not make the remaining ions move to the electrode surface, as it is covered by ions, resulting in no capacitive current. This indicates that almost all the cations that can be held on the electrode surface are electrosorbed between 0 and typically around 2 V. Thus, the decay of capacitive current at a voltage lower than the average 2 V can really be associated with the complete coverage of the electrode surface accessible to the desolvated cations.

This phenomenon also explains why the slower scan rate resulted in less decay and why there is no abrupt decay at saturation. This is due to the ion distortion, which permits the cations to enter pores smaller than their "rigid" size, or by an increase in the size of pores due to their deformation. At a slower regime, the distortion/intercalation effect permits the use of pores close in size to desolvated cations. There are also compressional effects such as electrostriction that increase molecular density which decrease the capacitance. Consequently, this saturation phenomenon makes it impossible to profit from higher voltage, which limits the energy and power density [130]. Frequency also plays a major role in measured capacitance.

When the frequency is increased, the capacitance shows a decreasing behavior towards zero and can even go to negative capacitance at frequencies higher than 1 MHz [128]. This trend from positive to negative capacitance, also called inductive behavior, is very common in several materials, which means the current lags behind the voltage [128]. Using 1 kHz instead of 1 MHz results in a greater capacitance measured per device as seen below in Figure 24, in which Figure 24 is a capacitance frequency measurement of a 100 uF capacitor that was purchased [131].
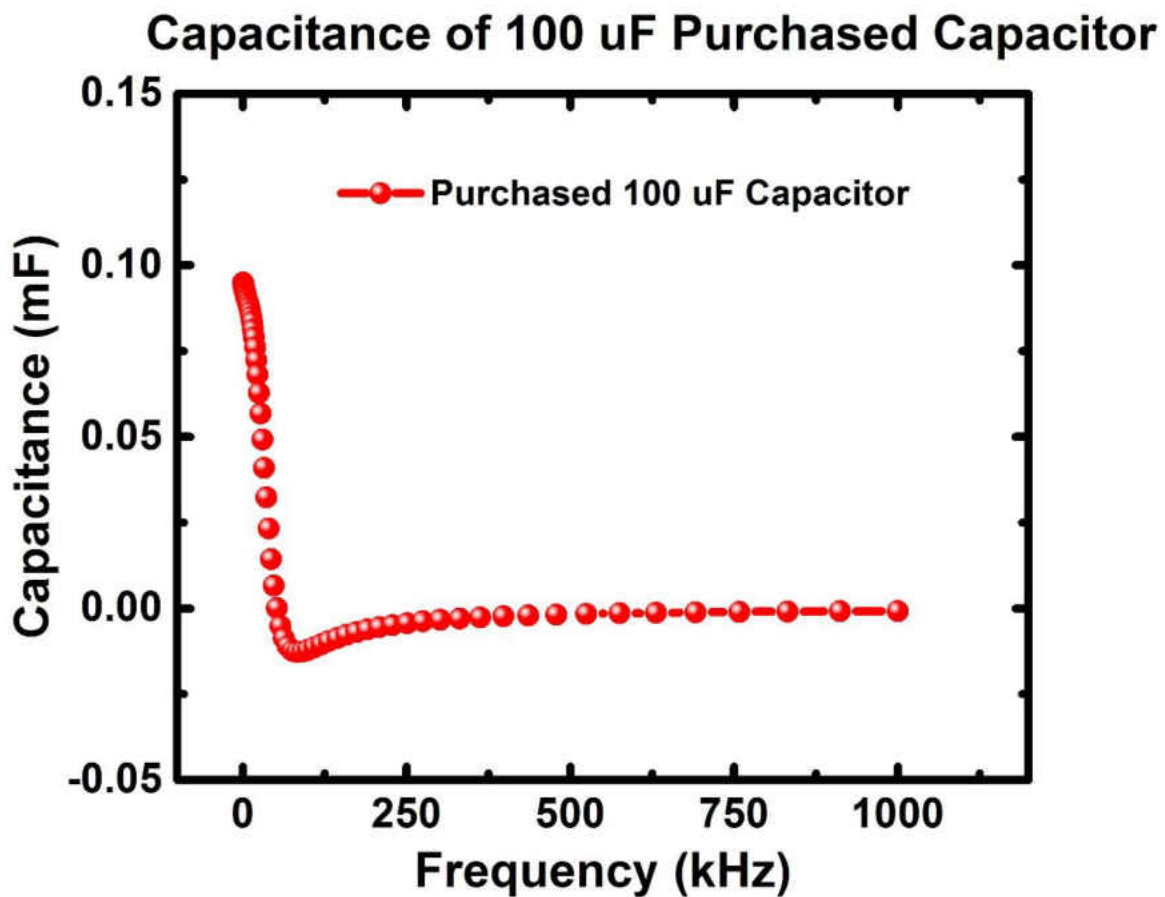
Figure 24: *CF measurement of 100 uF capacitor*

From Figure 24, it is clear that the capacitor did not measure 100 uF at 1 kHz, but instead there is a small error present. The machine has been recalibrated for phase compensation, load correction, short correction, and open correction SMU numerous times, and is consistently close to the optimal capacitance. If lesser frequency could be used in measurements, it is believed that the capacitor would measure closer to 100 uF. A capacitance voltage test was run with the same 100 uF capacitor, after calibrating, and the error was found to be about 5%.

The capacitance in the accumulation region increases consistently with decreasing frequency. Normally, the measured capacitance in the accumulation region should be independent of the signal frequency. Possible explanations for this occurrence may be due to the effect of direct carriers tunneling through the gate, the inability of the CV to accurately measure the capacitance in the presence of high leakage current, or due to the dielectric layer [131].

In the first case, if the tunneling currents become large, the effect of the series resistance is amplified, leading to a decrease in capacitance in the accumulation region. But this is seen in gate layers less than 4 nm [131]. The second possibility is the inability of the CV to accurately measure the capacitance. A dissipation factor (D), given in the CV data output, can be used to check the accuracy of the measurement and this can also be determined using measured capacitance and conductance [131]. Using the dissipation factor, the results remain at a very small error percentage, $< 0.25\%$ error. Frequency dispersion is not an instrumental error. Thus, the capacitance frequency variations in Figure 24 can be attributed to the presence of a dielectric layer. The dielectric layer

is filled with traps causing the dielectric layer to become highly frequency dependent [131]. The dielectric layer is the reason the devices vary capacitance with frequency.

CV RESULTS

All data recorded is at a frequency of 1 kHz. Measurements by other researchers go much lower in frequency, but the device is limited by a minimum of 1 kHz frequency for measurements [86], [89]. Nafion is one of the hardest materials to get CNTs to adhere to out of all the devices fabricated, but coating with BNNTs allows for an easier deposition of the CNTs. Some methods of fabrication allow the CNTs to adhere well as an electrode, but for other methods the CNTs struggle to leave a uniform coating. One the following page, in Figure 25, are the top performing devices measured capacitance graphed against each other. The two top performing devices had no BNNTs present, consisting of CNTs on nafion and CNTs on filter paper. Acid treated BNNTs did demonstrate relatively strong capacitance when applied to nafion and to CNTs that underwent acid treatment.
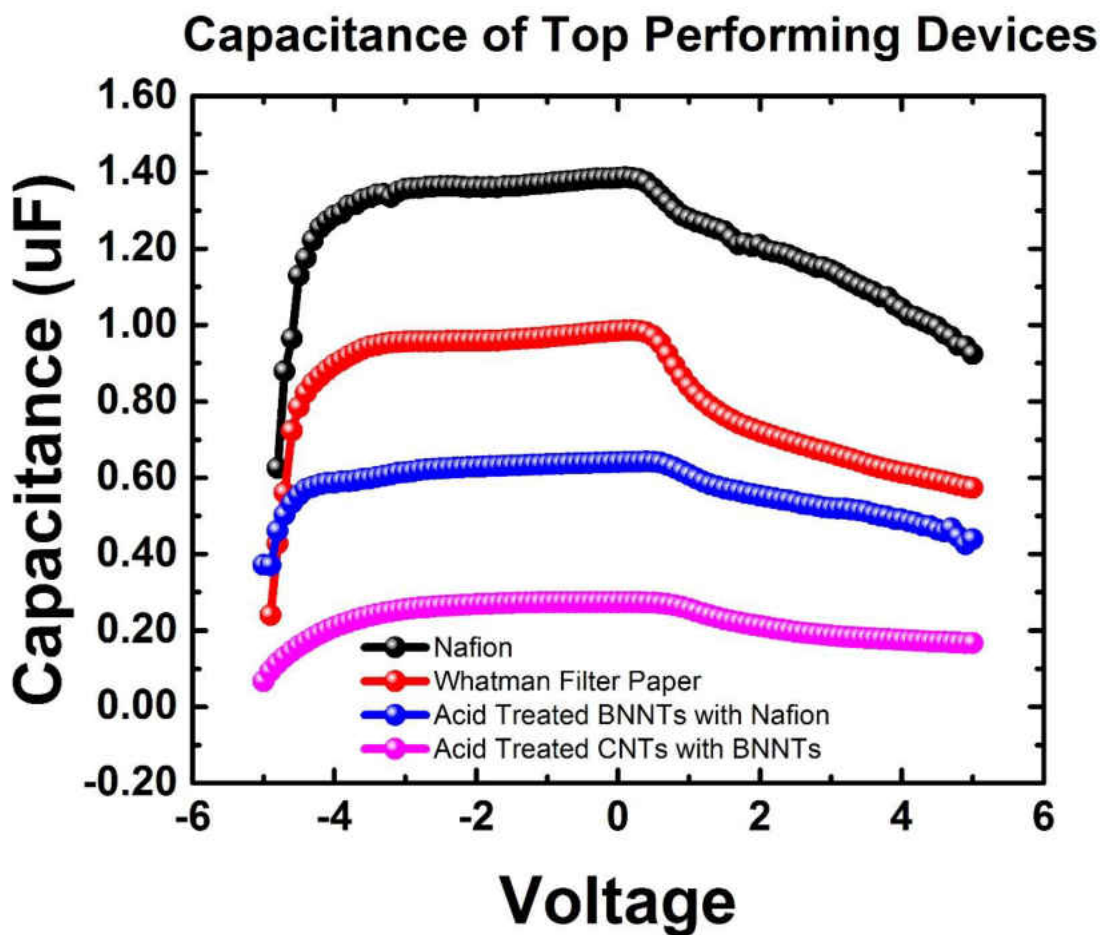
Figure 25: Measured capacitance of top performing fabricated devices

Using the measured capacitance, energy stored and energy density can be further calculated. More often, the data derived for supercapacitors is that of specific energy, sometimes referred to as energy density, although energy density is often used in terms of volumetric measurement, and is in the units of Watts-hour per kilogram [124]. The energy stored is calculated in Joules and calculations were taken using equation 5, shown below, in which capacitance (C) is multiplied by voltage (V) squared and divided by 2 [124]. Stored energy and energy density are very similar except that energy density, from equation 7, accounts for the mass of both electrodes in kilograms

[124]. Joules converts easily to Watts-hour as 1 Joule equals 278 mWh, and the mass (M) is found

from the total weight of both electrodes as seen previously in equation 7 [123]. The electrolyte

mass, separator mass, and current collector mass are not included in this calculation, as only the

mass of the active material in the two electrodes is used [125].

$$E = \frac{CV^2}{2} = \frac{QV}{2} \tag{5}$$

The stored energy can be seen graphically in Figure 26, on the following page. Because voltage

is squared, an increase is expected as the applied voltage increases. The data that increases at a

greater rate is expected to have a higher capacitance. Stored energy leads into energy density by

accounting for the mass of the electrodes. Energy density is the major difference between

capacitors and supercapacitors. Supercapacitors have a much greater energy density.
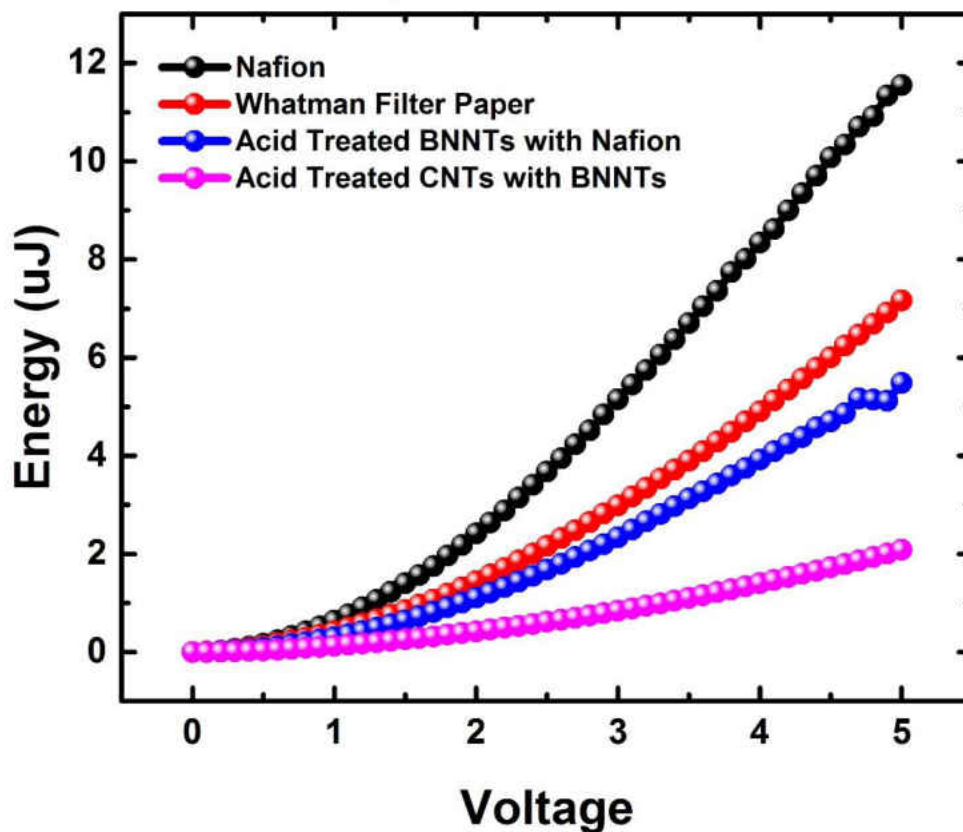
Figure 26: Stored energy for top performing fabricated devices

Because energy density uses stored energy divided by the mass of the two electrodes, a simple calculation was used to find the energy density of each device. Energy density can be seen graphically on the next page in Figure 27. Calculated energy density is close in many devices as the mass of the electrodes are accounted for in this calculation, while the stored energy calculations exhibit a greater difference in devices.
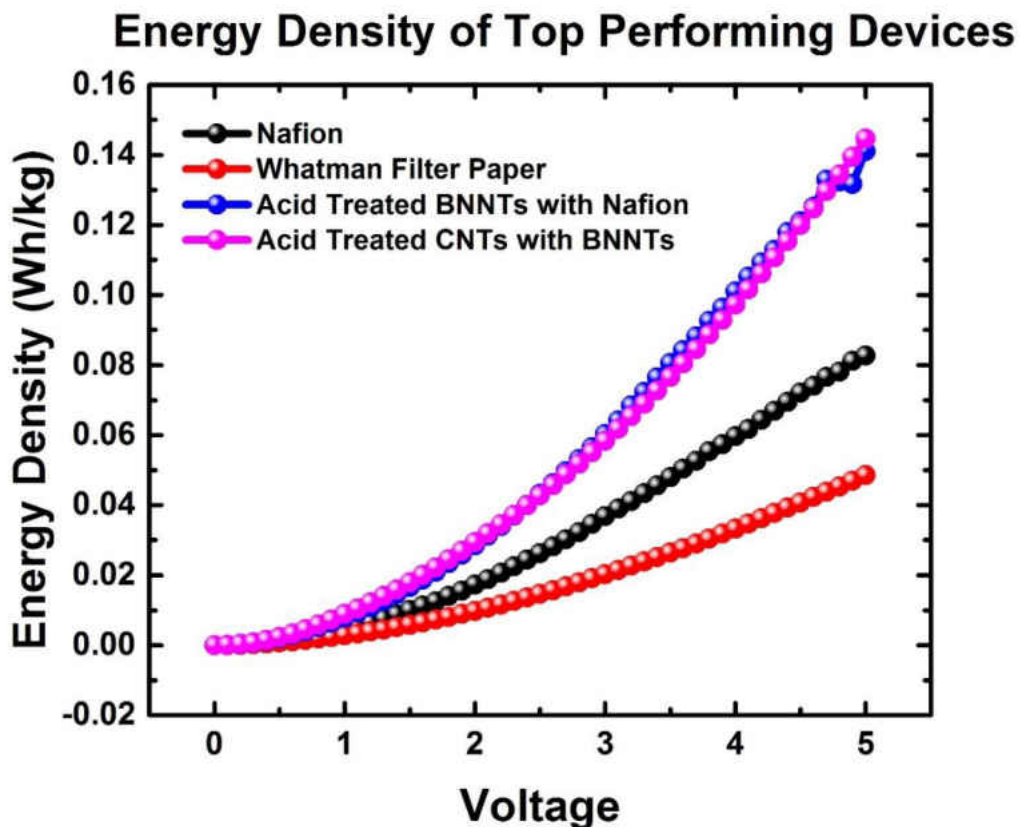
Figure 27: Energy density of top performing fabricated devices

Now that a few key capacitor characteristics have been introduced, Table 1 is shown below and contains these previously discussed values of all fabricated devices, and also includes more values discussed further in this section. Measured capacitance peaks were used in the top line of each row for all devices, and 5 volts was used on the second line of each row. Using a standard voltage in the table allows for a greater comparison between devices. Included in Table 1 by columns is the material being measured, as fabrication of such devices can be found in the experimental section, voltage measured at capacitance, mass of a single electrode, specific capacitance, energy density, and power density.

Material	Voltage (V)	Capac-itance (uF)	Active Material Mass per electrode (mg)	Specific Capacitance (mF/g)	Energy Density (Wh/kg)	Power Density (kW/kg)
PVDF	-1.7 V 5 V	0.46 uF 0.22 uF	4.7 mg	0.20 mF/g 0.10 mF/g	0.02 Wh/kg 0.08 Wh/kg	0.46 kW/kg 2.77 kW/kg
Nafion	.1 V 5 V	1.38 uF 0.92 uF	5.4 mg	0.51 mF/g 0.34 mF/g	0.09 Wh/kg 0.13 Wh/kg	0.002 kW/kg 3.02 kW/kg
Untreated BNNT Paper	-0.8 V 5 V	0.32 uF 0.18 uF	4.8 mg	0.13 mF/g 0.08 mF/g	0.003 Wh/kg 0.07 Wh/kg	0.07 kW/kg 1.74 kW/kg
Acid Clean BNNT Paper	1.8 V 5 V	0.63 uF 0.46 uF	5.3 mg	0.24 mF/g 0.17 mF/g	0.03 Wh/kg .015 Wh/kg	0.70 kW/kg 3.47 kW/kg
BNNT 1 Side Spray on Paper	0.2 V 5 V	0.47 uF 0.28 uF	5.4 mg	0.18 mF/g 0.11 mF/g	0.0002 Wh/kg 0.09 Wh/kg	0.008 kW/kg 2.4 kW/kg
Untreated BNNT Mat	4.4 V 5 V	0.12 uF 0.05 uF	35.2 mg	0.01 mF/g 0.003 mF/g	0.002 Wh/kg 0.003 Wh/kg	0.33 kW/kg 0.39 kW/kg
Whatman Filter Paper	.2 V 5 V	0.986 uF 0.573 uF	5.7 mg	0.35 mF/g 0.20 mF/g	0.0001 Wh/kg 0.05 Wh/kg	0.02 kW/kg 4.01 kW/kg
Acid Cleaned CNT with BNNT	-.4 V 5 V	0.274 uF 0.17 uF	2.0 mg	0.27 mF/g 0.17 mF/g	0.002 Wh/kg 0.15 Wh/kg	0.04 kW/kg 4.29 kW/kg
Acid Clean BNNT Mat	0.7 V 5 V	0.68 uF 0.50 uF	6.2 mg	0.22 mF/g 0.05 mF/g	0.004 Wh/kg 0.14 Wh/kg	0.006 kW/kg 0.42 kW/kg
Untreated BNNT Nafion	0.2 V 5 V	0.65 uF 0.49 uF	5.5 mg	0.24 mF/g 0.18 mF/g	0.0003 Wh/kg 0.15 Wh/kg	0.01 kW/kg 3.57 kW/kg
Acid Cleaned BNNT Nafion	0.4 V 5 V	0.64 uF 0.44 uF	5.4 mg	0.24 mF/g 0.16 mF/g	0.002 Wh/kg 0.14 Wh/kg	0.04 kW/kg 3.31 kW/kg

Table 1: Voltage, capacitance peak, mass per electrode, specific capacitance, energy density and power density

Another key characteristic of capacitors is specific capacitance, which can be measured using equations 9 or 10. As mentioned earlier, equation 10 will be used for specific capacitance equations due to the machine used for measurement, in which the measured capacitance is multiplied by 2 and divided by the mass of a single electrode [86], [88], [89]. The mass of a single electrode for each device can be found above in Table 1, along with the calculated specific capacitance. Specific capacitance of the top performing devices is also graphically represented below in Figure 28.

Figure 28: *Specific capacitance of top performing fabricated devices*

Because some devices have BNNTs, a comparison was made of the specific capacitances of only devices having a BNNT component to compare the samples cleaned with acid against untreated BNNTs. Below in Figure 29 is a graph that compares all the devices having BNNT as part of the fabrication process.
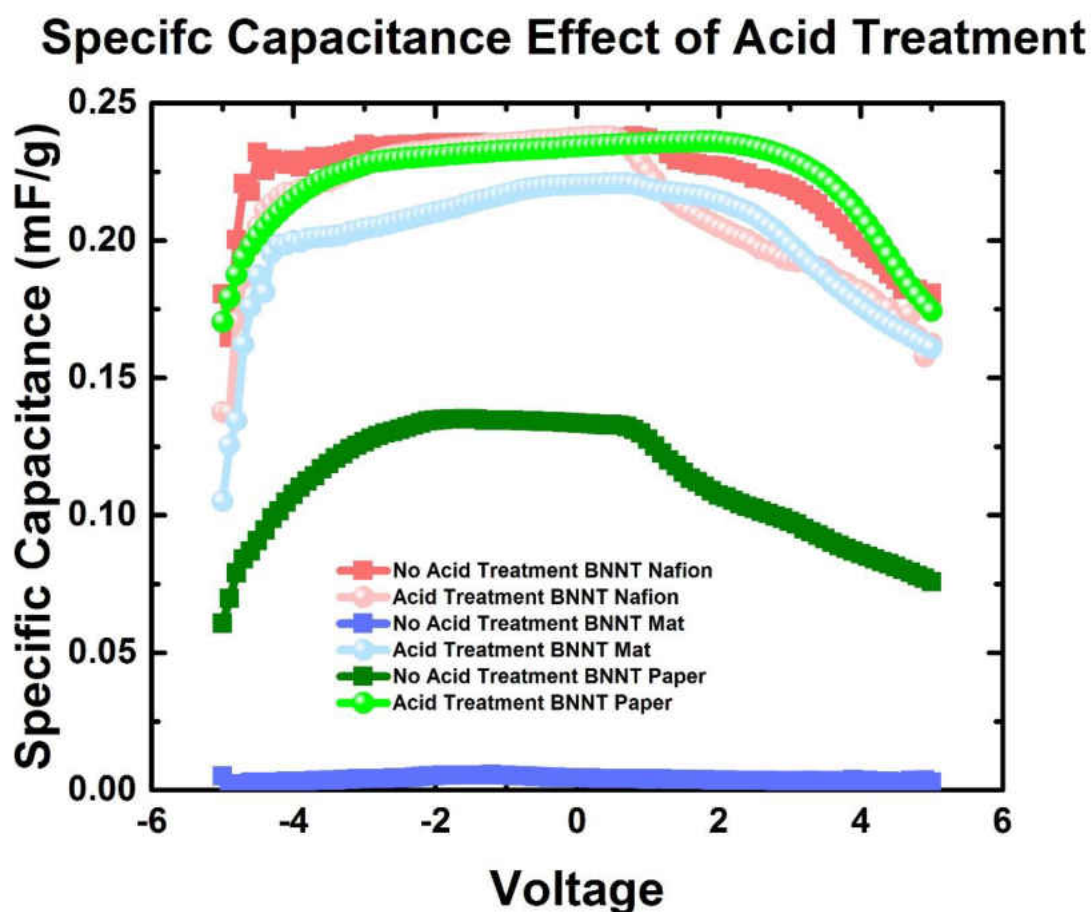
Figure 29: Specific capacitance of fabricated devices with BNNT with and without acid treatment

In Figure 29, it is obvious that the acid treatment increased the specific capacitance of the device in all the materials except for the devices also having a nafion membrane separator, in which the

values are very close. All the max specific capacitances can be seen in Table 1. The acid cleaned BNNTs sprayed on office paper with CNT deposition, was very similar to all nafion sprays. In addition, the deposition on paper results in lower fabrication costs when compared to the costs of fabrication when nafion is involved. The measured capacitances are similar with the nafion as the BNNT had little impact on the dielectric layer. The other two devices saw much greater differences. The non-acid treated BNNT mat is believed to have performed poorly due to a thicker separator layer that the vacuum filtration method produced. The acid treated BNNTs were more fine and compact to produce a slimmer mat. An increase in separator layer thickness is desired to a point for more optimal charge separation, however, too thick of a layer creates more resistance which will lower measured capacitance. The main point to take away from Figure 29 is that in most cases, acid treating the BNNTs did demonstrate higher capacitance measurements. Because there are such similarities in the specific capacitances of the BNNT nafion membranes, on the next page, in Figure 30 is all the devices with nafion as the separator layer.

Specific Capacitance of Nafion Devices
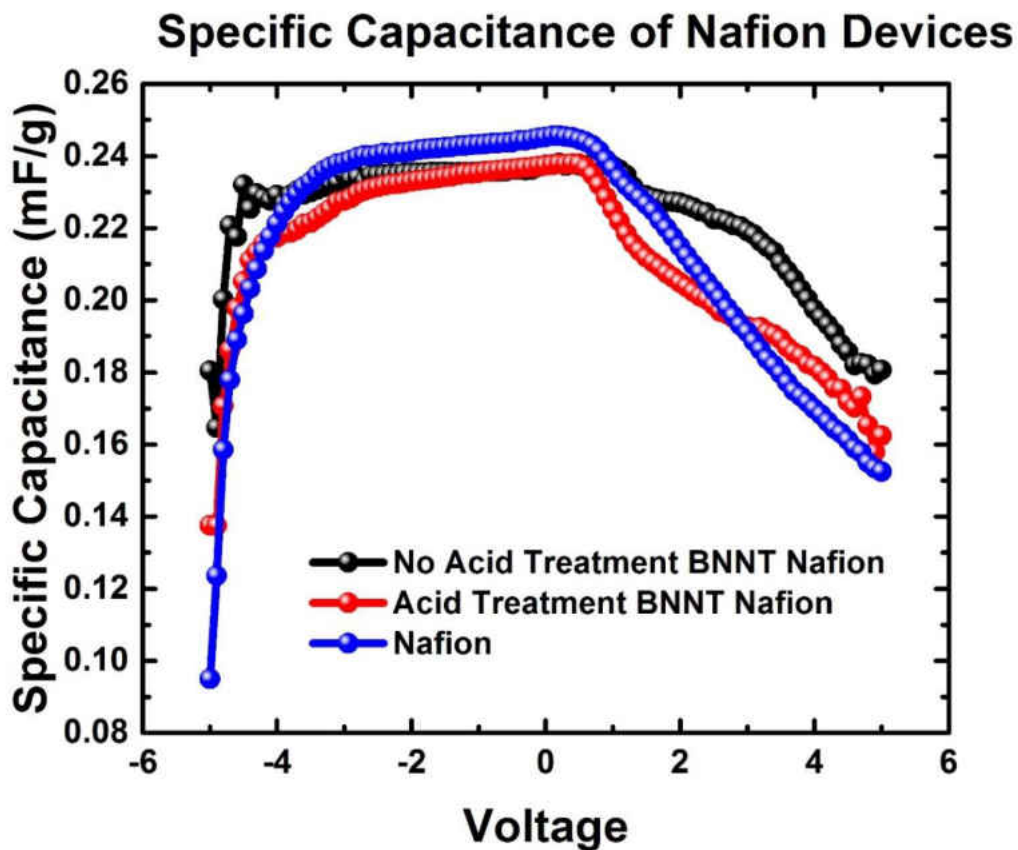
Figure 30: Specific capacitance of fabricated devices with nafion

All the results of nafion devices are very similar, as this is believed to be due to only a small amount of BNNTs adhering to the nafion. Around 1 mg of BNNTs were sprayed on each side of the nafion, but more BNNTs could be sprayed to see more variety in results. The CNTs adhered much better to the nafion that was sprayed with BNNTs as opposed to the nafion not coated with BNNTs. More coats of CNTs on the nafion and BNNT devices could lead to more stability, as the stand-alone nafion device had three coats of CNT spray, where the BNNT devices only needed one to achieve the same thickness of deposition. So, although there was not much difference in

measured capacitance, the deposition process improved tremendously and lowered fabrication costs with BNNTs being sprayed on the nafion separator layer.

Another typical key characteristic of supercapacitors is power density, which is found from max power. Max power, like stored energy, does not account for mass of the electrodes [124]. Max power is found by squaring the voltage (V), and dividing by 4 times the equivalent series resistance, ESR, as seen below in equation 6.

$$P = \frac{V^2}{4ESR} \tag{6}$$

The ESR is given from the B1500A measurements as the series resistance, but can also be calculated as it is the real resistance in impedance, which is also data given by the Agilent device. The power density is found by dividing the max power from the mass of the two electrodes [123]. The units are typically kW/kg [123], [124]. The results of max power for the top performing devices can be seen on the next page in Figure 31. Power density is shown graphically on page 94, in Figure 32, and numerically in Table 1.
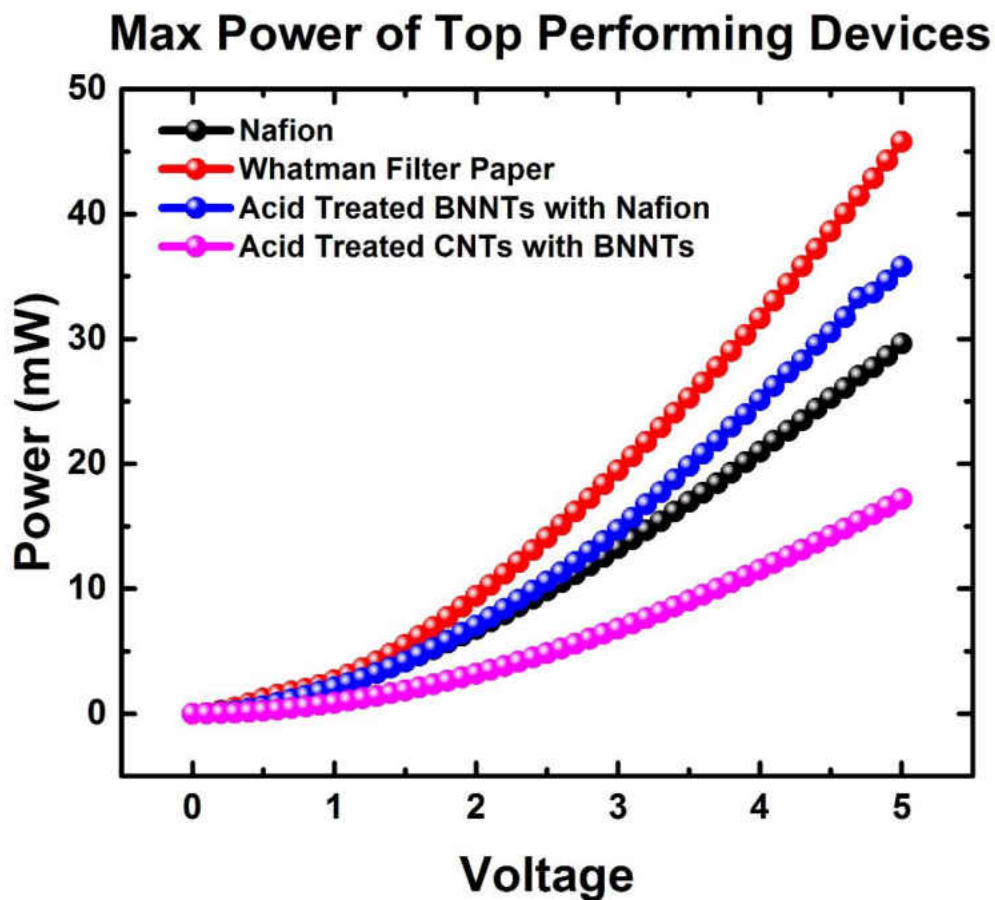
Figure 31: *Max Power of top performing devices*

The devices with the lower resistance will have higher max power. The higher performers in max power have a slightly larger amount of the active material, CNTs, deposited so when calculating the mass, the power densities will become closer than the max power results, which can be seen on the next page in Figure 32.
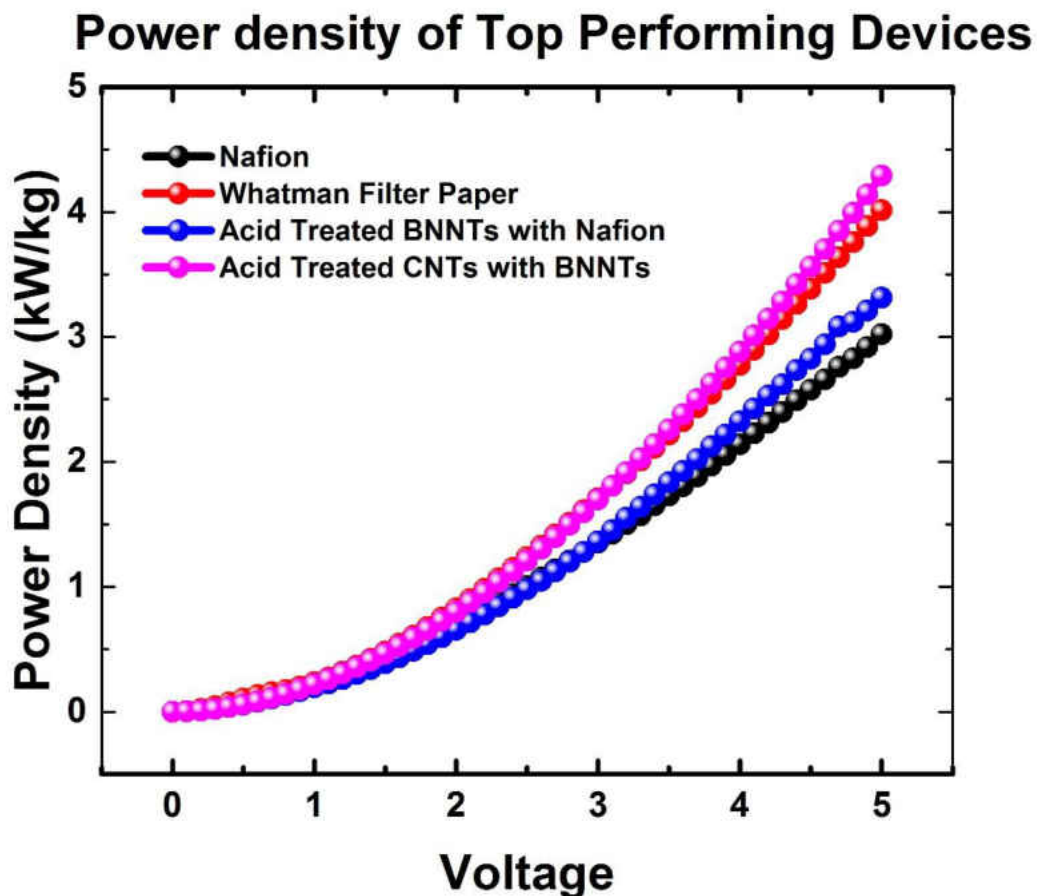
Figure 32: Power Density of top performing devices

Final conclusions can be found in a later section, but using less active material and cleaning the

CNTs and BNNTs with acid helped improve ideal characteristics of capacitors.

TEM IMAGE DATA

Also performed were TEM images of BNNTs dispersed in various solutions under controlled

ultrasonication times. All of the measured solutions were prepared using a 5:1 ml to mg ratio. The

solutions were all sonicated for four hours except the solution with DMF. The DMF solution was

stirred for 4 days, but clumps still existed, so shear mixing was used which left the solution capable of dispersion with only 15 minutes of ultrasonication time [116]. Similar to the results from the CV measurements, acid cleaned BNNTs underwent nitric acid treatment prior to dispersing the BNNTs in ethanol, and the untreated BNNTs did not receive acid treatment but are also dispersed in ethanol. All of the other solutions are named after the solvent used to disperse the BNNTs. The following figures are separated by zoom level and are expressed by the size of the scale bar in the bottom left of each image.

The first set of images in Figure 33 are at a 500 um scale bar, pictured on the next page, as 5 different solutions were examined under the TEM microscope are pictured below and on the next page.

In Figure 33, a far zoom allows a perspective of a larger sample region to view clumps and how the solution spreads when put on a flat surface. The large eclipse like pores are from the copper mesh in which the solutions were placed and dried prior to imaging. Although the cluster depends on position of image sampled, the acid cleaned BNNTs are more separated and evenly dispersed compared to the other images. The non ultrasonicated sample of DMF appears to be of the same consistency as ethanol, but with more clumps near the edges of dispersion where the sample should smooth out. The toluene sample has many broken nanotubes visible at such a large scale. Methanol suffers from the same issue as the toluene, but the chunks are more separated.
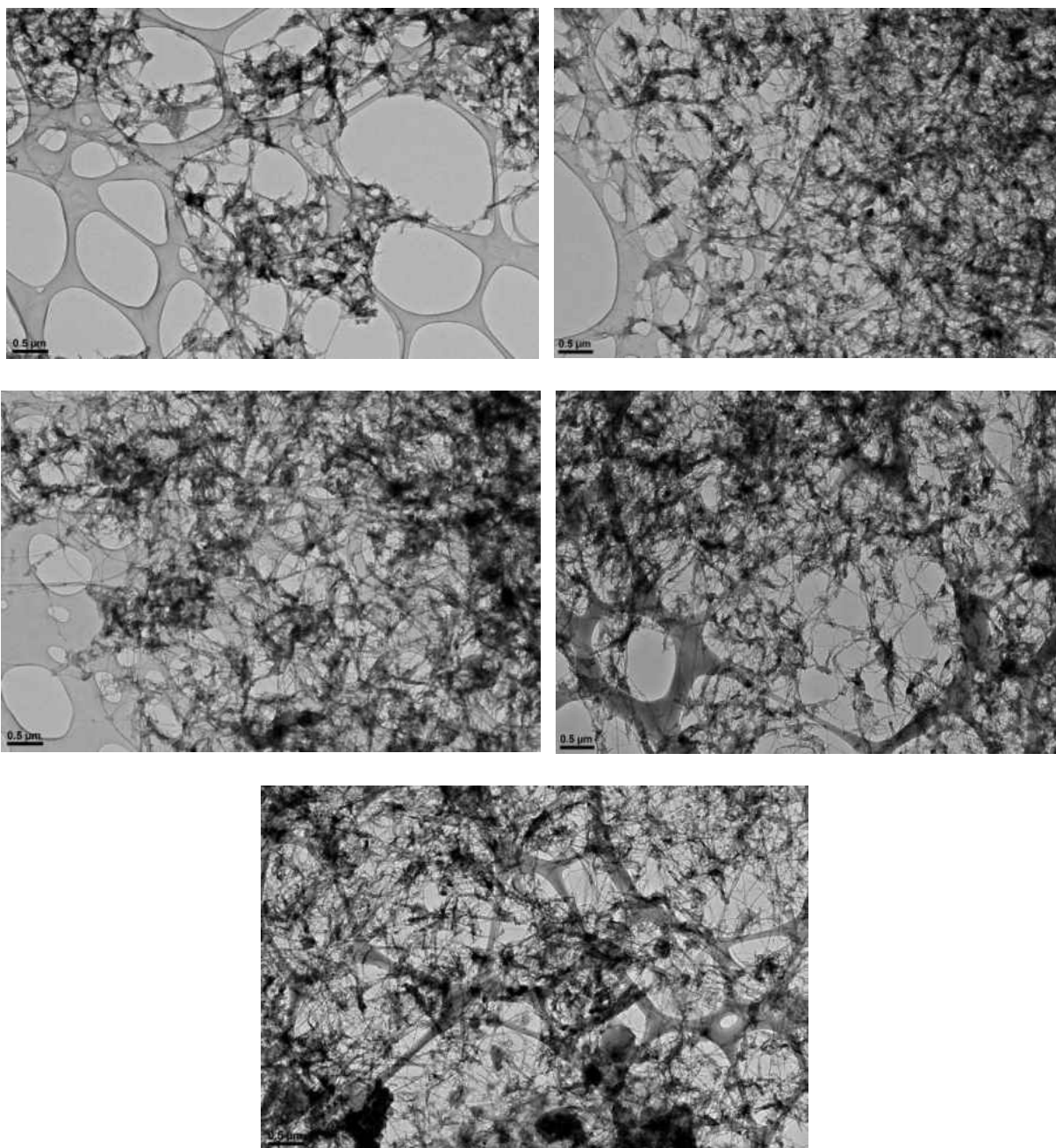
Figure 33: *500 um scale bar TEM of BNNTs acid cleaned in ethanol (top left), untreated in ethanol (top right), with solutions of DMF (middle left), methanol (middle right), and toluene (bottom)*

The next set of images are included in Figure 34, and zooms in using a 50 nm scale bar and are seen on the next page.
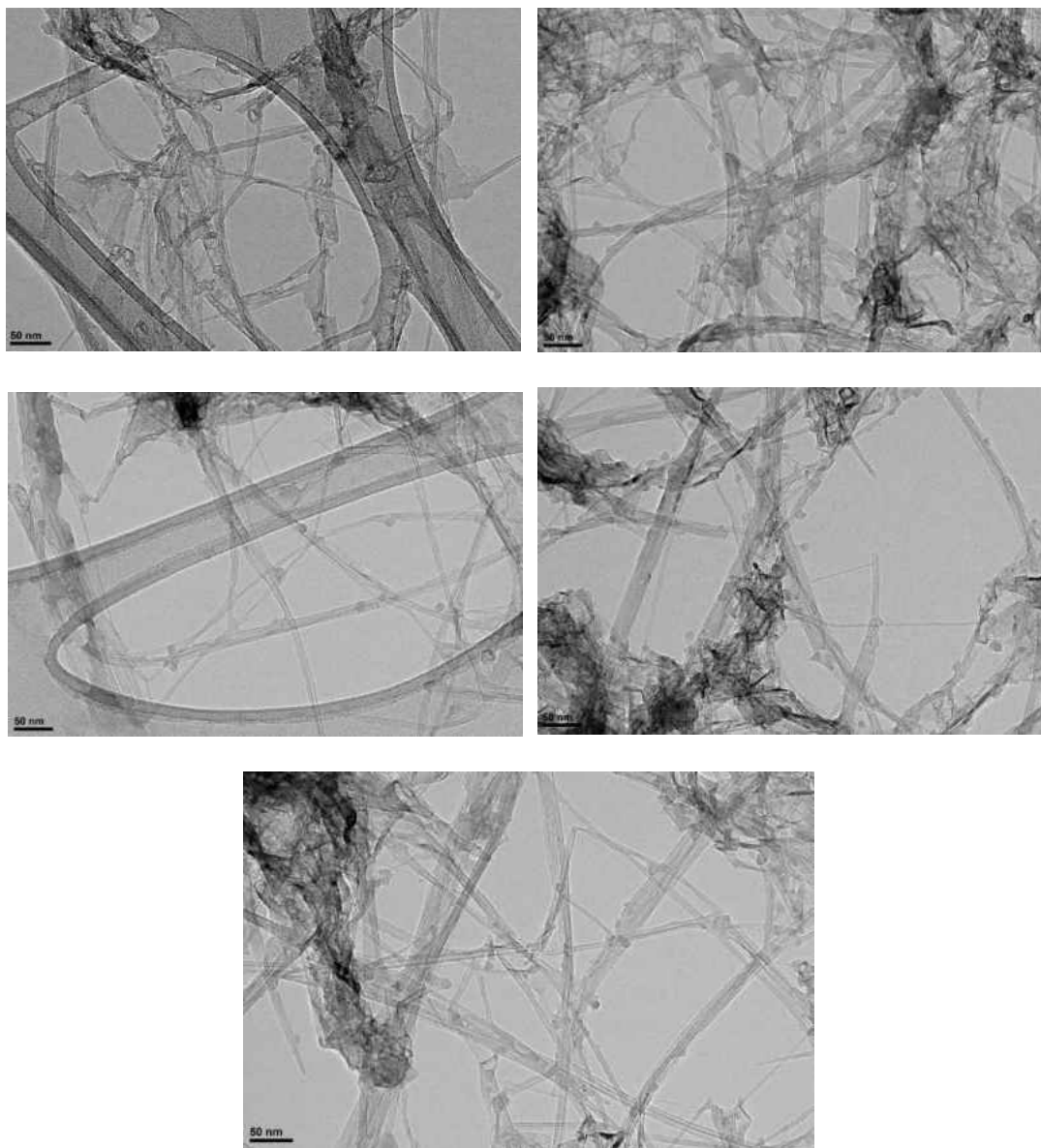
Figure 34: *50 nm scale bar TEM of BNNTs acid cleaned in ethanol (top left), untreated in ethanol (top right), with*

solutions of DMF (middle left), methanol (middle right), and toluene (bottom)

Zooming in, into regions where strands exists, the individual nanotube structures become visible. Although the individual walls are still not visible, it is possible to see the structure of the tubes, specifically any bends or breaks. The toluene and DMF samples are the only two images with any visible breaks at this zoom. The acid treated BNNTs do not have as much thick film present as both the untreated sample in ethanol and the sample dispersed in methanol. Although the DMF does have the least film present in this image, other images showed large conglomerations of nanotubes so the BNNTs did not disperse well with the minimal ultrasonication time, and because of the breaks that are present, the acid cleaned BNNTs are the best sampled image at the 50 nm scale bar. Figure 35 zooms in once again using a scale bar of 10 nm and is seen on the next page.
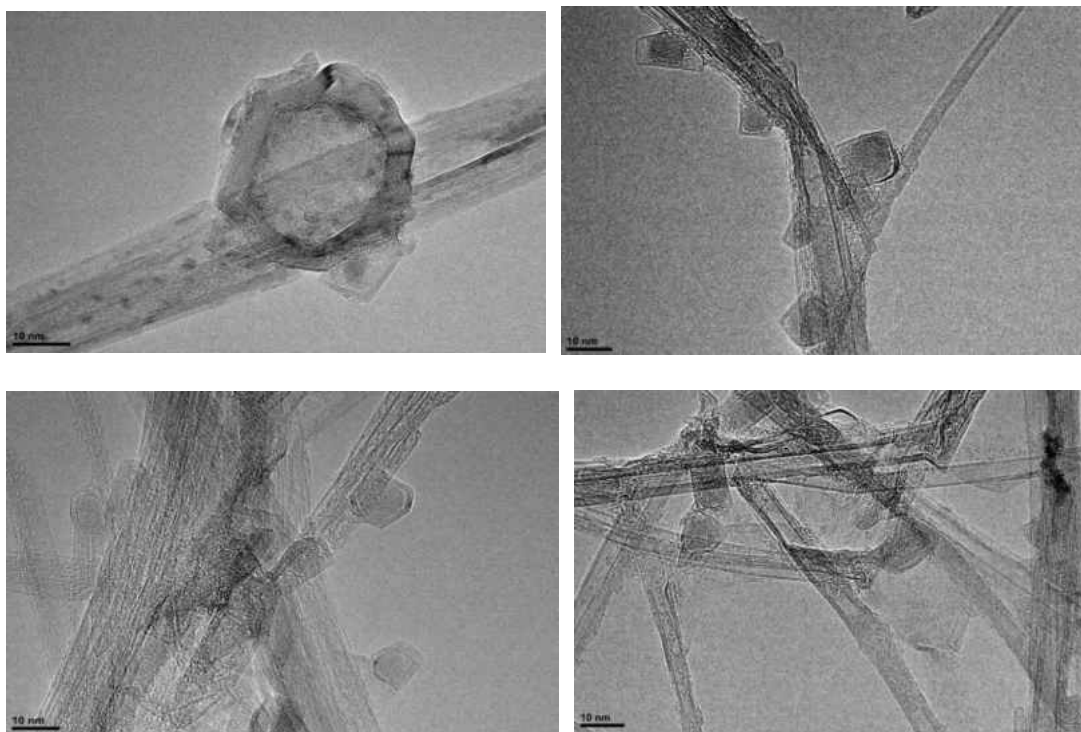
Figure 35: 10 nm scale bar TEM of BNNTs acid cleaned in ethanol (top left), untreated in ethanol (top right), methanol (bottom left), and toluene (bottom right)

In the 10 nm scale bar, the walls of the nanotubes become visible. It is clear that the methanol solution did not disperse well as clumps of broken BNNTs exist together. The nanotube walls look the most damaged in the methanol image. The toluene BNNTs separated, but there are many broken nanotubes. The untreated BNNTs clumped slightly but appear to have good structure. The acid cleaned BNNTs has a bundle on top of a strand and has very good structural characteristics with many undamaged walls. Having a minimal amount of damage to many walls increases the strength of the BNNT material as discussed in the literature section, as the nanotubes are capable of handling more stress. The next level of zoom is shown on the next page in Figure 36.
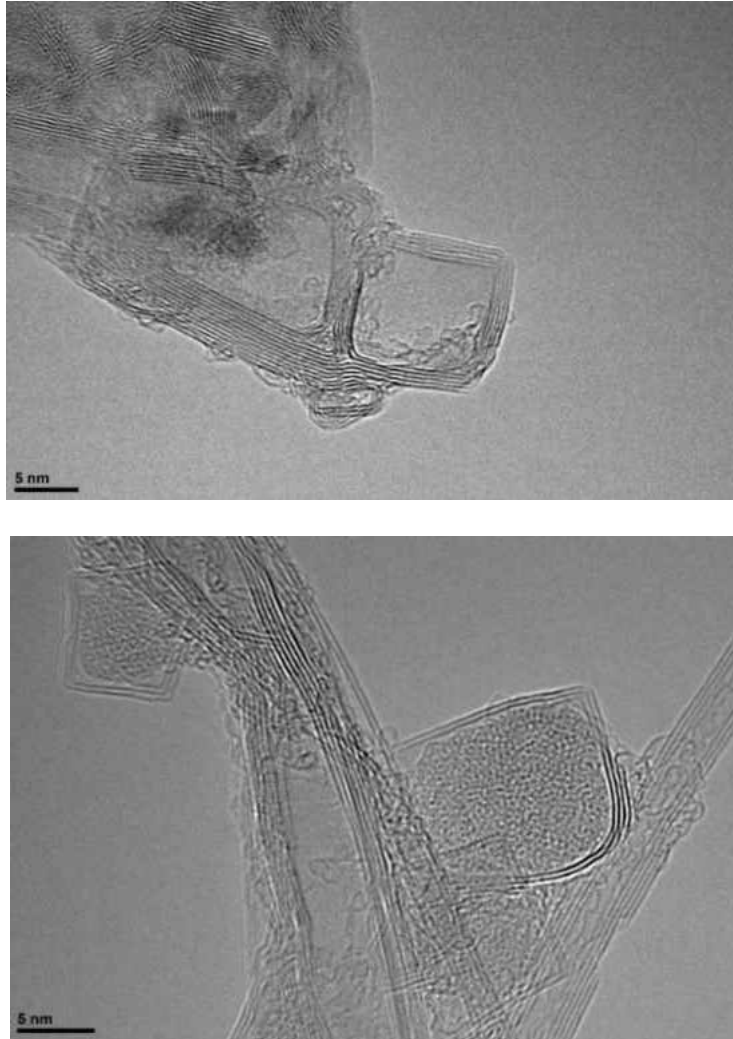
Figure 36: *5 nm scale bar TEM of BNNTs acid cleaned in ethanol (above) and untreated in ethanol (below)*

In this final zoom image in Figure 36, it is obvious that these samples have much better structure than the nanotubes that were pictured in Figure 5 from the beginning of the experiment. The acid cleaned BNNTs have more ideal structural properties as compared to the untreated BNNTs. The untreated BNNTs have little wall damage, but very few walls are present, which will lead to faster fracture under the same load stress. Even in a clump, the acid cleaned BNNTs have clear walls present that are undamaged. Also, in the untreated BNNTs, the nanotubes seem to cluster around

a thin film layer of BNNTs, where the acid treated BNNTs cluster formed with only a small amount of film in the corners. Both structures look adequate, but the acid cleaned BNNTs have more desirable properties for use in thermal or electrochemical applications, in which BNNTs are commonly being studied.

CHAPTER IV

CONCLUSION

Using the CV data and TEM data, the BNNTs that were cleaned with acid had better electrical and physical properties. It is recommended that all BNNT tests and measurements be taken of BNNTs that have undergone acid treatment. Ethanol appeared to cause very little damage to the wall structures as seen in the TEM images, so this can be used as the solvent of BNNTs moving forward. The few hours of ultrasonication time needed for dispersion had little effect on the walls when comparing the samples that had hours of ultrasonication time to the DMF solution, which only had 15 minutes. All the samples underwent some form of stirring or shear mixing, so eliminating this step could cause less defects in the wall structure, although some solutions showed very minimal damage to the nanotubes.

The capacitor devices that were fabricated showed higher ideal characterization levels than capacitors, but weak levels for supercapacitors. Despite reaching an ideal power density, energy density must be improved. Although some devices reached the mF/g specific capacitance range of supercapacitance, much improvement in the devices is still necessary to increase this level into the F/g range. The acid treated CNTs combined with acid treated BNNTs, which performed the best overall, shows the most promise moving forward, and a better layer of both nanotubes could be made through more regulated coats of spray. The power density of this device was on par with supercapacitors, but energy density was slightly lower than supercapacitor levels. Currently, the device is in between conventional capacitors and supercapacitors due to the energy density. The greater regulation of deposition sprays can be done through lowering the amount of CNTs deposited while strictly monitoring the thickness of the BNNTs deposited. All of the devices

performed well comparatively, and consistent data was found. More alterations in fabrication technique can be used to improve the fabricated devices characteristics.

IMPROVEMENTS

Improvements for CNTs, BNNTs, and electrolyte deposition could be made through stronger regulated thickness of depositions. Although milligrams of BNNTs were matched during depositions, overspray and BNNTs not settling on the membrane during vacuum filtrations could account for differences in amounts of BNNTs actually being deposited. Deposition will need to be adjusted as it is the only weak point of acid treated BNNTs, in that they appear to not adhere as well as untreated BNNTs to certain materials, such as nafion during spray depositions, and creating a BNNT mat without defects through vacuum filtration will need to be carefully performed. Untreated BNNTs can be used to easily and consistently produce BNNT mats, but acid treated BNNTs did not deposit so easily using the same procedure. Minor tweaks in methods can be performed to allow the acid treated BNNTs to deposit as easy as the untreated BNNTs, such as using an apparatus to hold the PCTE membrane down on the edges to keep the more dispersed acid treated BNNTs from seeping underneath the filter, or by adjusting ultrasonication time to manipulate the size of the particles used for deposition.

CNT deposition techniques will also need to be improved to not only increase stability, but also the capacitance characteristics. When CNTs have a good deposition, the capacitance, energy, and power increases. Stable data is also found when this occurs. Although various methods were tried, nafion and paper being dripped with CNTs did not have good results for deposition. The nafion depositions could be improved in terms of a solid thick layer of CNTs being deposited. The CNTs

did adhere better once the nafion was coated with BNNTs, so this may be a viable first step. The data in the nafion with and without BNNTs is similar, so more experiments could be run to see if the BNNTs, perhaps in thicker depositions, have any impact on the capacitance. Also, treating the CNTs with acid prior to deposition allowed for a deposition directly on aluminum foil to occur. Minimizing the deposited weight of the CNTs will improve specific capacitance, energy density, and power density. Cleaning CNTs with acid is vital to continue to improve device capacitance characteristics.

The electrolyte gel will be harder to regulate because even though a similar amount was applied to each device, the gel will leak out when the aluminum contacts are pressed against the device. However, using a liquid electrolyte did not allow the contacts to stick to the device, so there is much room for improvement in regards to a consistent, well-regulated electrolyte used in the devices.

FUTURE PLANS

Future plans could be to use purer materials in fabrication, in regards to minimizing potential contaminations. Although the black ink was used on the paper capacitor devices to be able to view the BNNT deposition, this ink could cause unwanted effects to the capacitor device. Using all white paper may yield different results. Stronger, or purer, metal used in the spray guns will be necessary in future sprays of the CNT and H_2SO_4 solutions as the sulfuric acid has begun stripping the metal coating on both the gun and the solution holder, resulting in corroded metal being exposed and likely deposited. The spray device lasted about a month, or roughly 20 sprays, so if this technique is continued, it would be cost effective to purchase better quality equipment.

Other improvements in capacitance measurements can be to add other chemicals such as Ruthenium Oxide to the CNTs to increase performance. Higher capacitance levels may also be achieved through using a higher grade of CNTs, as not all nanotubes are created under the same standards. The CNTs used in this experiment had 95% of purity, where better grades of CNT's exist for purchase. All of the above mentioned suggestions could be implemented to create better performing capacitive devices.

REFERENCES

[1]   L. L. Zhang, and X. S. Zhao. "Carbon-based Materials as Supercapacitor Electrodes." *Chemical Society Reviews*. 38.9 (2009): 2520-2531.

[2]   B. Scrosati. "Recent Advances in Lithium Ion Battery Materials." *Electrochimica Acta* 45.15-16 (2000): 2461-466.

[3]   K. H. An, W. S. Kim, Y. S. Park, J.-M. Moon, D. J. Bae, S. C. Lim, Y. S. Lee, and Y. H. Lee. "Electrochemical Properties of High-Power Supercapacitors Using Single-Walled Carbon Nanotube Electrodes." *Advanced Functional Materials* 11.5 (2001): 387-92.

[4]   C. Peng, C., S. Zhang, D. Jewell, and G. Z. Chen. "Carbon Nanotube and Conducting Polymer Composites for Supercapacitors." *Progress in Natural Science* 18.7 (2008): 777-88.

[5]   Q. Xiao and X. Zhou. "The Study of Multiwalled Carbon Nanotube Deposited with Conducting Polymer for Supercapacitor." *Electrochimica Acta* 48.5 (2003): 575-80.

[6]   V. V.N. Obreja, "On the Performance of Supercapacitors with Electrodes Based on Carbon Nanotubes and Carbon Activated Material—A Review.*" Physica E: Low-dimensional Systems and Nanostructures* 40.7 (2008): 2596-605.

[7]   X. Li, T. Li, J. Gao, H. Huang, L. Li, and J. Li. "A Novel "green" Solvent to Deeply Purify Quartz Sand with High Yields: A Case Study." *Journal of Industrial and Engineering Chemistry* (2016): 383-387.

[8]   Z. M. Xia, X. S. Li, Z. Y. Chen, G. Li, K. F. Yan, C. G. Xu, Q. N. Lv, and J. Cai. "Hydrate-based CO2 Capture and CH4 Purification from Simulated Biogas with Synergic Additives Based on Gas Solvent." *Applied Energy* 162 (2016): 1153-159.

[9]   D. Dasgupta, S. Manna, S. Malik, C. Rochas, J. M. Guenet, and A. K. Nandi. "Thermodynamic Structural and Morphological Investigation of Poly(Vinylidene Fluoride)−Camphor Systems, Preparing Porous Gels from a Solid Solvent." *Macromolecules* 38.13 (2005): 5602-608.

[10]   S. W. Kim, T. Kim, Y. S. Kim, H. S. Choi, H. J. Lim, S. J. Yang, and C. R. Park. "Surface Modifications for the Effective Dispersion of Carbon Nanotubes in Solvents and Polymers." *Carbon* 50.1 (2012): 3-33

[11]   T. Hargreaves. "Surfactants: The Ubiquitous Amphiphiles." *Chemistry in Britain* 39.7 (2003): 38-41.

[12]   M. J. Rosen and J. T. Kunjappu. *Surfactants and Interfacial Phenomena*. Hoboken, NJ: Wiley, 2012.

[13]   A. R. Biris, D. Lupu, A. Grüneis, P. Ayala, M. H. Rümmeli, T. Pichler, Z. Li, Y. Xu, I. Misan, E. Dervishi, and A. S. Biris. "High-Quality Double-Walled Carbon Nanotubes Grown by a Cold-Walled Radio Frequency Chemical Vapor Deposition Process." *Chemistry of Materials* 20.10 (2008): 3466-472.

[14]   T. Faraz, F. Roozeboom, H. C. M. Knoops, and W. M. M. Kessels. "Atomic Layer Etching: What Can We Learn from Atomic Layer Deposition?" *ECS Journal of Solid State Science and Technology* 4.6 (2015): N5023-N5032.

[15]   H. Papa, M. Gaillard, L. Gonzalez, and J. Chatterjee. "Fabrication of Functionalized Carbon Nanotube Buckypaper Electrodes for Application in Glucose Biosensors." *Biosensors* 4.4 (2014): 449-60.

[16]   J. H. Lee, B.S. Kong, S.B. Yang, and H.T. Jung. "Fabrication of Single-walled Carbon Nanotube/tin Nanoparticle Composites by Electrochemical Reduction Combined with Vacuum Filtration and Hybrid Co-filtration for High-performance Lithium Battery Electrodes." *Journal of Power Sources* 194.1 (2009): 520-25.

[17]   X. Song, S. Liu, Z. Gan, Q. Lv, H. Cao, and H. Yan. "Controllable Fabrication of Carbon Nanotube-polymer Hybrid Thin Film for Strain Sensing." *Microelectronic Engineering* 86.11 (2009): 2330-333.

[18]   S. Y. Chew, S.H. Ng, J. Wang, P. Novák, F. Krumeich, S.L. Chou, J. Chen, and H.K. Liu. "Flexible Free-standing Carbon Nanotube Films for Model Lithium-ion Batteries." *Carbon* 47.13 (2009): 2976-983.

[19]   A. S. Brady-Estévez, S. Kang, and M. Elimelech. "A Single-Walled-Carbon-Nanotube Filter for Removal of Viral and Bacterial Pathogens." *Small* 4.4 (2008): 481-84.

[20]   Y. A. Kim, H. Muramatsu, T. Hayashi, M. Endo, M. Terrones, and M. S. Dresselhaus. "Fabrication of High-Purity, Double-Walled Carbon Nanotube Buckypaper." *Chemical Vapor Deposition* 12.6 (2006): 327-30.

[21]   J. Zhang, D. Jiang, and H.X. Peng. "A Pressurized Filtration Technique for Fabricating Carbon Nanotube Buckypaper: Structure, Mechanical and Conductive Properties." *Microporous and Mesoporous Materials* 184 (2014): 127-33.

[22]   H. Kong, C. Gao, and D. Yan. "Constructing Amphiphilic Polymer Brushes on the Convex Surfaces of Multi-walled Carbon Nanotubes by in Situ Atom Transfer Radical Polymerization." *Journal of Materials Chemistry* 14.9 (2004): 1401-1405.

[23]   C. Huang, and P. S. Grant. "One-step Spray Processing of High Power All-solid-state Supercapacitors." *Scientific Reports*. Ser. 3.2393 (2013): 1-9.

[24]   D. Wang, P. Song, C. Liu, W. Wu, and S. Fan. "Highly Oriented Carbon Nanotube Papers Made of Aligned Carbon Nanotubes." *Nanotechnology* 19.7 (2008): 075609.1-609.7.

[25]   W. J. Zhang, I. Bello, Y. Lifshitz, and S. T. Lee. "Recent Advances in Cubic Boron Nitride Deposition." *MRS Bulletin* 28.03 (2003): 184-88.

[26]   M. F. Budyka, T. S. Zyubina, A. G. Ryabenko, S. H. Lin, and A. M. Mebel. "Bond Lengths and Diameters of Armchair Single Wall Carbon Nanotubes." *Chemical Physics Letters* 407.4-6 (2005): 266-71.

[27]   F. A. Carey. *Organic Chemistry*. 4th ed. Boston: McGraw-Hill, 2000.

[28]   Z. H. Xia, P. R. Guduru, and W. A. Curtin. "Enhancing Mechanical Properties of Multiwall Carbon Nanotubes via sp3 Interwall Bridging." *Physical Review Letters* 98.24 (2007) 245501.1-501.4

[29]   J. Robertson. "Mechanism of Sp3 Bond Formation in the Growth of Diamond-like Carbon." *Diamond and Related Materials* 14.3-7 (2005): 942-48.

[30]   J. Kanasaki, E. Inami, K. Tanimura, H. Ohnishi, and K. Nasu. "Formation of S P 3 -Bonded Carbon Nanostructures by Femtosecond Laser Excitation of Graphite." *Physical Review Letters* 102.8 (2009): 087402.1-402.4

[31]   S. Osswald, G. Yushin, V. Mochalin, S. O. Kucheyev, and Y. Gogotsi. "Control of Sp 2 /sp 3 Carbon Ratio and Surface Chemistry of Nanodiamond Powders by Selective Oxidation in Air." *Journal of the American Chemical Society* 128.35 (2006): 11635-1642.

[32]   M. Chubarov, H. Pedersen, H. Högberg, V. Darakchieva, J. Jensen, P. O. Å. Persson, and A. Henry. "Epitaxial CVD Growth of Sp2-hybridized Boron Nitride Using Aluminum Nitride as Buffer Layer." *Physica Status Solidi (RRL) - Rapid Research Letters* 5.10-11 (2011): 397-99.

[33]   W. H. Meyer. "Polymer Electrolytes for Lithium-Ion Batteries." *Advanced Materials* 10.6 (1998): 439-48.

[34]   V. Musolino, L. Piegari, and E. Tironi. "New Full-Frequency-Range Supercapacitor Model with Easy Identification Procedure." *IEEE Transactions on Industrial Electronics* 60.1 (2013): 112-20.

[35]   V. Marano, S. Onori, Y. Guezennec, G. Rizzoni, and N. Madella. "Lithium-ion Batteries Life Estimation for Plug-in Hybrid Electric Vehicles." *2009 IEEE Vehicle Power and Propulsion Conference* (2009): 536-43.

[36]   F. Zhang, T. Zhang, X. Yang, L. Zhang, K. Leng, Y. Huang, and Y. Chen. "A High-performance Supercapacitor-battery Hybrid Energy Storage Device Based on Graphene-enhanced Electrode Materials with Ultrahigh Energy Density." *Energy & Environmental Science Energy Environ. Sci.* 6.5 (2013): 1623-632.

[37]   Q. Wang, Z. H. Wen, and J. H. Li. "A Hybrid Supercapacitor Fabricated with a Carbon Nanotube Cathode and a TiO2–B Nanowire Anode." *Advanced Functional Materials* 16.16 (2006): 2141-146.

[38]   H. Pan, J. Li, and Y. P. Feng. "Carbon Nanotubes for Supercapacitor." *Nanoscale Research Letters* 5.3 (2010): 654-68.

[39]   F. Lufrano, and P. Staiti. "Performance Improvement of Nafion Based Solid State Electrochemical Supercapacitor." *Electrochimica Acta* 49.16 (2004): 2683-689.

[40]   D. Zhang, Y. Wu, T. Li, Y. Huang, A. Zhang, and M. Miao. "High Performance Carbon Nanotube Yarn Supercapacitors with a Surface-Oxidized Copper Current Collector." *ACS Applied Materials & Interfaces* 7.46 (2015): 25835-5842.

[41]   H. C. Wu, Y.P. Lin, E. Lee, W.T. Lin, J.K. Hu, H.C. Chen, and N.L. Wu. "High-performance Carbon-based Supercapacitors Using Al Current-collector with Conformal Carbon Coating." *Materials Chemistry and Physics* 117.1 (2009): 294-300.

[42]   M. Notarianni, J. Liu, F. Mirri, M. Pasquali, and N. Motta. "Graphene-based Supercapacitor with Carbon Nanotube Film as Highly Efficient Current Collector." *Nanotechnology* 25.43 (2014): 435405.1-405.7.

[43]   C. Du and N. Pan. "High Power Density Supercapacitor Electrodes of Carbon Nanotube Films by Electrophoretic Deposition." *Nanotechnology* 17.21 (2006): 5314-318.

[44]   G. Wang, L. Zhang, and J. Zhang. "A Review of Electrode Materials for Electrochemical Supercapacitors." *Chemical Society Reviews*. 41.2 (2012): 797-828.

[45]   K. Xia, Q. Gao, J. Jiang, and J. Hu. "Hierarchical Porous Carbons with Controlled Micropores and Mesopores for Supercapacitor Electrode Materials." *Carbon* 46.13 (2008): 1718-726.

[46]   Y. Wang, Z. Shi, Y. Huang, Y. Ma, C. Wang, M. Chen, and Y. Chen. "Supercapacitor Devices Based on Graphene Materials." *The Journal of Physical Chemistry C* 113.30 (2009): 13103-3107.

[47]   E. Perricone, M. Chamas, J.-C. Leprêtre, P. Judeinstein, P. Azais, E. Raymundo-Pinero, F. Béguin, and F. Alloin. "Safe and Performant Electrolytes for Supercapacitor. Investigation of Esters/carbonate Mixtures." *Journal of Power Sources* 239 (2013): 217-24.

[48]   D. Kalpana, N. G. Renganathan, and S. Pitchumani. "A New Class of Alkaline Polymer Gel Electrolyte for Carbon Aerogel Supercapacitors." *Journal of Power Sources* 157.1 (2006): 621-23.

[49]   I. Stepniak, and A. Ciszewski. "Grafting Effect on the Wetting and Electrochemical Performance of Carbon Cloth Electrode and Polypropylene Separator in Electric Double Layer Capacitor." *Journal of Power Sources* 195.15 (2010): 5130-137.

[50]   P. Arora, and Z. Zhang. "Battery Separators." *Chemical Reviews* 104.10 (2004): 4419-462.

[51]   K. Tõnurist, A. Jänes, T. Thomberg, H. Kurig, and E. Lust. "Influence of Mesoporous Separator Properties on the Parameters of Electrical Double-Layer Capacitor Single Cells." *Journal of The Electrochemical Society* 156.4 (2009): A334-A342.

[52]   K. Tõnurist, T. Thomberg, A. Jänes, I. Kink, and E. Lust. "Specific Performance of Electrical Double Layer Capacitors Based on Different Separator Materials in Room Temperature Ionic Liquid." *Electrochemistry Communications* 22 (2012): 77-80.

[53]   H. Wang, and L. Pilon. "Accurate Simulations of Electric Double Layer Capacitance of Ultramicroelectrodes." *Journal of Physical Chemistry C* 115.33 (2011): 16711-6719.

[54]   T. Brousse, D. Belanger, and J. W. Long. "To Be or Not To Be Pseudocapacitive?" *Journal of the Electrochemical Society* 162.5 (2015): A5185-A5189.

[55]   W. Chen, R. B. Rakhi, M. N. Hedhili, and H. N. Alshareef. "Shape-controlled Porous Nanocarbons for High Performance Supercapacitors." *Journal of Materials Chemistry A* 2.15 (2014): 5236-241.

[56]   P. Simon, and Y. Gogotsi. "Materials for Electrochemical Capacitors." *Nature Materials* 7.11 (2008): 845-54.

[57]   C. Liu, Z. Yu, D. Neff, A. Zhamu, and B. Z. Jang. "Graphene-Based Supercapacitor with an Ultrahigh Energy Density." *Nano Letters* 10.12 (2010): 4863-868.

[58]   M. S. Dresselhaus, G. Dresselhaus, and P. Avouris. "Carbon Nanotubes: Synthesis, Structure, Properties, and Applications." Berlin: Springer, 2001.

[59]   H. W. Kroto, J. R. Heath, S. C. O'brien, R. F. Curl, and R. E. Smalley. "C60: Buckminsterfullerene." *Nature* 318.6042 (1985): 162-63.

[60]   S. Iijima. "Helical Microtubules of Graphitic Carbon." *Nature* 354.6348 (1991): 56-58.

[61]   E. M. Byrne, M. A. Mccarthy, Z. Xia, and W. A. Curtin. "Multiwall Nanotubes Can Be Stronger than Single Wall Nanotubes and Implications for Nanocomposite Design." *Physical Review Letters* 103.4 (2009): 045502.1-502.4.

[62]   A. Zettl, C. Piskoti, and J. Yarger. "C36, a New Carbon Solid." *Nature* 393.6687 (1998): 771-74

[63]   W. Krätschmer, L. D. Lamb, K. Fostiropoulos, and D. R. Huffman. "Solid C60: A New Form of Carbon." *Nature* 347.6291 (1990): 354-58.

[64]   P. Enghag. *Encyclopedia of the Elements: Technical Data, History, Processing, Applications*. Weinheim: Wiley-VCH, 2004.

[65]   R. Ananthaiah. "Discovery of Fullerenes." *Resonance* 2.1 (1997): 68-73.

[66]   J. Tersoff, and R. S. Ruoff. "Structural Properties of a Carbon-Nanotube Crystal." *Physical Review Letters* 73.5 (1994): 676-79.

[67]   Y. Liu, A. Dobrinsky, and B. I. Yakobson. "Graphene Edge from Armchair to Zigzag: The Origins of Nanotube Chirality?" *Physical Review Letters* 105.23 (2010): 235502.1-502.4

[68]   I. V. Bondarev and P. Lambin. "The Van Der Waals Energy of an Atom near a Carbon Nanotube." *Optics and Spectroscopy* 99.3 (2005): 475-80.

[69] Y. J. Dappe and R. Scipioni. "Role of the Van Der Waals Forces in the Ability of a Double-walled Carbon Nanotube to Accommodate a C60 Molecule: The Example of C60 @ (15,0) @ (24,0)." *Physical Review B* 84.19 (2011):193409.1-409.4

[70] A. Jorio. *The Sp2 Nanocarbons: Prototypes for Nanoscience and Nanotechnology*. Weinheim: Wiley-VCH, 2011.

[71] R. J. Cartwright, S. Esconjauregui, R. S. Weatherup, D. Hardeman, Y. Guo, E. Wright, D. Oakes, S. Hofmann, and J. Robertson. "The Role of the Sp2:sp3 Substrate Content in Carbon Supported Nanotube Growth." *Carbon* 75 (2014): 327-34.

[72] Y. Matsuda, J. Tahir-Kheli, and W. A. Goddard. "Definitive Band Gaps for Single-Wall Carbon Nanotubes." *The Journal of Physical Chemistry Letters* 1.19 (2010): 2946-950.

[73] G. Kim, J. Bernholc, and Y. K. Kwon. "Band Gap Control of Small Bundles of Carbon Nanotubes Using Applied Electric Fields: A Density Functional Theory Study." *Applied Physics Letters* 97.6 (2010): 063113.1-113.6.

[74] N. A. Lanzillo, N. Kharche, and S. K. Nayak. "Substrate-induced Band Gap Renormalization in Semiconducting Carbon Nanotubes." *Scientific Reports* 4:3609 (2014): 1-5.

[75] C. H. Chen, M. H. Lee, and S. J. Clark. "Band Gap Modification of Single-walled Carbon Nanotube and Boron Nitride Nanotube under a Transverse Electric Field." *Nanotechnology* 15.12 (2004): 1837-843.

[76] L. G. Bulusheva, A. V. Okotrub, D. A. Romanov, and D. Tomanek. "Electronic Structure of (n,0) Zigzag Carbon Nanotubes: Cluster and Crystal Approach." *The Journal of Physical Chemistry* 102 (1998): 975-81.

[77] K. El Shabrawy, K. Maharatna, D. Bagnall, B. M. Al-Hashimi. "Modeling SWCNT Bandgap and Effective Mass Variation Using a Monte Carlo Approach." *Nanotechnology, IEEE Transactions* 9.2 (2010) 184-93.

[78] H. W. C. Postma, T. Teepen, M. Grifoni, and C. Dekker. "Carbon Nanotube Single-Electron Transistors at Room Temperature." *Science* 293.5527 (2001): 76-79.

[79] G. R. Li, F. Wang, Q. W. Jiang, X. P. Gao, and P. W. Shen. "Carbon Nanotubes with Titanium Nitride as a Low-Cost Counter-Electrode Material for Dye-Sensitized Solar Cells." *Angewandte Chemie International Edition* 49.21 (2010): 3653-656.

[80] R. Bhandavat, A. Feldman, C. Cromer, J. Lehman, and G. Singh. "Very High Laser-Damage Threshold of Polymer-derived Si(B)CN- Carbon Nanotube Composite Coatings." *ACS Applied Materials & Interfaces* 5.7 (2013): 2354-359.

[81] C. Niu, E. K. Sichel, R. Hoch, D. Moy, and H. Tennent. "High Power Electrochemical Capacitors Based on Carbon Nanotube Electrodes." *Applied Physics Letters* 70.11 (1997): 1480-82.

[82] A. Peigney, Ch. Laurent, E. Flahaut, R. R. Bacsa, and A. Rousset. "Specific Surface Area of Carbon Nanotubes and Bundles of Carbon Nanotubes." *Carbon* 39.4 (2001): 507-14.

[83] T. Chen and L. Dai. "Carbon Nanomaterials for High-Performance Supercapacitors." *Materials Today* 16.7/8 (2013) 272-80.

[84] R. Signorelli, D. C. Ku, J. G. Kassakian, and J. E. Schindall. "Electrochemical Double-Layer Capacitors Using Carbon Nanotube Electrode Structures." *Proceedings of the IEEE* 97.11 (2009): 1837-847.

[85] V. Srinivasan and J. W. Weidner. "Capacitance Studies of Cobalt Oxide Films Formed via Electrochemical Precipitation." *Journal of Power Sources* 108.1-2 (2002): 15-20.

[86] C. Portet, P. L. Taberna, P. Simon, and E. Flahaut. "Influence of Carbon Nanotubes Addition on Carbon–carbon Supercapacitor Performances in Organic Electrolyte." *Journal of Power Sources* 139.1-2 (2005): 371-78.

[87] P. L. Taberna, P. Simon, and J. F. Fauvarque. "Electrochemical Characteristics and Impedance Spectroscopy Studies of Carbon-Carbon Supercapacitors." *Journal of The Electrochemical* Society 150.3 (2003): A292-300.

[88] M. K. Seo, and S. J. Park. "Influence of Air-oxidation on Electric Double Layer Capacitances of Multi-walled Carbon Nanotube Electrodes." *Current Applied Physics* 10.1 (2010): 241-44.

[89] C. Kim, S. H. Park, W. J. Lee, and K. S. Yang. "Characteristics of Supercapaitor Electrodes of PBI-based Carbon Nanofiber Web Prepared by Electrospinning." *Electrochimica Acta* 50.2-3 (2004): 877-81.

[90] C. Peng, J. Lang, S. Xu, and X. Wang. "Oxygen-enriched Activated Carbons from Pomelo Peel in High Energy Density Supercapacitors." *RSC Adv.* 4.97 (2014): 54662-667.

[91] I. D. Rosca, F. Watari, M. Uo, and T. Akasaka. "Oxidation of Multiwalled Carbon Nanotubes by Nitric Acid." *Carbon* 43.15 (2005): 3124-131.

[92] H. Jeong, and J. Y. Park. "Local Electrical Investigations of Nitric Acid Treatment Effects on Carbon Nanotube Networks." *The Journal of Physical Chemistry* 119.17 (2015): 9665-668.

[93] N. Jha, E. Bekyarova, P. Ramesh, M. E. Itkis, and R. C. Haddon. "Ruthenium Oxide - Single Walled Carbon Nanotube Composite Based High Energy Supercapacitor." *International Conference on Advanced Nanomaterials & Emerging Engineering Technologies* (2013): 436-39.

[94] W. Wang, S. Guo, I. Lee, K. Ahmed, J. Zhong, Z. Favors, F. Zaera, M. Ozkan, and C. S. Ozkan. "Hydrous Ruthenium Oxide Nanoparticles Anchored to Graphene and Carbon Nanotube Hybrid Foam for Supercapacitors." *Scientific Reports* 4.4452 (2014): 1-9.

[95] X. Wang, Y. Yin, C. Hao, and Z. You. "A High-performance Three-dimensional Micro Supercapacitor Based on Ripple-like Ruthenium Oxide–carbon Nanotube Composite Films." *Carbon* 82 (2015): 436-45.

[96] T. F. Hsieh, C. C. Chuang, W. J. Chen, J. H. Huang, W. T. Chen, and C. M. Shu. "Hydrous Ruthenium Dioxide/multi-walled Carbon-nanotube/titanium Electrodes for Supercapacitors." *Carbon* 50.5 (2012): 1740-747.

[97] R. A. Fisher, R. A., M. R. Watt, R. Konjeti, and W. J. Ready. "Atomic Layer Deposition of Titanium Oxide for Pseudocapacitive Functionalization of Vertically-Aligned Carbon Nanotube Supercapacitor Electrodes." *ECS Journal of Solid State Science and Technology* 4.2 (2014): M1-M5.

[98] Z. Wang, Z. Liang, B. Wang, C. Zhang, and L. Kramer. "Processing and Property Investigation of Single-walled Carbon Nanotube (SWNT) Buckypaper/epoxy Resin Matrix Nanocomposites." *Composites Part A: Applied Science and Manufacturing* 35.10 (2004): 1225-232.

[99] K. Lau, M. Lu, H. Cheung, F. Sheng, and H. Li. "Thermal and Mechanical Properties of Single-walled Carbon Nanotube Bundle-reinforced Epoxy Nanocomposites: The Role of Solvent for Nanotube Dispersion." *Composites Science and Technology* 65.5 (2005): 719-25.

[100] D. Deepa, V. Nehrukumar, V. Chidambaranathan. "Synthesis and Evaluation of Functionalized Carbon Nanotubes (CNT) Based Polymer Composite Nanofiltration Membranes for Desalination." *International Journal of Advanced Technology in Engineering and Science* 3.2 (2015): 183-187.

[101] K. Sears, L. Dumée, J. Schütz, M. She, C. Huynh, S. Hawkins, M. Duke, and S. Gray. "Recent Developments in Carbon Nanotube Membranes for Water Purification and Gas Separation." *Materials* 3.1 (2010): 127-49.

[102] K. S. Kim, M. B. Jakubinek, Y. Martinez-Rubi, B. Ashrafi, J. Guan, K. O'neill, M. Plunkett, A. Hrdina, S. Lin, S. Dénommée, C. Kingston, and B. Simard. "Polymer Nanocomposites from Free-standing, Macroscopic Boron Nitride Nanotube Assemblies." *RSC Advances* 5.51 (2015): 41186-192.

[103] A. Rubio, J. L. Corkill, and M. L. Cohen. "Theory of Graphitic Boron Nitride Nanotubes." Phys. Rev. B *Physical Review B* 49.7 (1994): 5081-084.

[104] N. G. Chopra, R. J. Luyken, K. Cherrey, V. H. Crespi, M. L. Cohen, S. G. Louie, and A. Zettl. "Boron Nitride Nanotubes." *Science* 269.5226 (1995): 966-67.

[105] M. Cohen and A. Zettl. "The Physics of Boron Nitride Nanotubes." *Physics Today* (2010) 34-38.

[106] M. M. Wu, X. Zhong, Q. Wang, Q. Sun, R. Pandey, and P. Jena. "Anisotropy and Transport Properties of Tubular C-BN Janus Nanostructures." *The Journal of Physical Chemistry* 115.48 (2011): 23978-983.

[107] K. S. Kim, C. T. Kingston, A. Hrdina, M. B. Jakubinek, J. Guan, M. Plunkett, and B. Simard. "Hydrogen-Catalyzed, Pilot-Scale Production of Small-Diameter Boron Nitride Nanotubes and Their Macroscopic Assemblies." *ACS Nano* 8.6 (2014): 6211-220.

[108] S. Kalay, Z. Yilmaz, O. Sen, M. Emanet, E. Kazanc, and M. Çulha. "Synthesis of Boron Nitride Nanotubes and Their Applications." *Beilstein Journal of Nanotechnology* 6 (2015): 84-102.

[109] Y. K. Yap. *B-C-N Nanotubes and Related Nanostructures*. Dordrecht: Springer, 2009.

[110] H. Shin, J. Guan, M. Z. Zgierski, K. Su Kim, C. T. Kingston, and B. Simard. "Covalent Functionalization of Boron Nitride Nanotubes via Reduction Chemistry." *ACS Nano* 9.12 (2015): 12573-582.

[111] L. Hongxia, Z. Heming, S. Jiuxu, and Z. Zhiyong. "Electronic Structures of an (8, 0) Boron Nitride/carbon Nanotube Heterojunction." *Journal of Semiconductors* 31.1 (2010): 13001-003.

[112] E. Iyyamperumal, S. Wang, and L. Dai. "Vertically Aligned BCN Nanotubes with High Capacitance." *ACS Nano* 6.6 (2012): 5259-265.

[113] C. Y. Su, W. Y. Chu, Z. Y. Juang, K. F. Chen, B. M. Cheng, F. R. Chen, K. C. Leou, and C. H. Tsai. "Large-Scale Synthesis of Boron Nitride Nanotubes with Iron-Supported Catalysts." *The Journal of Physical Chemistry C* 113.33 (2009): 14732-738.

[114] D. Golberg, C. Zhi, P. Costa, X. Bai, C. Tang, Q. Huang, M. Mitome, and Y. Bando. "Boron Nitride Nanotubes: Recent Breakthroughs and Challenges." *ECS Transactions* 11.8 (2007): 15-21.

[115] A. L. Tiano, C. Park, J. W. Lee, H. H. Luong, L. J. Gibbons, S. H. Chu, S. Applin, P. Gnoffo, S. Lowther, H. J. Kim, P. M. Danehy, J. A. Inman, S. B. Jones, J. H. Kang, G. Sauti, S. A. Thibeault, V. Yamakov, K. E. Wise, J. Su, and C. C. Fay. "Boron Nitride Nanotube: Synthesis and Applications." *Nanosensors, Biosensors, and Info-Tech Sensors and Systems* 2014 (2014): 1-19.

[116] A. L. Tiano, L. Gibbons, M. Tsui, S. I. Applin, R. Silva, C. Park, and C. C. Fay. "Thermodynamic Approach to Boron Nitride Nanotube Solubility and Dispersion." *Nanoscale* 8.7 (2016): 4348-359.

[117] J. Cumings, and A. Zettl. "Mass-production of Boron Nitride Double-wall Nanotubes and Nanococoons." *Chemical Physics Letters* 316.3-4 (2000): 211-16.

[118] C. H. Lee, D. Zhang, and Y. K. Yap. "Functionalization, Dispersion, and Cutting of Boron Nitride Nanotubes in Water." *The Journal of Physical Chemistry C* 116.2 (2012): 1798-804.

[119] J. Robertson. "High Dielectric Constant Oxides." *The European Physical Journal Applied Physics* 28.3 (2004): 265-91.

[120] Y. Martinez-Rubi, B. Ashrafi, M. Jakubinek, S. Denommee, J. Guan, B. Simard. "Integration of Nanotube Paper into UHMWPE Multilayer Structures." in *Design, Manufacturing and Applications of Composites, Tenth Joint Canada-Japan Workshop on Composites* Vancouver, Canada (2014): 62-69.

[121] D. Lahiri, S. R. Bakshi, A. K. Keshri, Y. Liu, and A. Agarwal. "Dual Strengthening Mechanisms Induced by Carbon Nanotubes in Roll Bonded Aluminum Composites." *Materials Science and Engineering* A523.1-2 (2009): 263-70.

[122] J. Tao, N. Liu, W. Ma, L. Ding, L. Li, J. Su, and Y. Gao. "Solid-State High Performance Flexible Supercapacitors Based on Polypyrrole-MnO2-Carbon Fiber Hybrid Structure." *Scientific Reports* 3:2286 (2013): 1-7.

[123] L. Cai, S. Zhang, J. Miao, Q. Wei, and C. Wang. "Capacitance-Voltage Characteristics of Thin-film Transistors Fabricated with Solution-Processed Semiconducting Carbon Nanotube Networks." *Nanoscale Res Lett Nanoscale Research Letters* 10.291 (2015):1-6.

[124] S. Belahsene, N. A. Saqri, D. Jameel, A. Mesli, A. Martinez, J. D. Sanoit, A. Ougazzaden, J. Salvestrini, A. Ramdane, and M. Henini. "Analysis of Deep Level Defects in GaN P-i-n Diodes after Beta Particle Irradiation."Electronics 4.4 (2015): 1090-100.

[125] R. Comyn, Y. Cordier, V. Aimez, and H. Maher. "Reduction of the Thermal Budget of AlGaN/GaN Heterostructures Grown on Silicon: A Step towards Monolithic Integration of GaN-HEMTs with CMOS." *Physica Status Solidi (A)* 212.5 (2015): 1145-152.

[126] S. Jenatsch, R. Hany, A. C. Véron, M. Neukom, S. Züfle, A. Borgschulte, B. Ruhstaller, and F. Nüesch. "Influence of Molybdenum Oxide Interface Solvent Sensitivity on Charge Trapping in Bilayer Cyanine Solar Cells." *The Journal of Physical Chemistry C* 118.30 (2014): 17036-7045.

[127] E. C. Garnett, Y. C. Tseng, D. R. Khanal, J. Wu, J. Bokor, and P. Yang. "Dopant Profiling and Surface Analysis of Silicon Nanowires Using Capacitance–voltage Measurements." *Nature Nanotechnology* 4.5 (2009): 311-14.

[128] M. Atif, W. Farooq, A. Fatehmulla, M. Aslam, and S. Ali. "Photovoltaic and Impedance Spectroscopy Study of Screen-Printed TiO2 Based CdS Quantum Dot Sensitized Solar Cells." *Materials* 8.1 (2015): 355-67.

[129] C. Aramo, A. Ambrosio, M. Ambrosio, M. Boscardin, P. Castrucci, M. Crivellari, M. Cilmo, M. De Crescenzi, F. De Nicola, E. Fiandrini, V. Grossi, P. Maddalena, M. Passacantando, S. Santucci, M. Scarselli, and A. Valentini. "Observation of a Photoinduced, Resonant Tunneling Effect in a Carbon Nanotube–silicon Heterojunction."*Beilstein Journal of Nanotechnology* 6 (2015): 704-10.

[131] K. S. K. Kwa, S. Chattopadhyay, N. D. Jankovic, S. H. Olsen, L. S. Driscoll, and A. G. O Neill. "A Model for Capacitance Reconstruction from Measured Lossy MOS Capacitance voltage Characteristics." *Semiconductor Science and Technology* 18.2 (2002): 82-87.

[130] R. Mysyk, E. Raymundo-Piñero, and F. Béguin. "Saturation of Subnanometer Pores in an Electric Double-layer Capacitor." *Electrochemistry Communications* 11.3 (2009): 554-56.

APPENDIX A

IMAGE COPYRIGHT INFORMATION

Each of the following pages will demonstrate proper permission to reuse images taken from other authors work. I do not claim any right or fabrication of these images other than that of permission to reuse specifically in this work. If any of the images are needed for reuse, further permissions must be sought. I have included a brief description of the image, reference, as well as an image demonstrating my right to use the image in this document. 5 images ae used and 4 are copyright protected and the last is open access. All documentation is included.

The image used in Figure 1 of the text, which shows the basic supercapacitor structure is taken from:

[34] V. Musolino, L. Piegari, and E. Tironi. "New Full-Frequency-Range Supercapacitor Model With Easy Identification Procedure." *IEEE Transactions on Industrial Electronics* 60.1 (2013): 112-20.

Appendix A Image I: *Copyright permission for use of Figure 1*

The image used in Figure 2 of the text, which shows the Stern EDLC model is taken from:

[53]   H. Wang, and L. Pilon. "Accurate Simulations of Electric Double Layer Capacitance of Ultramicroelectrodes." *Journal of Physical Chemistry C* 115.33 (2011): 16711-6719.

Appendix A Image II: *Copyright permission for use of Figure 2*

The image used in Figure 3 of the text, which shows the CNT sheet cut types is taken from:

[1]   L. L. Zhang, and X. S. Zhao. "Carbon-based Materials as Supercapacitor Electrodes." *Chemical Society Reviews*. 38.9 (2009): 2520-2531.

ROYAL SOCIETY OF CHEMISTRY LICENSE
TERMS AND CONDITIONS

Mar 10, 2016

This Agreement between Derek C Demuth ("You") and Royal Society of Chemistry ("Royal Society of Chemistry") consists of your license details and the terms and conditions provided by Royal Society of Chemistry and Copyright Clearance Center.

License Number	3814941192110
License date	Feb 23, 2016
Licensed Content Publisher	Royal Society of Chemistry
Licensed Content Publication	Chemical Society Reviews
Licensed Content Title	Carbon-based materials as supercapacitor electrodes
Licensed Content Author	Li Li Zhang,X. S. Zhao
Licensed Content Date	Jun 12, 2009
Licensed Content Volume Number	38
Licensed Content Issue Number	9
Type of Use	Thesis/Dissertation
Requestor type	non-commercial (non-profit)
Portion	figures/tables/images
Number of figures/tables/images	1
Format	print and electronic
Distribution quantity	5
Will you be translating?	no
Order reference number	None
Title of the thesis/dissertation	Carbon and Boron Nitride Nanotube Fabricated Super Capacitors
Expected completion date	May 2016
Estimated size	80
Requestor Location	Derek C Demuth 6493 Walter Reed Dr
	GLOUCESTER, VA 23061 United States Attn: Derek C Demuth
Billing Type	Invoice
Billing Address	Derek C Demuth 6493 Walter Reed Dr
	GLOUCESTER, VA 23061 United States Attn: Derek C Demuth
Total	0.00 USD

Terms and Conditions

This License Agreement is between {Requestor Name} ("You") and The Royal Society of Chemistry ("RSC") provided by the Copyright Clearance Center ("CCC"). The license consists of your order details, the terms and conditions provided by the Royal Society of Chemistry, and the payment terms and conditions.
RSC / TERMS AND CONDITIONS
INTRODUCTION
The publisher for this copyrighted material is The Royal Society of Chemistry. By clicking "accept" in connection with completing this licensing transaction, you agree that the following terms and conditions apply to this transaction (along with the Billing and Payment terms and conditions established by CCC, at the time that you opened your RightsLink account and that are available at any time at .
LICENSE GRANTED
The RSC hereby grants you a non-exclusive license to use the aforementioned material anywhere in the world subject to the terms and conditions indicated herein. Reproduction of the material is confined to the purpose and/or media for which permission is hereby given.
RESERVATION OF RIGHTS
The RSC reserves all rights not specifically granted in the combination of (i) the license details provided by your and accepted in the course of this licensing transaction; (ii) these terms and conditions; and (iii) CCC's Billing and Payment terms and conditions.

Appendix A Image III: Copyright permission for use of Figure 3

The image used in Figure 6, which is protected under Crown copyright laws so permission was achieved through contact with the authors of the text, shows a TEM image of BNNTs taken from:

[107] K. S. Kim, C. T. Kingston, A. Hrdina, M. B. Jakubinek, J. Guan, M. Plunkett, and B. Simard. "Hydrogen-Catalyzed, Pilot-Scale Production of Small-Diameter Boron Nitride Nanotubes and Their Macroscopic Assemblies." *ACS Nano* 8.6 (2014): 6211-220.

Appendix A Image IV: *Conversation with ACS Nano to find specific copyright (left) email correspondence with author (right)*

The next image is classified as open access for copyright use.

The image used in Figure 23 of the text, which shows the CV measurements of devices:

[128] M. Atif, W. Farooq, A. Fatehmulla, M. Aslam, and S. Ali. "Photovoltaic and Impedance Spectroscopy Study of Screen-Printed TiO2 Based CdS Quantum Dot Sensitized Solar Cells." *Materials* 8.1 (2015): 355-67.

Appendix A Image V: *Copyright permission for use of Figure 24*

VITA

Derek Christian Demuth

Department of Study:

Electrical and Computer Engineering

Old Dominion University

231 Kaufman Hall

Norfolk, VA 23529

Background of Study:

I completed my first degree as a Bachelor of Arts at Virginia Tech in 2007 studying to be a reporter. After having to report on the shooting my direction was switched to that of working in retail management. Following one year in at Target as an Assistant Store Manager, I enrolled back in college at Old Dominion University in 2009. I completed my Bachelors of Science in Electrical and Computer Engineering in 2014 with a focus on networking and logic control systems. I started graduate school in 2015 in the Electrical and Computer Engineering Department at Old Dominion University to earn a Master's of Science. In my graduate research I have worked on such projects as TCSPC data measurements, perovskite solar cell two step method, and nanotube supercapacitor devices.